The influence of 17-β-estradiol on bio-energetic and estrogen metabolism in macrophages

A Tollemache

orcid.org/0000-0002-9411-1160

Dissertation accepted in partial fulfilment of the requirements for the degree *Master of Science in Biochemistry* at the North-West University

Supervisor:	Dr G Venter
Co-supervisor:	Prof E Erasmus
Co-supervisor:	Prof FH van der Westhuizen

Graduation May 2023

27026396

ACKNOWLEDGEMENTS

Firstly, I would like to extend my sincere gratitude to my family for encouraging me every step of the way during this journey. Special thanks go out to my parents:

To my dad: You will always be my greatest inspiration and the best example of great work ethic. To my mom: Your prayers, emotional support, and words of encouragement kept me going during times where I wanted to throw in the towel. Words cannot express what you both mean to me.

I am extremely grateful to my partner for his love, sacrifices and always finding a way to lift my spirits.

I would like to thank the following people, without whom this endeavour would not have been possible:

Dr. Venter- An exceptional woman of science and supervisor! Thank you for your patience and invaluable guidance throughout this study. It was a great privilege to study under you.

Prof Erasmus for his insightfulness, expertise and always having a solution to an obstacle.

Carien Van der Berg for teaching me the ins and outs of the LC-MS/MS and for offering her time and knowledge whenever I come knocking.

Mari van Reenen for her assistance in the statistical analyses of the data.

I am also grateful for the financial support from the following institutions, without whom this study would surely not have been possible:

The National Research Foundation (NRF): Grant no. 138745

The Struwig-Germeshuysen Cancer Research (SGKN) Trust

The North-West University Postgraduate bursary

Above all, I thank my Heavenly Father for His guidance and countless blessings throughout this study. All honour and praise go to Him.

ABSTRACT

Breast cancer is a multifactorial disease influenced by a variety of factors in the tumour microenvironment (TME), including hormones such as estrogen, and immune cells such as macrophages. Imbalances in estrogen metabolism and certain estrogen metabolites have been linked to breast cancer. Estrogen has also been shown to influence macrophage polarization. The metabolic and functional plasticity of macrophages allow these cells to play a dual role in breast cancer by either inhibiting or promoting tumourigenesis based on their activation (polarization) state. Considering the potential role of both estrogen and macrophages in breast cancer, it is possible that interaction between the two can further affect tumour dynamics. Macrophage polarization is tightly linked to metabolic state, however it is not known how estrogens affect the bio-energetic metabolism of naïve, pro-, or anti-inflammatory macrophages. Furthermore, estrogen metabolism in macrophages is not well studied. In this study the effect of 17-β-estradiol (E2) on macrophage bio-energetics was compared to that of lipopolysaccharide (LPS) and interleukin-4 (IL-4) at different glucose concentrations (5 mM, 11 mM, and 25 mM) using the Seahorse Extracellular Flux Analyzer to measure mitochondrial oxidative phosphorylation (OXPHOS). After identifying the most optimal glucose concentration from these and additional glucose consumption assays, the effect of E2 on the bio-energetic metabolism of pro- and anti-inflammatory RAW 264.7 cells and mouse bone-marrow derived macrophages (BMDMs) was also investigated. Finally, cell culture medium from RAW 264.7 cells (incubated with or without LPS, IL-4, and E2) was collected to analyse estrogen metabolite production with LC-MS/MS. Bio-energetics results reveal that the effect of LPS, IL-4, and E2 on macrophage metabolism is influenced by the glucose concentration in the culture medium. E2 induced an oxidative metabolism in macrophages, similar to IL-4 treatment. Moreover, E2 caused a shift in the bio-energetic metabolism of LPS-treated (pro-inflammatory) cells towards a metabolic profile comparable to naïve cells. Since macrophage polarization and metabolism is reciprocally coupled, this may mean that E2 present in the breast tissue may dampen or limit pro-inflammatory, anti-cancer macrophages (present during the early stages of tumor development) by inducing a metabolic switch. This may favor tumor initiation and progression. LC-MS/MS results showed that macrophages can synthesise and secrete estradiol (particularly the less active 17-α-estradiol) into their environment, where it may have the potential to affect the functionality of other neighboring cells in the TME. Furthermore, LPS-treated macrophages seemed to produce more 17-α-estradiol and 17-β-estradiol compared to anti-inflammatory cells. This may be due to the involvement of LPS in aromatase modulation. The findings from this study suggest that the interplay between estrogen and macrophages (which can also be influenced by other factors such as glucose concentration) may alter tumour dynamics, but probably not via the production of carcinogenic estrogen metabolites by macrophages.

Key terms: Breast cancer, metabolism, estrogen, LC-MS/MS, macrophages, bio-energetics, tumour microenvironment

TABLE OF CONTENTS

LIST OF FIGURES

LIST OF TABLES

LIST OF SYMBOLS AND ABBREVIATIONS

ADP	Adenosine diphosphate
ANOVA	Analysis of variance
ATP	Adenosine triphosphate
BCKDC	Branched-chain α-keto acid dehydrogenase complex
BDK	Branched-chain α-keto acid dehydrogenase kinase
BMDMs	Bone-marrow derived macrophages
CCL2	C-C motif chemokine ligand 2
CD	Cluster of differentiation
CO_2	Carbon dioxide
COMT	Catechol-O-methyltransferase
CSC	Cancer stem cell
CSF-1	Colony-stimulating factor-1 receptor
CYP	Cytochrome P450
dH_2O	Distilled water
DHEA	Dehydroepiandrosterone
DMEM	Dulbecco's Modified Eagle's Medium
DMSO	Dimethylsulfoxide
E1	Estrone
E2	17-β-estradiol
E3	Estriol
ECAR	Extracellular acidification rate
ECM	Extracellular matrix
EGF	Epidermal growth factor
EM	Estrogen metabolites
ER	Estrogen receptor
ERE	Estrogen response elements
ESI	Electrospray ionisation
ETC	Electron transport chain
FA	Fatty acid
$FADH_2$	Flavin adenine dinucleotide
FBS	Fetal bovine serum
FSH	Follicle-stimulating hormone
GLUT	Glucose transporters

GPER	G protein-coupled estrogen protein
HER2	Human epidermal growth factor receptor 2
hMDMs	Human monocyte-derived macrophages
HR	Hormone receptor
HIF-α	Hypoxia-inducible factor-alpha
HRP	Horseradish peroxidase
HSD	Hydroxysteroid dehydrogenase
IL-4	Interleukin-4
IL-6	Interleukin-6
ILIS	Isotope-labelled internal standards
iNOS	Nitric oxide synthase
IFN	Interferons
KLF-4	Krüppel-like factor 4
LC-MS/MS	Liquid chromatography tandem mass spectrometry
LDH	Lactate dehydrogenase
LOD	Limit of detection
LOQ	Limit of quantification
LH	Luteinizing hormone
LLE	Liquid-liquid extraction
LPS	Lipopolysaccharides
MAMs	Metastasis associated macrophages
MAPK	Mitogen-activated protein kinase
MCP	Monocyte chemoattractant protein
MCSF	Macrophage colony-stimulating factor
ME2	Methoxyestradiol
ME1	Methoxyestrone
MeOH	Methanol
MIF	Macrophage migration inhibitory factor
MISS	membrane-initiated steroid signaling
MMP	Matrix metalloproteinases
MS/MS	Tandem mass spectrometry
MyD88	Myeloid differentiation primary response 88
NADH	Nicotinamide adenine dinucleotide
NADPH	Nicotinamide adenine dinucleotide phosphate
NaCl	Sodium chloride

NaOH	Sodium hydroxide
NF-kβ	Nuclear factor-kappa β
NOS	Nitric oxide synthase
NWU-AnimCare REC	North-West University Animal Care, Health, and Safety research ethics commitee
OCR	Oxygen consumption rate
OHE2-3,4-Q	Hydroxyestradiol-3,4-quinone
OHE2-2,3-Q	Hydroxyestradiol-2,3-quinone
OHE2	Hydroxyestradiol
OHE1	Hydroxyestrone
OH	Hydroxyl
OXPHOS	Oxidative phosphorylation
P450scc	Cholesterol side chain cleavage
PBS	Phosphate buffered saline
PCDDP	Preclinical Drug Development Platform
PGE2	Prostaglandin E2
PIM kinase	Proto-oncogene serine/threonine-protein
PMA	Phorbol 12-myristate-13 acetate
PPAR-γ	Peroxisome proliferator-activator receptor gamma
PR	Progesterone receptor
ROS	Reactive oxygen species
RRHD	Rapid resolution high-definition
SIRP	Signal regulatory proteins
SLAM	Signaling lymphocyte activation molecules
SPE	Solid phase extraction
STAT	Signal transducer and activator of transcription
SULTs	Sulfotransferase
TAM	Tumour-associated macrophages
TC	Tissue culture
TCA cycle	Tricarboxylic acid cycle
TCA	Trichloroacetic acid
TGF	Transforming growth factor
TLR	Toll-like receptor
TME	Tumour microenvironment
TNBC	Triple negative breast cancer

TNF	Tumor necrosis factors
TRIF	TIR-domain-containing adapter-inducing interferon-β
Tris-HCl	Trisaminomethane hydrochloric acid
UGTs	UDP-glucuronosyltransferase
VCAM	Vascular cell-adhesion molecule
VEGF	Vascular endothelial growth factor
XF	Extracellular Flux
α	Alpha
β	Beta
γ	Gamma
mL	Millilitre
L	Litre
µL	Microlitre
g	Gram
ng	Nanogram
x g	Relative centrifugal force
°C	Degrees Celcius
%	Percentage
M	Molar concentration
mM	Milimolar concentration
nM	Nanomolar concentration
nM	Nanometres wavelength
v/v	Volume/volume %
w/v	Weight/volume %
psi	pound-force per square inch
V	Volts
ppb	Parts per billion
ppm	Parts per million
Pmol	Picomoles per litre
m/z	Mass to charge ratio
Min	Minute
Sec	Second

CHAPTER 1 INTRODUCTION

Breast cancer remains a formidable enemy and is the second most common cancer type that accounts for mortality in women worldwide (Bray *et al.*, 2018). The recalcitrant nature of breast cancer towards treatment may be attributed to various factors such as tumourigenesis stage, estrogen receptor (ER) status, and components in the tumour microenvironment (TME) such as estrogen and infiltrating macrophages.

Substantial research has shown that estrogen may have a significant role in the onset of breast cancer. It has been found that postmenopausal women are at an increased risk for breast cancer, probably due to the unbalanced estrogen levels that arise after menopause (Samavat & Kurzer, 2015). Furthermore, studies have indicated that endocrine therapy such as estrogen replacement in postmenopausal women is linked to a significant increase in breast cancer risk (Shah & Wong, 2006). In the last two decades, estrogen metabolism has emerged as an important contributor to the pathogenesis of breast cancer. Imbalances in estrogen metabolism as well as certain estrogen metabolites such as catechol estrogen quinones were found to cause mutagenicity (Cavalieri *et al.*, 2006). It is, therefore, evident that these molecules may have an immense impact on breast cancer pathogenesis and that the study of estrogens and their metabolites is important.

The tumour microenvironment also comprises a variety of signaling molecules and immune cells such as macrophages. These tumour-associated macrophages (TAMs) are prime topics in the study of tumour malignancy, since a dynamic interplay exists between these specialised cells and the tumour (Wei *et al.*, 2019). The incredible metabolic plasticity of macrophages allows these cells to be activated to different states in response to exposure to certain stimuli such as extracellular metabolites, bacterial components (e.g. lipopolysaccharides), cytokines (e.g. interleukin-4), and hormones (estrogen). This enables the macrophages to either promote or inhibit cancer progression by secreting certain factors and cytokines (Poh & Ernst, 2018). This flexibility in the activation state of TAMs is coupled with differences in the metabolic mechanisms of these cells which may cause alterations in the TME. TAMs may, therefore, largely contribute to the phenomenon that all types of breast tumour cells do not respond equally to cancer treatments (Avagliano *et al.*, 2019).

It is clear that estrogen, estrogen metabolism, as well as its effect on macrophage metabolism and function, are important factors that need to be considered when studying breast cancer. Although much has been done to characterise macrophage metabolism (Geeraerts *et al.*, 2017;

Viola *et al.*, 2019) and the effect of estrogen on macrophage activation (Keselman *et al.*, 2017), the effect of estrogen on already polarized macrophages as well as estrogen metabolism in macrophages has not been thoroughly studied up to now. The crux of this study, therefore, is to evaluate the effect of estrogen on the bio-energetic metabolism in different macrophage cell lines and activation states as well as to investigate estrogen metabolism in macrophages. This study aims to shed light on the potential role of estrogen metabolism in macrophages in the onset and progression of breast cancer. The knowledge generated from the study will contribute to the fundamental understanding of macrophage biology and can be employed towards the development of novel therapy options, such as the manipulation of estrogen metabolism and immune engineering (Rezvani *et al.*, 2017).

Chapter 2 covers existing literature regarding components in the tumour microenvironment (with a special focus on estrogen and macrophages). A problem statement as well as the aim and objectives are presented in this chapter.

Chapter 3 encompasses the materials and methods used in the study. An overview of the principles of the experimental procedures and the statistical procedures followed to analyse the experimental data are described.

Chapter 4 covers the results and a discussion of the experimental analyses.

Chapter 5 summarises the major findings and overall biological interpretation of the study. The chapter concludes with a discussion about the shortcomings of this study as well as future prospects.

CHAPTER 2 LITERATURE REVIEW

2.1 The influence of components in the TME on cancer progression

Stephen Paget was the first to introduce the concept of microenvironmental influences on tumour progression and paved the way for other pioneering research on the TME (Wits, 2009). It is now well understood that conditions in the TME differ from that in normal tissue and that this is pivotal to our understanding of tumour interactivity. The TME is comprised of cellular components such as extracellular macromolecules, connective tissue, lymph, adipose tissue, red blood cells, fibroblasts, and immune cells (Wang *et al.*, 2017), as well as non-cellular factors secreted by other cells in the TME. These include growth factors, nucleic acids, metabolites, cytokines, and hormones (Patel *et al.*, 2018).

2.1.1 The role of estrogen in the TME

Estrogen is the most abundant female hormone (Samavat & Kurzer, 2015) and the hormone most commonly linked to breast cancer, which suggests that it constitutes a significant part of the breast TME. Estrogen levels in the TME fluctuates considerably during the menstrual cycle, pregnancy, and postmenopause (Pozzi *et al.*, 2006). Variations in the estrogen concentration may also be influenced by estrogen production by the tumour itself, as well as by other tumour-associated cells such as stromal cells, fibroblasts, and macrophages. The aromatase enzyme present in these cells catalyze the conversion of androstenedione to estrogen (Navarro *et al.*, 2018). The current knowledge regarding the exact mechanisms by which estrogen affects tumour progression is limited. However, several studies have described estrogen as having an oncogenic role in breast cancer (Cavalieri *et al.*, 2006; Russo & Russo, 2006).

2.1.2 Macrophages in the TME

Immune cells, such as macrophages, play a particularly important role and have drawn attention in TME studies as these cells can make up 50% of the TME (Poh & Ernst, 2018). These specialised phagocytes form part of the body's first line of defense and protect against harmful cells such as pathogens and cancerous cells by means of phagocytosis, apoptosis, and secretion of reactive oxygen species (ROS) (Pathria *et al.*, 2019). Macrophages can invade the region surrounding the tumour. These TAMs can either impede or assist tumour growth depending on their activation state. The M1 (pro-inflammatory) state is known as the cancer-killing type. On the other hand, the M2 (anti-inflammatory) state is characterised by its cancer-promoting abilities. It

is thus clear that macrophages can play a dual role in the progression of breast cancer. Cancer cells can exploit this versatility by increasing the activation of M2 macrophages via the secretion of M2 stimulating factors and lactic acid production. This allows the tumour to harness the cancer-promoting qualities of M2 macrophages as a survival mechanism (El-Kenawi *et al.*, 2019). Due to the significant role that both estrogen and macrophages play in the TME, these two factors will be the focal point of discussion in this study.

2.2 Estrogen: biologically important hormone

Estrogens are essential steroid hormones that play a plenitude of key roles in both women and men. Therefore, knowledge regarding the synthesis and metabolism of this hormone is necessary to fully understand its biological role. The following sections present a discussion about this important aspect.

2.2.1 Estrogen production, regulation, and metabolism

Estrogen production in females occurs mainly in the ovaries, however, the brain, adrenal gland, breast adipose tissue, bone-forming cells, blood vessel endothelium, and the liver are also sites of estrogen production (Simpson, 2003). Estrogen production is mainly regulated by follicle-stimulating hormone (FSH). The hypothalamus in the brain is responsible for secreting FSH, which then stimulates the ovaries to produce estrogen. FSH receptors have also been found to be expressed in other estrogen-producing tissues such as breast adipose tissue (Lizneva *et al.*, 2019). According to Simpson (2003), postmenopausal estrogen production differs greatly from that seen before menopause. Premenopausal estrogen, which is predominantly produced in the ovaries, is distributed in and acts on other parts of the body whereas in postmenopausal women this is not the case. Perturbations in postmenopausal FSH hamper estrogen production in the ovaries. Estrogen is then rather produced in other sites such as breast- and adipose tissue. Although smaller amounts of estrogen are produced the biological effect thereof is greater since the influence is directly localized at these sites. The three types of naturally produced estrogens found in the body are estrone (E1), 17-β-estradiol (E2), and estriol (E3), with E2 being the most biologically active estrogen (Hariri & Rehman, 2019). Therefore, special focus will be placed on E2.

Following FSH and luteinizing hormone (LH) release in the hypothalamus (Raju *et al.*, 2013), the formation of cholesterol is upregulated. As indicated in Figure 1, cholesterol is cleaved by the cytochrome P450scc (cholesterol side chain cleavage) enzyme to form pregnenolone, which is metabolised to either progesterone via hydroxysteroid dehydrogenases (HSDs) or via a series of enzymatic steps by the cytochrome P450 (CYP) family to dehydroepiandrosterone (DHEA).

Androstenediol is formed from DHEA (via 17β-HSDs) and androstenedione from progesterone and DHEA (via CYP and 3β-HSD enzymes, respectively). These androgen metabolites are converted to testosterone via 17β-HSDs. E2 and E1 are produced from the aromatization of testosterone and androstenedione, respectively, by the aromatase enzymes. E1 can then be converted to E2 via 17β-HSD enzymes (Samavat & Kurzer, 2015).

E2 and E1 and their related metabolites can further be metabolised to sulphates via sulfotransferase (SULTs), undergo glucuronidation via UDP-glucuronosyltransferase (UGTs), or be hydroxylated by CYP enzymes in a reversible fashion to form hydroxy (OH) metabolites (such as 6α/β-OH E2, 7α/β-OH E2, 15α/β-OH E2, 16α/β-OH E2, and 16α-OH E1) (Raftogianis *et al.*, 2000). The catechol estrogen metabolites 2-hydroxy-E1/E2 and 4-hydroxy-E1/E2 are also formed via CYPs, which in turn can be converted to 2-methoxyestrone (2-ME1), 4-methoxyestrone (4-ME1), 2-methoxyestradiol (2-ME2), and 4-methoxyestradiol (4-ME2) via Catechol-O-methyltransferase (COMT) or be oxidised by peroxidase enzymes to form estrogen quinones (E1/E2- 2,3 quinones and E1/E2-3,4 quinones). These quinones can be converted back to the hydroxyl quinones via quinone reductase (Gaikwad *et al.*, 2009). Additionally, estrone-2-hydroxy-3-methyl ether can be formed from 2-hydroxyestrone via CYPs (Eliassen *et al.*, 2008). The less biologically active estriol metabolites (which include 16-epiestriol, 17-epistriol, 16-ketoestradiol) are formed from 16α-OH estrone (via 16α-HSD). Like E1 and E2, estriol can undergo sulfonation and glucuronidation (Eliassen *et al.*, 2008). Estrogen metabolites may then be eliminated from the body, for example as estriol metabolites (Pizzorno *et al.*, 2016). Tight regulation of this metabolic pathway is required to ensure that estrogens and estrogen metabolites are produced and perform their respective functions in the body.

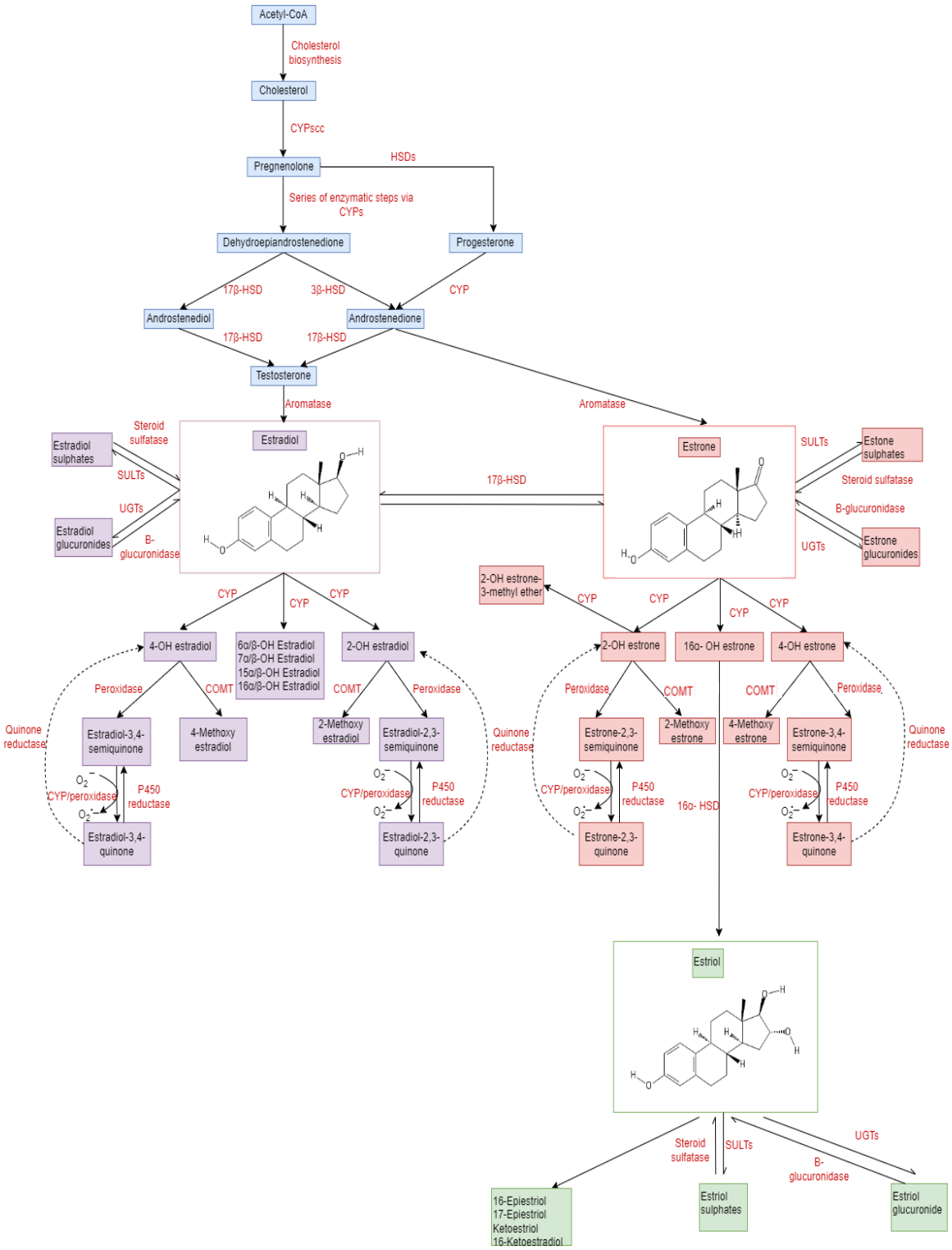

Figure 1: A schematic overview of estrogen production and metabolism— Reconstructed from Samavat *et al.*, (2015); Raftogianis *et al.*, (2000); Gaikwad *et al.*, (2009) and Eliassen *et al.*, (2008).

2.2.2 Importance of estrogen and estrogen metabolites

Although the most prevalent role of estrogen is the development of secondary sexual characteristics in women, it is also involved in numerous other important biological processes such as vasodilation, neuroprotection, and immune regulation (Hamilton *et al.*, 2017). The numerous functions of estrogens in the body as well as their functional efficiency may be attributed to the molecular structure of these hormones. Conformation is often directly linked to function, which is also the case for estrogens. According to Smiley and Khalil (2009) estrogens which are structurally alike perform similar purposes in the body. Estrogens are particularly well suited for their role as hormones in the body due to their aromatic structures. Although slight differences are observed for the three types of estrogens, they all consist of 18 carbons and a benzene ring with a hydroxyl group. This aromaticity significantly increases the stability of these hormones (Samavat & Kurzer, 2015). As already mentioned, E2 is the predominant estrogen hormone and has potent estrogenic activity (Smiley & Khalil, 2009). E2 has several biological roles in the body. Calcium regulation is one such process which is crucial for maintaining cardiovascular health. E2 modulates calcium channels and ensures sufficient calcium supplies to allow electrical signals in the heart (Mahmoodzadeh & Dworatzek, 2019). The mitochondrion is essential for life and is the main site for energy production. E2 is responsible for maintaining mitochondrial homeostasis by increasing mitochondrial protein expression as well as increasing mitochondrial oxygen consumption in order to limit ROS production (Klinge, 2008). Another important function of estradiol is its involvement in synapse formation in the fetal brain (McCarthy, 2008). Estrone is the weakest form of estrogen and is mainly involved in sexual development but often serves as a reserve for when extra estrogen is required since it can be readily converted to estradiol (Nichols, 2020). However, the involvement of estrone in other parts of the body such as the brain was made evident in a study that aimed to investigate the potential role of estrone on brain recovery in rats who suffered from brain lesions. The researchers found a decrease in neuronal damage upon estrone administration, which suggests a possible role of estrone in brain protection and brain tissue renewal (Gatson *et al.* (2012). Estriol is an important hormone during fetal development and higher levels of this hormone are typically detected during pregnancy. As such, estriol is often used as a biochemical marker for screening abnormalities during pregnancy. Estriol is furthermore involved in uterine development, blood vessel formation, and blood flow between the mother and fetus (Falah *et al.*, 2015). Even though the biological functions of estrogens as a whole are well understood, it is important to note that different estrogen metabolites can have different effects in the body. Zhu and Conney (1998) reviewed these biological functions of estrogen metabolites. Estradiol metabolites such as 2-hydroxyestradiol and 4-hydroxyestradiol are involved in the release of gonadotropins and the ovulation cycle. 2-

Hydroxyestradiol stimulates prostaglandin production, which triggers inflammatory and growth responses, and regulates neuronal signaling as well as dopamine activity. Similar to 2-hydroyxestradiol, the metabolite 4-hydroxyestradiol is involved in prostaglandin production and development of the uterus. 15α-Hydroxyestradiol is another metabolite speculated to be involved in fetal development, due to high levels detected during pregnancy. Finally, the 2-methoxyestradiol metabolite has been shown to inhibit cell growth and angiogenesis. Estrone metabolites, 2-hydroxyestrone and 4-hydroxyestrone display functions similar to that of 2-hydroxyestradiol and 4-hydroxyestradiol and regulate gonad development and ovulation. 2-Hydroxyestradiol has an additional growth inhibitory effect, whereas 16α-hydroxyestrone displays a pro-proliferative effect (Eliassen *et al.*, 2008). The estriol metabolite, 17-epistriol, was found to upregulate the transforming growth factor (TGF)-β3 and play a role in prenatal development (Zhu & Conney, 1998).

Considering the biological significance of estrogen and its metabolites it is clear that disturbances in estrogen metabolism can have negative effects. Unbalanced estrogen levels may facilitate inflammation and result in type 2 diabetes, especially after menopause, when estrogen levels are more disturbed (Monteiro *et al.*, 2014). Neurological disorders are coincident with estrogen perturbations (Ratnakumar *et al.*, 2019). Coronary artery disease in 100 women was assessed and found to be significantly increased in postmenopausal women with unbalanced estrogen levels compared to premenopausal women (Dosi *et al.*, 2014). Disruptions in the levels of certain estrogen metabolites have been associated with different diseases. Disturbances in the 16α-hydroxyestrone/2-hydroxyestrone ratio were linked to osteopenia. Higher levels of 16α-hydroxyestrone and low levels of 2-hydroxyestrone were detected in patients who suffered from decreased bone density (Lim *et al.*, 1997). It is also known that estrogens can promote breast cancer (Mufudza *et al.*, 2012). Tight regulation of estrogen metabolism is thus important in the prevention of diseases such as obesity, type 2 diabetes, and neurological and cardiovascular disorders (Monteiro *et al.*, 2014). However, perturbations in estrogen metabolism have mostly been implicated in breast cancer as outlined next.

2.2.3 The role of estrogen in breast cancer pathogenesis

Disturbances in estrogen levels (especially E2), typically seen in women after menopause, have extensively been described as a risk factor for breast cancer. A study which included over 16 000 postmenopausal women found a strong correlation between estrogen metabolites and breast cancer risk (Farhat *et al.*, 2013). It was also found that participants with breast cancer had considerably higher levels of estrones, estrone sulfates, and estradiol compared to the control group. The association of estrogen (such as estrone and estradiol) and breast cancer risk was

again confirmed in a study conducted by Sampson *et al.* (2017); see also (Dallal *et al.*, 2014). Although the exact way estrogen facilitates tumourigenesis is still uncertain, several possible mechanisms have been proposed.

The most well-known mechanism of estrogen-associated breast cancer is via estrogen receptors (ERα, ERβ and G protein-coupled receptors [GPERs]). Based on the cellular expression pattern of hormone receptors, breast cancer can be divided into two main classes: Hormone receptor positive (HR+) and hormone receptor negative (HR-) cancer. HR+ tumours can display receptors for hormones such as estrogen and progesterone. HR+ breast cancer subtypes are further described as estrogen positive (ER+), progesterone positive (PR+), or both. These types of cancer can be treated with endocrine therapy. The most prevalent breast cancer subtype is ER+ (Yersal & Barutca, 2014). In ER+ tumours, estradiol interacts strongly with the estrogen receptor (a ligand-activated transcription factor) via a hydrogen bond which causes a conformational change in the ER, resulting in the transcription of proliferation activators (Williams & Lin, 2013). This interaction of hormones on proliferation is not observed for HR- breast cancers. The HR- subtypes may include ER- and PR- and do not express receptors for the hormones to bind to (Putti *et al.*, 2005). Another type of cancer, in which too much of the human epidermal growth factor receptor 2 (HER2) is made, is referred to as HER2+ (Callahan & Hurvitz, 2011). Triple-negative breast cancer (TNBC) display a decreased expression of the HER2 protein in addition to the absence of estrogen and progesterone receptors, and is a stubborn form of breast cancer i.e. difficult to treat. This subtype does not respond to endocrine treatment (Anders & Carey, 2008). ER- tumours, therefore, do not follow the same estrogen-induced mechanism as ER+ breast cancer. ER+ breast cancer is more susceptible to endocrine treatment, which may entail the use of estrogen inhibitors, compared to ER- cancer. Tamoxifen is an example of an estrogen antagonist, owing to the fact that it is structurally similar to estrogen. Hence, competition for an ER binding site occurs between Tamoxifen and estrogen, which can barricade the effect of estrogen on proliferation (Yu & Bender, 2001). However, Tamoxifen has a lower binding affinity for the ER than estradiol and therefore endogenous estrogen levels must still be controlled (Zlotos *et al.*, 2023).

Estrogen-induced receptor-mediated tumourigenesis can also occur by means of estrogen-oncogene interaction. Estrogen was shown to activate the oncogenic nature of several genes. Proto-oncogene serine/threonine-protein kinase (PIM) is one such gene, which is implicated in multiple cancers, including breast cancer. PIM-1 promotor contains a major binding site for the estradiol-ERα complex. After the ligand-bound ER binds to estrogen response elements (ERE) on the PIM-1 promoter, the oncogene is activated to disable cell cycle inhibitors which thereby enhances cellular proliferation (Malinen *et al.*, 2013). Another prominent oncogene, c-MYC, is

regulated by estrogen in a non-promotor binding fashion. The ligand-activated ER tethers to AP-1 proteins, which in turn, binds to the c-MYC promoter, leading to its transcriptional activation (Wang *et al.*, 2011).

Over the last two decades, estrogen-receptor-independent mechanisms of cancer progression have also been identified. Ample evidence proposes estrogen-induced genotoxicity as another mechanism of inducing breast cancer. As described earlier, a disruption in the estrogen metabolic pathway can result in unbalanced levels of estrogen metabolites, such as the catechol estrogens 2-hydroxyestradiol-2,3-quinones, 4-hydroxyestradiol-3,4-quinones, 2-hydroxyestrone-2,3-quinones, and 4-hydroxyestrone-3,4 quinones. These catechol quinones have been implicated in breast cancer and the mechanisms involved are portrayed in Figure 2. Firstly, the covalent bonding of these metabolites with DNA can form depurinating adducts (Chen & Li, 2019). Fallible DNA repair mechanisms of these apurinic sites in the DNA can then result in mutations associated with increased proliferation(Torgovnick & Schumacher, 2015). Another way by which estrogen metabolites can induce mutagenicity is via the production of ROS (such as hydroxyl radicals) from the conversion of the semiquinones to quinone molecules. These hydroxyl radicals may cause damage to DNA and other biologically important molecules (Cavalieri *et al.*, 2006).

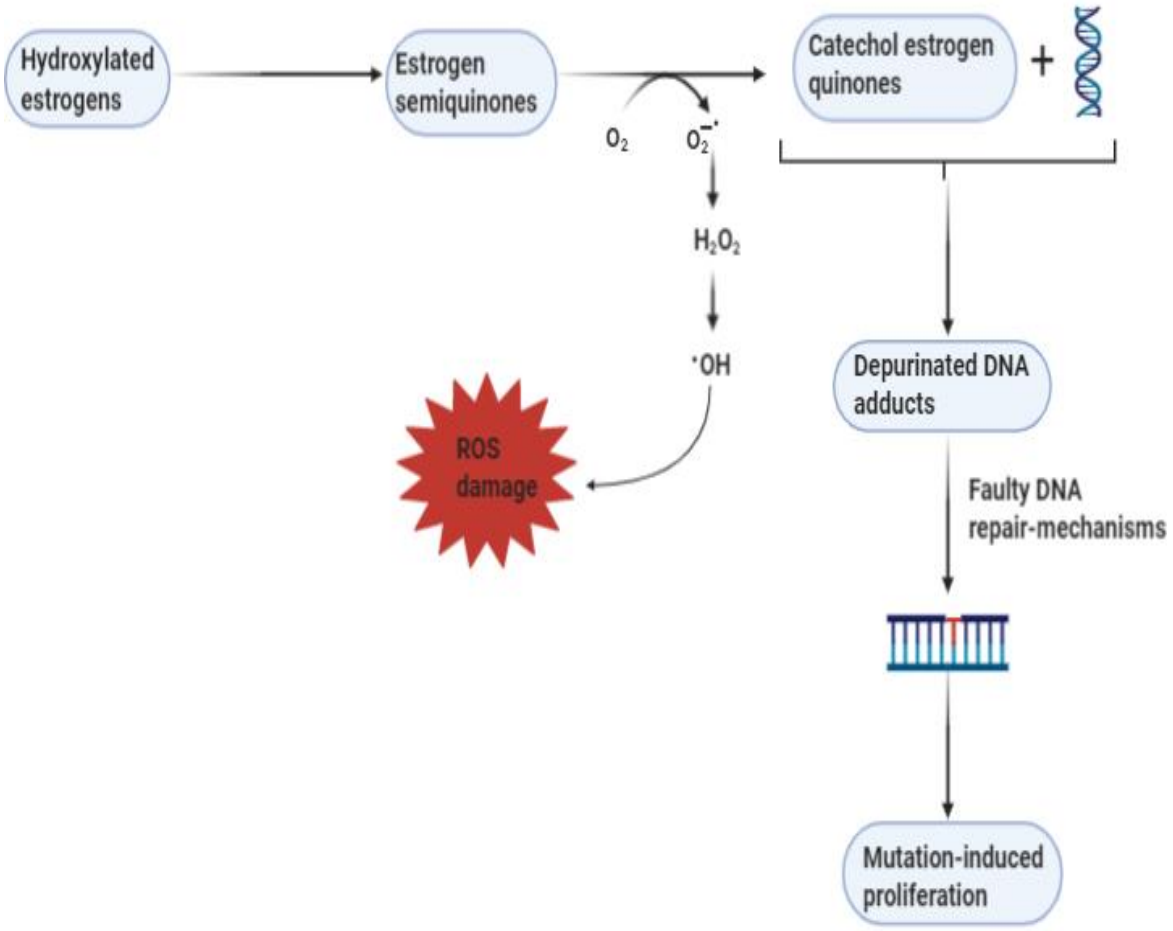

Figure 2: Schematic representation of the mechanism of catechol estrogen quinones in the initiation of breast cancer via DNA damage- Reconstructed from Cavalieri *et al*., (2006).

2.3 Macrophages: important immune cells

Élie Metchnikoff was awarded a Nobel prize in 1908 for his pioneering work in immunology. He was the first to birth the concept of phagocytosis and defined the cells which were responsible for this phenomenon as *macrophages*, i.e. “big eaters” (Epelman *et al.*, 2014). These immune cells have sparked interest among scientists owing to their versatile abilities and functions in the body ever since. First and foremost, these cells act at the frontline of the immune system and engulf and digest invasive particles that can harm the system. These cells, however, do not solely participate in phagocytosis but are involved in other biological processes as well. Macrophages are thought to participate in brain tissue regeneration by initiating apoptosis of damaged neurons and to facilitate cell signaling and angiogenesis to ensure cardiovascular health. Regeneration of damaged epithelial and muscle is another important function of macrophages. Lastly, these cells

allow optimal iron absorption by destroying damaged haemoglobins (Theret *et al.*, 2019). Seeing that macrophages have multiple roles in maintaining homeostasis and immune responses in the body, knowledge regarding the biological mechanisms of these cells remains important.

2.3.1 Macrophage polarization

Understanding macrophage origin, polarization, and metabolism may offer insight into the role and mechanisms by which these specialised cells affect immune responses and disease pathogenesis. Macrophages originate from stem cells, which are present in embryos, fetal liver, and bone marrow. These cells give rise to monocytes, which can differentiate into either dendritic cells or macrophages. These specialised phagocytes can reside in the bloodstream or tissues, or be recruited to the site of injury during an immune response and undergo polarization in order to perform their specialised functions (Corliss *et al.*, 2016). Macrophage polarization is the process of macrophage activation towards different states in response to environmental stimuli. The two outermost states of the activation spectrum are M1 and M2. However, *in vivo* macrophages exhibit complex states which can vary between these two extremes. The activation state greatly affects the phenotypic and metabolic characteristics of macrophages and determines the functional role of these cells (Parisi *et al.*, 2018).

Macrophages that display properties of the M1 type are commonly referred to as the pro-inflammatory type, since these cells produce immuno-regulatory proteins such as interferons (IFN), tumour necrosis factors (TNF), and nitric oxide synthase (NOS) enzymes, which elicit inflammatory responses. *In vitro*, external factors such as IFN-*γ* and LPS stimulate macrophages towards an M1 state. LPS endotoxin is found in bacterial membranes (Rosenfeld & Shai, 2006) which is a common inflammation inducer for *in vitro* studies. A study conducted by Zheng *et al.* (2013) also confirmed the strong influence of LPS on M1 polarization, since it was found that M2 macrophages were stimulated back to the M1 state when exposed to LPS. The molecular signaling involved in macrophage polarization was also studied. IFN-*γ* can interact with macrophages by binding to the IFN-*γ* receptor expressed by the immune cells. This activates signal transducer and activator of transcription (STAT)-1 and the consequent expression of NOS genes. LPS mediates inflammation by binding to macrophage toll-like receptors, which lead to a series of events regulated by myeloid differentiation primary response 88 (MyD88) and TIR-domain-containing adapter-inducing interferon-β (TRIF). This ultimately stimulates the secretion of nuclear factor-kappa β (NF-kβ,) IFN, and TNF which mediates inflammation (Wang *et al.*, 2014).

The M2 type macrophages differ greatly from the M1 type, in the sense that they are involved in anti-inflammatory processes via the release of cytokines such as TGF-β, arginase, and epidermal

growth factor (EGF). TGF-β decreases ROS production by inhibiting NOS enzyme activity (Bi *et al.*, 2019). Arginase is considered an anti-inflammatory agent since it is a potent inhibitor of inflammatory cytokine Th2 (Pesce *et al.*, 2009). EGF is important in cellular growth and tissue repair, but also alleviates inflammation (Choi *et al.*, 2018). Stimuli such as IL-4 and IL-13 are known to polarize macrophages towards the M2 state. IL-4 is the most common M2 stimulant and is a particularly important factor in immune and disease studies, given that this cytokine assists the differentiation of T-cells into B lymphocytes, key players in adaptive immunity. The importance of IL-4 in M2 stimulation was confirmed in a study in which it was shown that IL-4 is required for M2 macrophages to initiate tissue repair in the brain (Liu *et al.*, 2016). The activation of M2 macrophages on the molecular level can be described as follows: IL-4 binds to the IL-4α receptor expressed by macrophages and activates transcription factors which include c-MYC and STAT-6 (Wang *et al.*, 2014). C-MYC is a well-known agent in cancer research due to its upregulation in tumour cells and pro-cancer abilities. Krüppel-like factor 4 (KLF-4), expressed via STAT-6, was found to significantly decrease inflammation associated with LPS stimulation which suggests an anti-inflammatory role of this factor (Li *et al.*, 2018). It is clear that the macrophage activation state determines their functionality. In addition, macrophage activation is tightly linked with the metabolic state of these cells (Langston *et al.*, 2017).

2.3.2 Macrophage metabolism

Energy metabolism is fundamental for the functioning and survival of all cells in the body. ATP is the 'energy currency' of the cell and transports energy to cells to drive biochemical reactions. The two major metabolic pathways by which a cell produces ATP is mitochondrial oxidative phosphorylation (OXPHOS) and glycolysis. Glycolysis entails the catabolism of glucose to pyruvate and the generation of two ATP molecules per glucose molecule. The pyruvate then enters the tricarboxylic acid (TCA) cycle. Important electron carriers, NADH and $FADH_2$, are produced in this cycle. These electron carriers drive oxidative phosphorylation in the electron transport chain (ETC), located in the mitochondria. During OXPHOS, oxygen is consumed, and ADP is phosphorylated to ATP. Mitochondrial OXPHOS is the main energy producing pathway in most cells, since it produces up to 36 ATPs per cycle, which is considerably more energetically beneficial compared to glycolysis (Wang *et al.*, 2020). This is, however, not the case for all cell types. Alterations in energy metabolism are often observed for different macrophage activation states.

LPS-stimulated M1 macrophages have a distinct metabolic profile. These cells are metabolically well adapted to combating pathogens via inflammation. Great amounts of energy are required to elicit an inflammatory response; therefore, these macrophages must attune to the increased

energy demands. This is done by upregulating glycolysis, which serves as a quick source of energy. Pyruvate kinase is a key enzyme involved in glycolysis, which was found to be upregulated in M1 macrophages (Palsson-McDermott *et al.*, 2015). These cells are also highly equipped in glucose uptake since the expression of glucose transporters (GLUT) is increased. The tricarboxylic acid cycle (TCA) is shortened in these cells. This is a result of a decrease in the activity of isocitrate dehydrogenase and succinate dehydrogenase activity, with a consequent accumulation of citrate succinate. Since the TCA cycle is an important source of electron carriers (NADH and $FADH_2$) for mitochondrial OXPHOS, it is evident that the decrease in TCA activity will result in an altered OXPHOS activity as well (Geeraerts *et al.*, 2017). Citrate serves as a precursor for fatty acid (FA) synthesis and, therefore, an accumulation of this metabolite will cause an upregulation of FA anabolism in LPS-activated macrophages. FA, such as arachidonic acid is required to form prostaglandins, which can regulate inflammation (Viola *et al.*, 2019). Another metabolic adaptation which is important for M1 functioning is an increased pentose phosphate- and aspartate-arginosuccinate shunt pathway. These pathways produce NADPH, which is an important electron donor used by NADPH oxidase to produce ROS such as nitric oxide (Koo & Garg, 2019). Both inflammation and ROS production contribute to the dualistic role of M1 macrophages on disease. Although the cytotoxic abilities of this type can damage cancer cells, the same abilities can damage other non-cancerous cells in the body and is thus responsible for the onset of several auto-immune diseases such as rheumatoid arthritis (Li *et al.*, 2013).

IL-4 also notably affects the metabolic mechanisms of macrophages. M2 macrophages predominantly make use of mitochondrial OXPHOS to fulfil energy demands. Contrary to M1 macrophages certain glycolytic intermediates, for instance, fructose 2,6-biphosphate, are downregulated which leads to a decrease in glycolysis. Another key difference that is evident in M2 macrophages is an intact TCA cycle (Geeraerts *et al.*, 2017). To maintain the TCA cycle, despite a downregulated glycolysis, alternative sources are needed to drive the TCA cycle. FA can serve as an additional fuel because FA is catabolized via β-oxidation to acetyl CoA, which then enters the TCA cycle. Glutamine metabolism is another important pathway which can sustain both the TCA cycle as well as other amino acid anabolism pathways. Glutamine synthetase expression is increased in M2 macrophages, which can explain the remarkable ability of these cells to regenerate tissues, considering that amino acids are the building blocks that are required to repair damaged cells (Koo & Garg, 2019). Arginine metabolism in M2 macrophages differs from that of the M1 state in the sense that arginine is involved in M1-associated ROS production, whereas in M2 macrophages arginine is cleaved to ornithine and urea during the urea cycle. Ornithine then serves as a precursor for collagen synthesis, which is essential for the characteristic M2-associated tissue renewal (Diskin & Pålsson-McDermott, 2018). The wound-

healing, anti-inflammatory abilities of the M2 type makes these cells an intriguing treatment prospect for diseases such as diabetes, Parkinson's disease and atherosclerosis (Murray & Wynn, 2011). However, these positive attributes can also be harnessed by malignant cells. The metabolic differences between the two outermost extreme activation states again emphasises the plasticity of macrophages. Due to these cells' great plasticity, it is therefore possible that other factors such as cell type may also affect their function and metabolism.

2.3.3 Polarization and functional characteristics in different macrophage cell lines

Metabolism in macrophages has only recently emerged as a key player in regulating macrophage biology in health and disease. As a result, the number of studies about macrophages has significantly increased over the last decade. Researchers have extensively studied overall macrophage polarization, yet discrepancies in these studies make interpretation of the results somewhat difficult. Inconsistencies in culturing duration, culture medium, and especially different cell lines are often seen in studies of macrophages. This is surprising, especially since it is known that the greatest characteristic of macrophages is their functional plasticity. It is thus possible that even the slightest difference may significantly alter the functioning of these cells. Chamberlain *et al.* (2015) have aimed to emphasise the importance of considering the aptness of cell line type by highlighting the differences between macrophage cell lines. Cell shape, proliferation rate, and cytokine secretion were compared between RAW 264.7 cells and murine-derived bone-marrow derived macrophages (BMDMs). The researchers found that a clear distinction could be made between the two cell lines based on morphology. This difference is biologically important since it is known that cell size and shape can affect aspects such as the rate of oxygen consumption (Wagner *et al.*, 2011). Another finding was the increased proliferation rate of the RAW 264.7 cells compared to the BMDMs. Cytokine expression analyses after M2 stimulation revealed IL-6 expression in BMDMs, whereas TNF was detected in RAW 264.7, which is interesting since TNF is a pro-inflammatory cytokine, this can suggest a difference in the degree of polarisation between different cell lines (Chamberlain *et al.*, 2015). Dissimilarities in functional responses were also observed between the above-mentioned cell lines. Work by Levenson *et al.* (2018) showed that BMDMs are more efficient in responding to viral infections compared to RAW 264.7. After viral infection BMDMs swiftly upregulated TNF expression, whereas the rate of TNF secretion was significantly reduced in RAW 264.7 cells. The latter also displayed decreased lipid synthesis in comparison to BMDMs.

Differences in polarization markers between THP-1 (a model for human monocytes) cells and human monocyte-derived macrophages (hMDMs) were also reported (Tedesco *et al.*, 2018). M1-stimulated hMDMs showed significant increases in interleukin 6 (IL-6), toll-like receptor (TLR)-2

and hypoxia-inducible factor 1-alpha (HIF-α), whereas M1-activated THP-1 showed a significant increase in monocyte chemoattractant protein (MCP)-1 expression. After M2 stimulation, hMDMs displayed a significant increase in peroxisome proliferator-activated receptor gamma (PPAR)-γ compared to THP-1 cells. The researchers further analysed phagocytosis ability after polarization between the two cell lines. Although M2-activated THP-1 cells were still capable of phagocytosis, they found that phagocytosis in M2-activated THP-1 cells was considerably compromised as opposed to hMDMs. The authors concluded that immortalised cell lines, such as THP-1, may not always be suitable for all macrophage-related studies due to the significant differences in some of the polarization markers.

Seeing that there can be great differences between immortalised cell lines and primary cells, it is possible that there may be differences in macrophages from different species as well. Similarities between human and murine macrophage cell lines were reviewed and although the authors agreed that there is homogeneity between the species, they also emphasised that there are dissimilarities as well. Certain genes such as NOS genes are highly expressed in murine cells but to a much lower extent in human cell lines, and expression of other genes such as STAT-4 genes is increased in human models (Reynolds & Haniffa, 2015) compared to murine cells. Some studies (e.g. that of Rodríguez-Prados *et al.* (2010)) have assessed metabolic differences between peritoneal macrophages and RAW 264.7 cells. The authors observed a higher metabolic flux (including the pentose phosphate pathway) in RAW 264.7 cells compared to peritoneal macrophages. although information about this is still scarce. These findings, therefore, suggest that the choice of cell type may affect study outcomes with regard to polarization, metabolism, and function, and that it is important to compare findings between different cell types to obtain a complete picture of macrophage biology.

2.3.4 The effect of glucose concentration on macrophage polarization and metabolism

Extracellular glucose concentration is another aspect that should be considered when designing a macrophage study. There is often large variability in the culturing conditions applied in macrophage studies. Different types of culturing medium are used that vary in composition, especially regarding the glucose concentration in each medium (varying from 5 mM to 11 mM and even up to 25 mM glucose). This is surprising, firstly because the use of high glucose medium may not be physiologically relevant because the normal physiological blood glucose concentration in humans ranges between 3.5 mM and 5.5 mM, and for mice, it can range between 4 mM and 6 mM (Güemes *et al.*, 2016). Secondly, macrophage polarization and metabolism may be greatly influenced by glucose levels. A study conducted by Freemerman *et al.* (2014) reported that macrophages treated with high glucose levels displayed an M1-like phenotype. Thapa and

Lee (2019) also stated that high glucose induces pro-inflammatory macrophage activation as well as an increase in the glycolytic activity in these cells. However, long-term exposure to high glucose levels also appeared to hamper glycolysis. Pavlou *et al.* (2018) showed that long-term high glucose treatments led to an upregulation of cytokines such as TNF-α and a decrease in NOS levels in LPS-activated (M1) BMDMs, and an increase in arginase gene expression. Research by Ayala *et al.* (2019) verified the decrease in NOS levels observed in LPS-stimulated BMDMs after treatment with high glucose. They further observed that increased glucose levels considerably decreased TLR-4 expression and upregulated lactate production. Contrary to BMDMs, high glucose concentrations did not affect TLR-4 production in THP-1 cells (Grosick *et al.*, 2018), which suggests that the macrophage function is not just affected by single factors but rather by the contribution of various different factors (e.g., glucose concentration and cell type, etc.). In addition to alterations in polarization and glycolysis activity, glucose levels were found to impact other metabolic pathways as well. Kaplan *et al.* (2008) demonstrated that upon exposure to high levels of glucose, cholesterol anabolism in macrophages was increased. Considering the large impact that medium glucose concentration may have on macrophage function and phenotypes, it is necessary to carefully consider experimental conditions when investigating macrophage biology and the effect of certain stimuli (e.g. estrogen).

2.3.5 The role of macrophages in breast cancer pathogenesis

The involvement of macrophages in breast cancer and the association of macrophage infiltration with a bad prognosis, has convincingly been demonstrated before (Belgiovine *et al.*, 2020). Breast and lymph tissue-resident macrophages and recruited macrophages can gain entry into tumour-associated tissue via high endothelial venules, direct interaction, or in response to macrophage migration inhibitory factor (MIF) secreted by mural cells which outline the endothelial capillaries (Corliss *et al.*, 2016). TAMs play an important role in tumourigenesis: they are able to constantly alter their functional characteristics, and thereby exert different effects on the tumour cell depending on the activation state (Anfray *et al.*, 2020).

2.3.5.1 M1 macrophages and breast cancer

As previously mentioned, the M1 TAMs are known to have a tumouritoxic effect. These cells are functionally and metabolically well adapted in their role as biological guardians against infections and cancer. The M1 state can decrease tumourigenicity via multiple mechanisms. The phagocytic ability of macrophages is the most renowned mechanism for tumour clearance. In a study that compared phagocytic efficiency between M0 (unpolarized), M1, and M2 types, polarized macrophages (M1 and M2) displayed significantly increased phagocytic activity compared to the M0 type. Furthermore, the M1 macrophages displayed a more efficient phagocytosis capability

compared to the M2 type (Lam *et al.*, 2016). Phagocytosis of tumours occurs after the attachment of macrophages to the tumour cell, which can be mediated via receptors expressed by macrophages or the recruitment of antibodies. According to Pahl *et al.* (2014), macrophages express several receptors which are important in recognizing particles and cells to be phagocytosed, including Fcγ receptors (Cluster of differentiation [CD] 16, CD32 and CD64) and signaling lymphocyte activation molecules (SLAM). The identification of tumours that originate in the blood and lymph tissue by macrophages is facilitated by SLAM (Marcus *et al.*, 2014). Since breast tissue extends to the lymph nodes, this is an important receptor for breast tumour recognition as well. Cancer cells can, however, circumvent this direct type of phagocytosis since they express CD47 which binds to the macrophage signal regulatory proteins (SIRP)-α. This interaction inhibits macrophage-induced phagocytosis (Chen *et al.*, 2019). Antibody-mediated phagocytosis can then serve as an important alternative to remove tumours. For instance, antibodies impede the anti-phagocytic strategies of tumours by enabling macrophages to recognize tumours without direct contact. The paratope of the antibody binds to the antigen presented by the tumour and the Fc tail of the antibody binds to the Fcγ receptors on the macrophage (Gül & van Egmond, 2015), after which the tumour cell can be engulfed by the macrophage. Besides phagocytosis, the M1 type can initiate the destruction of cancer cells by eliciting an inflammatory response. This enables vasodilation and increases the transport efficiency of other immune cells, such as T-cells, to the TME (Harrison *et al.*, 2011). T-cells may also be directly recruited to the tumourigenic site by secretion of M1 cytokines (Boutilier & Elsawa, 2021). Continuous inflammation is known to initiate DNA damage which can cause tumour dysfunction and ultimate apoptosis (Ioannidou *et al.*, 2016). The production of free radicals is another mechanism by which these cells can cause mutagenesis. Nitric oxide is an example of an extremely reactive free radical which damages DNA via oxidation, deamination, and inhibition of DNA synthesising enzymes (Burney *et al.*, 1999). A study on the antitumour role of macrophages indicated that proteases and chitinases produced by M1 macrophages caused tumour lysis after just 24 hours, and that this lysis was tumour specific as non-cancerous cells were not damaged (Pan, 2012). Furthermore, Jarosz-Biej *et al.* (2018) showed that stimulation of TAMs towards an M1 phenotype markedly reduced the deformity of tumour blood vessel structure, and that the combination of M1 stimulation and treatment with the chemotherapeutic drug doxorubicin showed a significant decrease in tumour progression. These studies point to the potential therapeutic use of M1 macrophage activation alongside existing therapy, e.g. chemotherapy.

2.3.5.2 M2 macrophages and breast cancer

In contrast to pro-inflammatory macrophages, the M2 type macrophage is known to be pro-tumourigenic and tumours may calamitously take advantage of the pro-tumourigenic properties of M2 macrophages (Boutilier & Elsawa, 2021). The secretion of a macrophage colony-stimulating factor (MCSF) which interacts with a colony-stimulating factor-1 (CSF-1) receptor expressed by macrophages, enables the cancer cell to stimulate macrophage polarization towards the M2 type, and thereby profit from its several proliferative abilities (Lu *et al.*, 2019). The M2 cells secrete cytokines and growth factors which boost the tumour's blood vessel and collagen formation (Shrivastava & Shukla, 2019), and enhance oxygen supply and tissue regeneration (Trenti *et al.*, 2018). Tumour cell angiogenesis is mediated by M2 macrophages in several ways. The first and foremost mechanism by which the M2 type stimulates blood vessel formation is via the expression of angiopoietin receptors as well as the release of vascular endothelial growth factor (VEGF), which is responsible for tumour-associated vascular endothelial growth, as well as matrix metalloproteinases (MMP) enzymes which cause proteolysis of extracellular matrix (ECM) proteins and allows reformation of the ECM (Anfray *et al.*, 2020). Another course of action by which angiogenesis is stimulated is by the expansion of arterial vessels via the secretion of VEGF. This blood vessel development delivers oxygen supplies, tissue building blocks, and other reparative cells (such as fibroblasts) to the tumour. Angiogenesis can promote the infiltrative abilities of cancer cells and allow optimal invasion into surrounding tissue (Argyle & Kitamura, 2018). Phagocytosis may be employed in this regard to remove any damaged tissue before new blood vessel formation can occur. The stunted healing of injured tissue in the absence of M2 macrophages emphasises the necessity of these cells in collagen formation and tissue restoration (Aitcheson *et al.*, 2021). As already mentioned, the M2 type can produce significant amounts of collagen, which can maintain the structural integrity of the cancer cell and is required in the formation of new tissue (Rømer *et al.*, 2021). An additional important requirement for tissue development is M2-related growth cytokines which enhance cell division of endothelial cells and other cells that make up the capillaries and venules (Minutti *et al.*, 2017). Furthermore, the presence of M2 TAMs protects the tumour from immune responses. Prostaglandin E2 (PGE2) TGF-β, and IL-10 which are upregulated by M2 cells, inhibit immune responses such as those elicited by T-cells. It is, therefore, feasible that M2 macrophages may impede cancer-induced immune retaliation (Hirayama *et al.*, 2018). A study on tumour invasion in TNBC cell lines conducted by Little *et al.* (2019) found that upon IL-4 treatment and subsequent M2 activation, a significant increase in tumour migration was induced. The researchers discovered that higher VEGF levels secreted by the M2 macrophages directly correlated with migration efficiency and concluded that the secretion of VEGF and its promotion of cancer migration may be another way

by which M2 TAMs assist cancer growth. As already described, the oncogene c-MYC is upregulated in tumour cells and is partly responsible for the fast division of cancer cells. This oncogene was found to be highly expressed in mouse M2-activated macrophages, and may be another way in which these macrophages induce proliferation (Jablonski *et al.*, 2015). The abundance of c-MYC in M2 macrophages is of particular interest since it was found that c-MYC significantly enhances efferocytosis of M2 BMDMs (Zhong *et al.*, 2018). Efferocytosis is the process in which damaged cells that underwent apoptosis are removed by M2 macrophages. Under normal circumstances, this is a mechanism by which M1 macrophage numbers are decreased and M2 macrophages are recruited to resolve the inflammatory response and revert physiological conditions back to normal. However, this process contributes to cancer progression as tumour cells may take advantage of the regression of inflammation in order to circumvent M1 activity and survive (Werfel & Cook, 2018).

A remaining challenge in designing anticancer therapies is the resistance of tumours to existing treatments which include chemotherapy, endocrine therapy, and radiotherapy. M2 macrophages may act as accomplices in obstinate cancers: M2 TAMs typically reduce chemotherapy efficiency by inhibiting apoptotic pathways in tumours. Another example of M2-mediated chemo resistance is the interference with the action of cisplatin (a DNA alkylating chemo drug) by modulation of the PI3/Akt pathway which suppresses anti-tumour p53 activity (Larionova *et al.*, 2019). Tamoxifen, an anti-estrogen drug, is often used as a viable hormone therapy option, yet Tamoxifen-resistant cancers still remain problematic. Xuan *et al.* (2014) investigated the possible involvement of M2 macrophages in Tamoxifen resistance and cancer severity using immunohistochemical staining and found that CD163+ (M2) macrophage numbers of Tamoxifen resistant cells were considerably higher compared to the non-resistant cells. The researchers also found an increase in the EGF receptor levels in the resistant tissue and concluded that M2 macrophages may assist Tamoxifen resistance via the secretion of EGF. Activation of M2 macrophages may also play a role in the promotion of cancer migration after radiotherapy (Pinto *et al.* (2016). Finally, M2 TAMs appear to be involved in cancer stem cell (CSC) development (therefore in the initiation of tumour formation) through upregulation of the STAT-3 signaling pathway which mediates cell growth and division (Aramini *et al.*, 2021).

2.3.5.3 The clinical value of assessing M1/M2 ratio in breast cancer

When considering the role macrophages play in cancer and other diseases, it becomes apparent that regulation of macrophage activation is necessary to maintain homeostasis and avoid disease. Each macrophage type has a distinct role in the body and both pro-inflammatory and anti-inflammatory macrophages are required to maintain homeostasis. For eg. pro-inflammatory

macrophages are involved in the inflammatory response to destroy pathogens, whereas anti-inflammatory macrophages resolve the inflammatory response and is involved in repairing damaged tissue (Redka *et al.*, 2018).Under normal physiological conditions, the ratio of M1 and M2 macrophages in the body is tightly controlled. However, in diseases such as cancer a disruption in this equilibrium is often observed. A study on the role of macrophage balance in the onset and prognosis of ovarian cancer progression revealed that TAM density was increased in more severe, malignant cancers (Colvin, 2014). A direct correlation between a lower M1/M2 ratio and the severity of cancer progression was also found since a higher amount of M1 TAM was linked to a better long-term prognosis for the patients (Zhang *et al.*, 2014). In another study by Fadhil *et al.* (2019), the number of infiltrating TAMs was significantly higher in breast cancer patients as opposed to the healthy control groups. It was further found that the ratio of M2 to M1 TAMs of the non-malignant cancer group was significantly higher compared to the control group and that the malignant tumour group displayed an even higher M2/M1 ratio than the benign cancer group. Finally, a higher M2/M1 ratio is also correlated with increased resistance to chemotherapy treatments by means of evading induced cell death via activating the STAT-3 and IL-10 pathways (Parisi *et al.*, 2018). Regulation of the M1/M2 ratio thus plays a critical role in cancer development and severity.

2.3.5.4 The role of MAMs in breast cancer

In addition to the influence of TAMs on breast cancer progression, another key player that must be taken into consideration is a subgroup of TAMs that is directly involved in metastasis. These macrophages are known as metastasis-associated macrophages (MAMs) (Doak *et al.*, 2018). Metastasis occurs when a tumour cell spreads from the original site to other distant areas in the body. It is characteristic of the advanced stages of cancer and is typically the principal cause of mortality. The main steps of the metastatic cascade are as follows (Qian & Pollard, 2012): (1) The tumourous cells must first infiltrate the basement membrane (invasion), (2) after which single or small clusters of tumour cells are released into circulation (intravasation). (3) The tumour cells proliferate while being transported through the bloodstream to distant tissue (survival). (4) The cells then exit the bloodstream into tissue (extravasation), where cell division proceeds. MAMs (typically displaying M2-like properties) were found to be involved in various steps of the metastatic state and even suggested to play a key role in cancer morbidity (Boutilier & Elsawa, 2021). At the site of origin, the tumour is surrounded by TAMs and bombarded with other immune cells. The tumour circumvents the immune responses by initiating the metastatic cascade and in essence escapes by entering the bloodstream and migrating to another location, referred to as the metastatic site. MAMs are recruited to the metastatic site by tumour-induced secretion of C–C motif chemokine ligand 2 (CCL2) cytokines, where these cells promote tumour survival and

metastasis in several ways. Firstly, MAMs enable extravasation by releasing the angiogenic VEGF, which also allows cell growth and division in the new site. Much like M2 TAMs, the MAMs contribute to cancer survival by inhibiting apoptosis and other immune responses (Argyle & Kitamura, 2018). Secondly, MAMs can support tumour survival via the expression of *α*4-integrins which can bind to a tumour vascular cell-adhesion molecule (VCAM)-1, and activate the PI3/Akt signaling pathway (Nielsen & Schmid, 2017). Lastly, MAMs' involvement in stimulating myofibroblasts is also an interesting topic in cancer metastasis research since these cells are involved in the production of ECM proteins. MAMs produce considerable amounts of granulin proteins which activate myofibroblast ECM proteins, which in turn, are used during clonal expansion of the tumour cell. A study by Nielsen and Schmid (2017) showed that exhaustion of granulins decreased the proliferation and metastasis of liver tumour cells. This MAM-associated granulin production was also observed in breast cancer and high granulin levels were linked to a poor prognosis (Elkabets *et al.*, 2011). Taken together it is evident that macrophages contribute to the pathogenesis of breast cancer. Even though multiple possible mechanisms of contribution have been proposed, there is still a great deal of information with respect to macrophages and their involvement in breast cancer that is still not fully explored.

2.4 The link between estrogen and macrophages in breast cancer

It has become increasingly apparent that breast cancer is a multifactorial disease and cannot be attributed to one factor alone. Tumourigenicity rather originates because of the complex intertwinement and interaction of several genetic, environmental, and other non-genetic components. Considering this together with the fact that estrogen-responsive mammary tissue is relatively densely populated with macrophages (Anfray *et al.*, 2020), it is important to consider the interplay between estrogen and macrophages in the onset and/or progression of breast cancer.

2.4.1 ER expression and signaling in macrophages

The TME is an ideal environment for interaction between estrogen and macrophages via the transduction of signals and estrogen receptors. Molecules in the TME play crucial roles in cell signaling of which galectin is one such signaling molecule that can allow estrogen-macrophage associations. Galectin is described as an important cell signaling molecule in the TME. These proteins are expressed in both cancer cells and immune cells where it exerts pro-proliferative functions (Sundblad *et al.*, 2013). Estrogen was proposed as a possible inducer of galectin-3 in proliferative endometrial cells (Yang *et al.*, 2016). Galectin-1 and galectin-3 then bind to CD4, a glycoprotein expressed by immune cells such as T-cells and macrophages which thereby facilitates tumour evasion from these immune cells (Gál *et al.*, 2017). Estrogen-macrophage

signaling can also be accomplished by membrane-initiated steroid signaling (MISS). This signaling results in the regulation of the PI3/Akt pathway, which is known to modulate macrophage polarization (Kovats, 2015).

Although the various ER-independent pathways are involved in mediating estrogen-macrophage signaling, estrogen receptors still have a prime involvement because most of the estrogenic activity is mediated by ERs (Bolego *et al.*, 2013). Direct interactivity between estrogen and macrophages is enabled by the estrogen receptors which are expressed by macrophages. Estrogen can bind to ERα or ERβ or GPER-1 on macrophages which results in alterations in chromatin conformation and transcriptional modifications (Bolego *et al.*, 2013). Although these receptors are very similar and exhibit specificity for estrogen, there are some differences in terms of location, function, and estrogen affinity. ERα is prominent in reproductive organs, the liver, and breast tissue (Lee *et al.*, 2012). Studies have suggested that this receptor is biologically the most active receptor since the absence of the ERα results in various disturbances which may include low insulin sensitivity and increased inflammation (Trenti *et al.*, 2018). ERα is also of particular importance because E2, which is involved in most biological processes preferentially binds to this receptor (Barkhem *et al.*, 1998). This is notable since ERα is the most abundant estrogen receptor expressed by macrophages, which may suggest a strong interaction of estrogens (such as E2) with macrophages. Moreover, it was proven that *in vivo* estrogen treatment results in increased ERα expression in macrophages (Trenti *et al.*, 2018).

2.4.2 The effect of estrogen on macrophage polarization

Estrogen has been shown to regulate macrophage polarization by an estrogen receptor-mediated mechanism (Keselman *et al.*, 2017). This was illustrated by the absence of polarization markers in macrophages *in vitro* after the addition of an ER antagonist (Villa *et al.*, 2015). M2 polarization markers in both female and male mice were investigated in response to different *in vivo* and *in vitro* stimuli, which included estrogen treatment. The main findings were that estrogen stimulated macrophage activation towards an anti-inflammatory M2 state. Female mice also displayed more M2 macrophages compared to male mice, which also expressed a larger amount of ERα. Another interesting discovery was the significant reduction in M2 markers after ERα inhibition using a ERα-deficient mouse model, which led the authors to propose ERα as the major receptor involved in M2 polarization (Keselman *et al.*, 2017). Activation of ERα increases the expression of macrophage TLRs. This is accomplished via the binding of ERα to ERE on TLR genes (Cunningham *et al.*, 2014). Despite the prevalence of Erα, ERβ may also play a significant role in estrogen-macrophage signaling. ERβ is present in the reproductive organs, brain, and bone-marrow (Lee *et al.*, 2012). Unlike estradiol, most phytoestrogens such as 16-epiestriol, and 17-

epistriol show a predilection towards ERβ (Barkhem *et al.*, 1998)**.** Contrary to ERα, estrogen levels do not seem to upregulate the expression of macrophage ERβ. It is also important to note that ERβ is considerably downregulated in females who use oral contraceptives (Millas *et al.*, 2011). This may suggest that estrogen in birth control pills may cause a decrease in ERβ, although more studies are needed to confirm this. Despite limited research, though, it was shown that ERβ inhibits immune responses by decreasing CD16 and TNF-α, which is a characteristic that is consistent with M2 polarization (Bolego *et al.*, 2013). Experiments on ERα and ERβ knockout mice revealed that estrogenic effects on the cardiovascular system was still intact. This implied that another receptor had to be involved in binding and regulating estrogen in the body. The plasma membrane receptor GPER-1 was only recently studied in depth and was shown to facilitate estrogenic activity in various parts of the body including the heart, brain, muscles, and reproductive organs. This receptor was also described as exerting anti-inflammatory effects in murine macrophages when activated by estrogen (Zimmerman *et al.*, 2016). It was demonstrated that the binding of estrogen to murine macrophage GPER-1 reduced TLR-4, which decreases LPS-induced inflammation (Rettew *et al.*, 2010). This is consistent with the anti-inflammatory characteristics of the M2 type. It is also possible that GPER-1 is an important receptor in maintaining balance during estrogen-macrophage signaling since it may act in a feedback inhibition mechanism and decrease ERα expression by triggering the mitogen-activated protein kinase (MAPK) pathway (Bolego *et al.*, 2013).

The interaction between estrogen and macrophages via estrogen receptors can signal certain pathways involved in various processes including adhesion, chemotaxis, and polarization. 17-β-estradiol reduced the adhesion abilities of macrophages by decreasing Rac-1, an important GTPase which is involved in maintaining structural integrity and support (Friedrich *et al.*, 2006). The chemotactic abilities of macrophages are diminished by the estrogen-induced reduction of MCP-1 (Frazier-Jessen & Kovacs, 1995). The effect of estrogen on macrophage polarization has been extensively studied but remains controversial. Estrogen treatment has been linked to anti-inflammatory M2 polarization, which was further reported to inhibit several immune-related cytokines (Campbell *et al.*, 2014). However, there are inconsistencies regarding this as some studies suggest an increase in factors such as TNF-γ*,* which elicits inflammatory responses (Bolego *et al.*, 2013). An investigation of the effect of E2 on joint inflammation indicated that estrogen treatment increased the number of M1 macrophages and M1-linked nitric oxide production (Kou *et al.*, 2015). The phenomenon that females are more prone to developing autoimmune diseases (typically characterised by high inflammation) implies that estrogen is a key initiator of uncontrolled inflammation. It is then plausible that the action of estrogen in immunity and inflammation is contradictory and much more complex than once thought.

2.4.3 The effect of estrogen on macrophage metabolism

General energy homeostasis and metabolism are tightly controlled by hormones, including estrogens (Mauvais-Jarvis *et al.*, 2013). The necessity of this estrogen-regulated balance is especially observed in postmenopausal women. Imbalances in estrogen levels that occur after menopause result in a significant increase in visceral adipose tissue (Feigelson *et al.*, 2004). This phenomenon was also observed in murine models. ER-knockout female mice displayed a higher food consumption, reduced ability to burn energy, and greater fat percentage compared to mice that had sufficient estrogen activity. This may be due to the fact that estrogen reduces FA and lipid biosynthesis by decreasing FA synthase and lipoprotein lipase, respectively (Mauvais-Jarvis *et al.*, 2013). Glucose metabolism may also be altered by circulating estrogens. Impaired estrogenic activity (via ERα) causes low insulin sensitivity and impedes glucose metabolism. Studies on Erα-knockout mice indicate a direct correlation between ERα levels and GLUT-4 expression (Barros *et al.*, 2009). The opposite is true for ERβ for which increased levels are linked to the downregulation of GLUT-4 (Gupte *et al.*, 2015). A study conducted on female rats indicated that estrogen plays a role in amino acid metabolism too. The main finding was that branched-chain α-keto acid dehydrogenase complex (BCKDC) was increased and branched-chain α-keto acid dehydrogenase kinase (BDK) was decreased post ovariectomization, and that E2 treatment replenished levels back to normal (Obayashi *et al.*, 2004). Although the information about the effect of estrogen on macrophage metabolism is limited, estrogen may indeed have a significant role in regulating macrophage metabolism since estrogen has an impact on metabolism in general. Estrogen is known to affect lipoprotein metabolism in macrophages by decreasing low-density lipoprotein absorption and ultimately inhibiting cholesterol build-up (Sulistiyani, 1997). The influence of estrogen on other metabolic pathways in macrophages, however, is not well studied. In a pilot study on BMDMs by our group, estrogen's effect on macrophage metabolism appeared to be more complex and co-regulated by other factors. BMDMs that were treated with E2 tended to exhibit mitochondrial OXPHOS and glycolytic activity similar to IL-4-treated BMDMs, although different medium glucose concentrations seemed to influence the effect of estrogen on cellular metabolism. Better controlled assays are therefore required to verify the effect of estrogen on pathways such as glycolysis and mitochondrial oxidative phosphorylation, and to fill the gaps in the knowledge regarding estrogen metabolism in macrophages.

2.4.4 Estrogen metabolism in macrophages

Macrophages possess aromatase enzymes, which can produce estradiol and estrone from testosterone and androstenedione respectively. The aromatase enzyme is important since it is the rate-limiting step in estrogen anabolism (Au *et al.*, 2017). Expression analyses conducted by

Mor *et al.* (1998) demonstrated that breast tissue-resident macrophages, as well as monocytes and THP-1 cells (once differentiated into macrophages), produce a considerable amount of aromatase enzymes. The estrogen production of these cell lines was found to be sufficient to enhance cell division in breast tumour cell line MCF-7. Another intriguing finding from this study was that tumour proliferation was suppressed by the incubation of THP-1 macrophages with aromatase antagonists.

Some evidence of other estrogen-metabolizing enzymes in macrophages has been reported. Baron *et al.* (1998) analysed the expression of the cytochrome P450 (CYP) enzyme family in human blood macrophages. Several CYPs were found to be expressed, which included CYP1A1, CYP3A4, and particularly CYP1B1 (the major CYPs involved in estrogen metabolism). COMT enzymes which convert 4-hydroxyestradiol and 2-hydroxyestradiol to their methoxy derivatives were reported to be expressed in macrophages, found in the intestines (Myöhänen *et al.*, 2010). In addition, peroxidase, which converts 4-hydroxyestradiol and 2-hydroxyestradiol to their respective semiquinone metabolites was found to be active in both blood and bone marrow-derived macrophages (Deimann, 1984). Evidence of estrogen biosynthesis in macrophages was confirmed. Monocyte-derived macrophages were incubated with radiolabelled DHEA and low levels of E1 and E2 and higher levels of E3 were detected (Schmidt *et al.*, 2000).

The estrogen metabolites produced by macrophages may have an intracrine or autocrine effect, or may be secreted into the extracellular environment and have a paracrine effect on other neighboring cells' metabolism and functionality (Rubinow, 2018; Schmidt *et al.*, 2000). As already described, estrogen metabolites, in particular catechol estrogens such as 2-hydroxyestradiol and 4-hydroxyestradiol, induce DNA mutations and thereby tumourigenesis. In terms of mutagenic potency, estradiol and 4-hydroxyestradiol were implicated as the major cause of mutations and tumour formation (Khan & Khan, 2013). On the other hand, 2-hydroxyestradiol was found to be tumourigenic only at extremely high doses. Some studies have even recorded an anti-proliferative effect of moderate concentrations of 2-hydroxylated estrogens (Seeger *et al.*, 2006). The levels of 4-hydroxyestradiol metabolites have been reported to be higher in the urine and breast tissue of breast cancer patients compared to healthy women (Park, 2018). It is, however, not known to what extent macrophages contribute to the production and secretion of these metabolites in the breast tissue. This may, in turn, be dependent on the macrophage polarization state. However, no information is available about estrogen metabolism in different macrophage cell lines and activation states.

2.4.5 Macrophage-mediated regulation of estrogen metabolism in the TME

Although estrogen influences macrophage biology in several ways, several studies have indicated that the opposite is also true: macrophages can regulate estrogen signaling and metabolism in other cells. M1-activated macrophages were shown to secrete ROS such as H_20_2 which can upregulate ERβ expression in MCF-breast cancer cells (Tamir *et al.*, 2002). TNF is another factor secreted by M1 macrophages, and has been shown to regulate estrogen metabolism in MCF-7 breast tumour cells (Kamel *et al.*, 2012). TNF-α treatment in these cells increased the levels of estrogen and estrogen metabolites 4-hydroxyestradiol, 2-hydroxyestradiol, and DNA adducts. This was accompanied by a decrease in COMT, the E1/E2 ratio, as well as 2-methoxyestradiol levels. The M2 cytokine IL-6 was, in turn, found to decrease estrogen biosynthesis in human follicular tumour cells via a MAPK-dependent mechanism (Deura *et al.*, 2005). Besides the influence that macrophages can have on estrogen metabolism via the secretion of certain cytokines, macrophages themselves also express enzymes involved in estrogen biosynthesis and metabolism. However, only a few studies have been published on this (Au *et al.*, 2017; Baron *et al.*, 1998; Deimann, 1984; Mor *et al.*, 1998; Myöhänen *et al.*, 2010).

2.5 Estrogen and macrophages as a therapeutic tool

Early stages of breast cancer are treatable with surgery, chemotherapy, and radiotherapy. However, numerous side-effects often coincide with these treatments (Beisecker *et al.*, 1997). Moreover, metastatic tumours and cancer recurrence still pose a problem. Endocrine therapy is a viable option in the treatment of HR+ breast cancers, yet it is not effective for HR- tumours (Podo *et al.*, 2010). Innovative strategies are therefore still required for the optimal treatment of all breast cancer stages and types. The TME is a ‘hot topic’ in cancer therapy research. It is a complex network of interactions that constantly affect the tumour’s sustainability. By manipulating conditions in the TME, tumour survival may be crippled. For example, a low TME pH is typically consistent with a poor prognosis and alkaline treatments have proven valuable in limiting cancer severity (Falcone *et al.*, 2016). Another feasible approach may be hyperbaric oxygen treatment to slow cancer progression (Moen & Stuhr, 2012). Since metabolism is central to normal cellular function, manipulation thereof may be a viable approach to alter tumour function and survival. Diet adaptations and glycolytic intermediate inhibitors have proven to be successful in reducing the proliferation rate of cancer cells (Netea-Maier *et al.*, 2018). Furthermore, suppressing tumour glycolytic activity and lactic acid production in the TME conditions may become favourable for the recruitment of anti-tumour macrophages (de la Cruz-López *et al.*, 2019).

The macrophage-estrogen axis remains an unexplored target area for the treatment of obstinate breast tumours. Suppression of estrogen production and metabolism may assist in reducing

carcinogenic estrogen metabolites. Several treatments can accomplish this. The use of aromatase antagonists such as Megestrol and selective ER modulators such as Tamoxifen are often used as a therapy for breast cancer. These antagonists could block estrogen production by competing for an aromatase binding site, resulting in testosterone and androstenedione not being converted to estrogen metabolites (Santen & Harvey, 1999). The reduction in estrogen levels may, in turn, limit the recruitment of pro-tumour M2 macrophages. The direction of the immune system against cancer has proven effective in combating skin melanoma (Rosenberg & Restifo, 2015), and the employment of macrophage-targeted therapies in breast cancer may also be possible in the near future. Preclinical studies have proven that the limitation of macrophages in the TME via the use of monoclonal antibodies, as well as hindering macrophage recruitment and transport are associated with decreased cancer severity (Poh & Ernst, 2018). Advancements in nanotechnology can optimise the manipulation of macrophage polarization and metabolism by controlling factors such as IL-4, LPS, and E2 as well as targeting metabolic pathways (which include glycolysis, OXPHOS, and estrogen metabolism) to limit pro-cancer M2 TAMs and increase the number of tumouritoxic M1 TAMs (Reichel *et al.*, 2019).

2.6 Problem statement

Macrophages play a fundamental role in the pathophysiology of breast cancer and are, therefore, viable cancer prevention and treatment targets. However, it is essential to understand the fundamental biology and metabolic mechanisms of these cells before it can be used in the development of new cancer prevention and treatment approaches. Estrogen metabolism has been implicated in the pathogenesis of breast (and other) cancers. Although much has been done to characterise macrophage metabolism and the effect of estrogen on macrophage activation, information regarding the effect of estrogen on pro- and anti-inflammatory macrophage bioenergetics is still lacking, as well as a thorough understanding of estrogen metabolism in macrophages. These gaps need to be addressed since estrogen, estrogen metabolism, as well as its effect on macrophage metabolism, are important factors that need to be considered when studying breast cancer.

2.7 Aim and Objectives

The main aim of this study is to assess bio-energetic and estrogen metabolism of pro- and anti-inflammatory macrophages (using RAW 264.7, THP-1, and mouse BMDM cell lines) in the presence of 17-β-estradiol. This will be accomplished by the following objectives:

1. Aseptically isolate mouse bone marrow cells and differentiate them into macrophages.
2. Optimise THP-1 cell differentiation protocol.

3. Determine optimal glucose concentration for *in vitro* metabolic studies of macrophages.
4. Determine the effect of estrogen on the metabolism of pro- and anti-inflammatory macrophages with bio-energetics analyses.
5. Collect medium from estrogen-treated pro- and anti-inflammatory macrophages and perform solid phase extraction (SPE) and LC-MS/MS (liquid chromatography tandem mass spectrometry) analysis of estrogen metabolites in culture medium.
6. Statistical analyses, metabolite comparison between different cell lines and activation states and biological interpretation (estrogen metabolism comparison).

CHAPTER 3

3.1 Cell culture

3.1.1 Preparation of cell culture medium

A) L929 conditioned medium

L929 cells (mouse fibroblasts) were cultured in RPMI 1640 medium (11 mM glucose) supplemented with 10% fetal bovine serum (FBS), 100 U/mL penicillin and 100 µg/mL streptomycin, and 1 mM sodium pyruvate until 80% confluent. The medium was collected and centrifuged at 200 x g to pellet any cells. The supernatant was used for supplementing BMDM differentiation medium (see point C). Medium from different L929 cell cultures was pooled, filtered, stored in aliquots of 45 mL at -20°C, and thawed as needed.

B) RAW 264.7 culture medium (5 mM, 11 mM, and 25 mM)

RPMI 1640 medium (glucose free) was supplemented with 5 mM, 11 mM, or 25 mM glucose, 10% FBS, 100 U/mL penicillin and 100 µg/mL streptomycin, and 1 mM sodium pyruvate.

C) BMDM differentiation medium (5, 11, and 25 mM)

RPMI 1640 medium (glucose free) was supplemented with a 20% L929 conditioned medium, 20% FBS, 100 U/mL penicillin and 100 µg/mL streptomycin, 1 mM sodium pyruvate and 5 mM, 11 mM, or 25 mM glucose.

D) BMDM culture medium (5 mM, 11 mM, and 25 mM)

RPMI 1640 medium (glucose-free) was supplemented with 10% L929 conditioned media, 10% FBS, 100 U/mL penicillin and 100 µg/mL streptomycin, 1 mM sodium pyruvate and 5 mM, 11 mM, or 25 mM glucose.

F) THP-1 culture medium (11 mM)

RPMI 1640 medium (11 mM glucose) was supplemented with 10% FBS, 1% 100 U/mL penicillin and 100 µg/mL streptomycin, and 1 mM sodium pyruvate.

G) Seahorse base medium

One vial of Dulbecco's Modified Eagle's Medium (DMEM) powder was dissolved in 990 mL tissue culture (TC)-grade H_20, which contained 143 mM NaCl and 0.5 M NaOH.

3.1.2 Cell counting

Cell count and viability tests were performed with the Guava® Muse® Cell Analyzer (obtained from Merck Millipore). This instrument makes use of laser fluorescence and flow cytometry for cell analysis. A small quantity of the cell suspension (50 µL) is mixed with Count and Viability reagent (450 µL). The Count and Viability reagent contains a DNA-binding dye that stains the nuclei of dead or dying cells (cells of which the membrane is no longer intact), which will give an indication of the cellular viability. Another dye which can penetrate the membrane stains all nucleated cells and allows the instrument to distinguish between cells with a nucleus from debris to allow an exact representation of cell numbers. The cell and Count and Viability mixture is then allowed to incubate for 5 min in the dark and loaded onto the instrument (Millipore, 2012). The cells are drawn up one at a time into the microcapillary and detected with laser fluorescence. This allows the rapid, reliable, and repeatable quantification of cells, which is not always the case for other methods (Herculano-Houzel *et al.*, 2015).

3.1.3 Microscopic evaluation of cells

Visual inspection of cells is crucial since cellular morphology is tightly linked to cell health, function, and differentiation and is used to inspect for contamination (Hart *et al.*, 2018). Cells were inspected with the Nikon Eclipse TE2000-S light microscope (LWD 0.52 Japan) at x10 magnification. The criteria for healthy macrophages were as follows: clear cells with a round or amoeboid shape, an intact nucleus, and often pseudopodia (Lee *et al.*, 2013). The following were indicative of dead or dying cells: small, shrivelled cells with cellular debris. Murky/yellow cell culture medium and small particles moving between cells are indicative of bacterial contamination (Gray *et al.*, 2010). Differentiated cells were distinguished from undifferentiated cells as follows: differentiated cells attach to the Petri dish and have an amoeboid shape whereas non-differentiated cells do not attach and are mostly round and smaller in shape and size.

3.1.4 Cells

A) RAW 264.7 cells

RAW 264.7 cells are macrophage-like cells that originated from BALB/c mouse cells that were transformed with the Abelson leukemia virus (Raschke *et al.*, 1978). These cells are often used

as macrophage models due to their robustness, availability, and expression of typical macrophage characteristics and genes. These cells are also stable for up to 30 passages (Taciak *et al.*, 2018). RAW 264.7 cells were obtained from Cellonex South Africa, via the distributor Separations.

The RAW 264.7 cells were already in stock and kept frozen at -80 °C in cryovials. The frozen cells were thawed at 37°C, resuspended in culture medium (5 mM glucose), and centrifuged at 200 x g for 5 min. The DMSO-containing supernatant was removed, and the cells were resuspended in either 5 mM, 11 mM, or 25 mM culture medium. Cells were maintained at 37ºC and 5% CO_2 and passaged when between 80% and 90% confluent. To passage cells, the medium was replaced with fresh medium and the cells were detached with cell scrapers. A tenth of the cells was resuspended in fresh medium in a new T25 or T75 flask. Cells were passaged around three times before analyses were performed to ensure full recovery from cryopreservation.

B) Mouse bone marrow-derived macrophages (BMDMs)

Bone marrow is an ideal source of naïve (non-activated) primary macrophages for metabolomics studies since the exposure of bone marrow-resident cells to activating factors such as estrogen (which can affect cellular metabolism) is not as profound compared to blood-derived monocytes (Han *et al.*, 2017). Bone marrow also yields high numbers of monocytes, thereby limiting the number of animals needed. This cell type is included in the study since the phenotype and metabolism of transformed cell lines such as RAW 264.7 cells may differ from primary cells (Unger *et al.*, 2002).

Ethics approval for the isolation of mouse bone marrow was obtained from the North-West University Animal Care, Health, and Safety Research Ethics Committee (NWU-AnimCareREC). The NWU ethics approval number for this study is: NWU-00517-20-A5. The housing, caretaking, and handling of the animals used for bone marrow collection were managed by trained personnel at the Vivarium of the Preclinical Drug Development Platform (PCDDP) of the NWU. Sexually mature (8 weeks), wild type C57BL/6 female mice were euthanized via cervical dislocation and the murine femurs and tibiae dissected by a trained laboratory animal technologist. Cervical dislocation was determined (by former PCDDP animal technician Mr. Hylton Bunting, NWU) as the most appropriate method for the harvesting of drug-free, undamaged tissue. Since metabolic analyses will be done on these cells, other choices of euthanasia (pharmacological/anaesthesia) are not ideal. These methods introduce extra chemicals and metabolites, which can affect the metabolic profiles of the mice.

Bone marrow isolation was done according to Amend *et al.* (2016) and summarised in Figure 3. The tibiae and femurs were dislocated, after which the condyles, patella, and epiphysis were removed. Muscle and connective tissue were removed with 70% ethanol wipes. The femurs and tibiae were placed knee-end down in 0.5 mL micro-centrifuge tubes (punctured at the bottom with an 18 G needle) and placed inside a 1.5 mL micro centrifuge tube. The tubes were centrifuged at 10 000 x g for 15 sec, after which the pellet was resuspended in freezing medium (90% FBS, 10% DMSO), counted, and stored at -80°C.

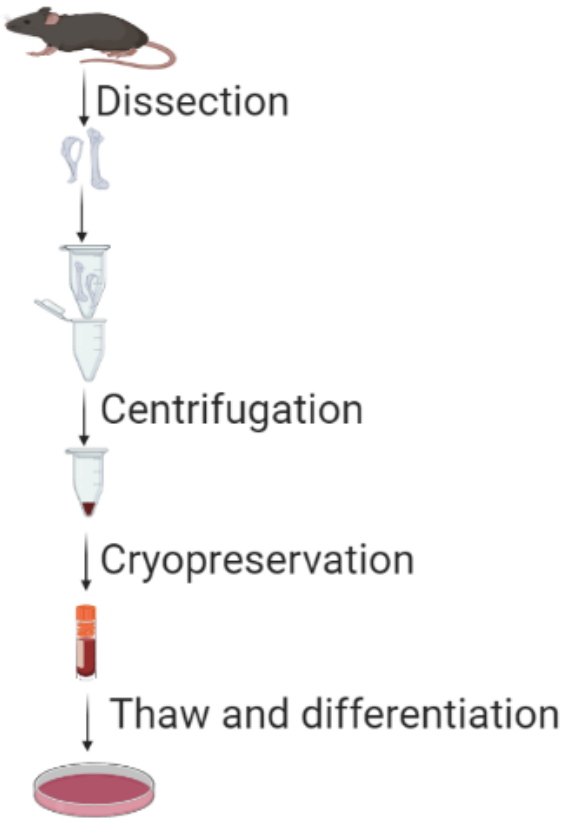

Figure 3: Summary of the isolation of mouse bone marrow cells and differentiation into BMDMs.

The procedure described by Marim *et al.* (2010) was followed for differentiation of bone marrow cells into BMDMs. Frozen bone marrow cells were thawed at 37ºC, suspended in 15 mL PBS, and centrifuged at 200 x g for 5 min. The supernatant was discarded and the cells were resuspended in 1 mL differentiation medium (5 mM glucose) and counted. The cells were seeded at 2 million cells in 10 mL differentiation medium (5 mM, 11 mM, or 25 mM glucose) per non-tissue culture treated Petri dish. A corresponding differentiation medium (10 mL) was added after four days of incubation at 37ºC in a humidified atmosphere with 5% CO_2. The cells were allowed

to incubate for another three days. The medium was removed and the BMDMs were detached by rinsing with 10 mL ice-cold PBS and subsequent gentle scraping with cell scrapers. The cells in the PBS were transferred to tubes and centrifuged at 200 x g for 5 min. The supernatant was discarded and the pellet resuspended in 1 mL of the appropriate freezing medium (90% differentiation medium with 5 mM, 11 mM, or 25 mM glucose, and 10% DMSO). The BMDMs were counted and then stored in cryovials at -80ºC until further analysis.

C) THP-1 cells

THP-1 is a spontaneously immortalised human cell line and was included in this study since the phenotype and metabolism may differ from that of mouse cells such as the RAW 264.7 macrophages and BMDMs. THP-1 cells are non-adherent human monocytic cells. For macrophage studies, these cells should be differentiated into adherent macrophages. The protocol for this has not been established in our lab and had to be optimised. Furthermore, THP-1 differentiation protocols differ greatly between different studies in terms of phorbol 12-myristate-13 acetate (PMA) concentration and differentiation period (Starr *et al.*, 2018). Another problem that was encountered previously by our lab is that THP-1 cells' viability decreases after treatment with the bacterial endotoxin LPS which will be used in this study.

THP-1 cells were a kind gift from the NWU Centre of Excellence for Pharmaceutical Sciences (Pharmacen™) and was stored at -80ºC. The frozen cells were thawed at 37ºC, suspended in a culture medium, and centrifuged at 200 x g for 5 min, after which the supernatant was discarded and the pellet resuspended in a culture medium and incubated at 37ºC in a humidified atmosphere with 5% CO_2.

Based on work by others (Baxter *et al.*, 2020; Biriken *et al.*, 2018; Starr *et al.*, 2018) different PMA concentrations as well as differentiation times were tested for optimal differentiation. THP-1 cells were seeded at 500 000 cells per well (2 mL) in 6-well plates. Initially, the cells were incubated with 20 ng/mL PMA for 72 hours (Annexure A, Figure A1) according to Starr *et al.* (2018). For further optimisation of the differentiation protocol, cells were incubated with 0 ng/mL (control), 50 ng/mL, 100 ng/mL, or 200 ng/mL PMA for 24 hours, 48 hours, and 72 hours in duplicate (Annexure A, Figure A2). After the specified incubation time the PMA was removed and the cells were allowed to rest for 24 hours in a PMA-free culture medium. The cells were then detached by gentle scraping, and cell number and viability determined. The cells were then seeded in a 12-well plate and incubated with or without LPS for 24 hours as depicted in Figure A3 (Annexure A).

3.2 Glucose measurement

3.2.1 Cell culture medium collection

A) RAW 264.7

The cells were seeded in triplicate for each of the three different glucose concentrations that were tested (5 mM, 11 mM, and 25 mM) at a density of 400 000 cells per T25 flask containing 5 mL culture medium. The cells were incubated at 37ºC with 5% CO_2 until confluent (three days). Three control flasks containing only a RPMI medium with either 5 mM, 11 mM, or 25 mM glucose but no cells were also included. Medium samples (350 µL) were collected after every 24 hours and centrifuged for 5 min at 200 x g and 4°C to remove any cells. The supernatant (300 µL) was collected and stored at -20ºC until further analysis (Figure 4). Cells were harvested and counted after the final medium collection on day three.

B) BMDMs

Bone marrow cells from three mice were differentiated at three different glucose concentrations (5 mM, 11 mM, or 25 mM) and medium samples (350 µL) were collected before the addition of a fresh medium (day four) and every 24 hours thereafter for another three days. Medium samples were collected and centrifuged at 200 x g at 4°C for 5 min to remove any cells. The supernatant (300 µL) was collected and stored at -20ºC until further analysis. The remaining medium was removed and the differentiated cells (BMDMs) detached and resuspended in freezing medium as described in *3.1.4 B*. The BMDMs were counted and stored at -80ºC.

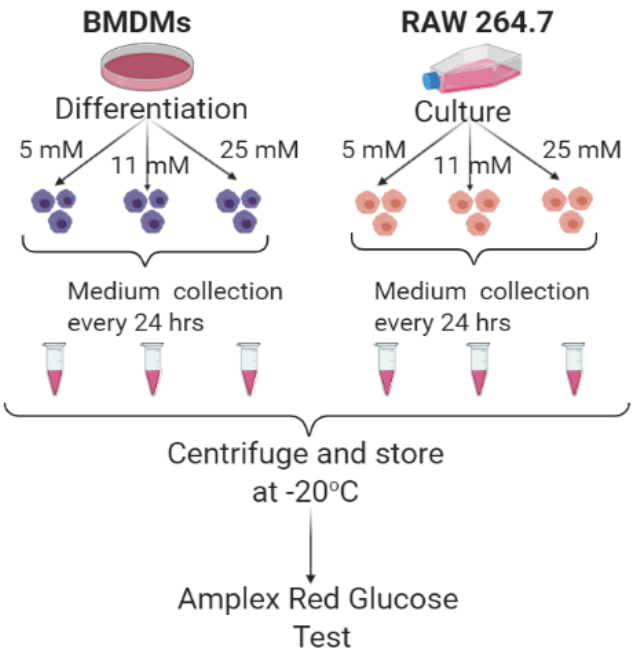

Figure 4: Cell culture medium collection for Amplex Red Glucose Assay tests.

3.2.2 Amplex Red assay

The Amplex™ Red Glucose assay allows the accurate quantification of glucose concentration in a sample. The glucose in the sample reacts with glucose oxidase to form gluconolactone and hydrogen peroxide, which reacts linearly with the Amplex reagent in the presence of horseradish peroxidase (HRP) to form a product that can be measured spectrophotometrically. The absorbance measured for a standard series of known glucose concentrations are used to construct a standard curve. The glucose concentration of the medium samples can then be calculated from this standard curve.

A glucose standard series (0 µM, 5 µM, 10 µM, 15 µM, 20 µM, 25 µM, 30 µM, 35 µM, 40 µM, 45 µM, 50 µM, 55 µM) was prepared in a reaction buffer (1 M Tris-HCl). Frozen cell culture medium samples were thawed at room temperature and vortexed. The 5 mM glucose samples were diluted stepwise to 1:200 and the 11 mM and 25 mM glucose samples diluted to 1:1 000 in the reaction buffer. A reaction mix was prepared containing 50 µL Amplex Red reagent (2,56 µg/mL), 100 µL HRP (10 U/mL), 100 µL glucose oxidase (100 U/mL), and 4,75 mL reaction buffer. Of this reaction mix, 50 µL together with 50 µL of the diluted medium sample was added to each well of a 96-well spectrophotometer microplate in triplicate (see Annexure A, Figure A4-Figure A7). Each plate was incubated for 30 min at room temperature in the dark and the absorbance measured at 560 nm on a Synergy™ HT Multi-Mode microplate reader from BioTek Instruments.

3.3 Bio-energetics analyses

The bio-energetic metabolism (mitochondrial oxidative phosphorylation and glycolysis) of the cells were analysed with the Seahorse 96-well Extracellular Flux (XF) Analyzer from Agilent. This instrument allows the sensitive, rapid, and real-time measurement of the most well-known bio-energetics pathways: mitochondrial oxidative phosphorylation and glycolysis. Bio-energetics analysis using this instrument does not have the drawbacks of other conventional methods that often require large amounts of cells and reagents, and radioactive substances (Van der Windt *et al.*, 2016). The Seahorse XF Analyzer is, therefore, a valuable instrument to analyse the bio-energetic metabolism of cells. The biochemical principle on which the Seahorse Analyzer operates is as follows: in the presence of oxygen cells favour mitochondrial OXPHOS, during which oxygen is taken up from the culture medium. Highly sensitive probes on the XF instrument measures this metabolic change as the change in oxygen levels in the assay medium (OCR = oxygen consumption rate) that serves as a measure of mitochondrial respiration. During glycolysis, and in the absence of oxygen, cells produce lactic acid, which donates protons into the medium and, thereby, decrease the pH of the medium. The XF sensor probes measure the change in pH as the extracellular acidification rate (ECAR) which represents cellular glycolytic rate. The Mitochondrial Stress tests were used in this study since these tests are reliable and widely accepted for assessing mitochondrial bioenergetics and give an indication of parameters such as non-mitochondrial respiration, basal respiration, maximal respiration, proton leak, ATP production, spare respiratory capacity, and coupling efficiency. During this test, OCR and ECAR are measured at baseline and after the injection of specified electron transport chain (ETC) inhibitors oligomycin, antimycin A and rotenone as well as uncoupler FCCP. Oligomycin inhibits ATP synthase resulting in a decreased OCR with a compensatory increase in ECAR. The uncoupler FCCP causes leakage of protons across the mitochondrial membrane and disrupts the mitochondrial membrane potential. This disruption leads to fast oxidation of substrates and therefore an increased OCR as a compensation mechanism. The inhibitors rotenone and antimycin A inhibit Complex 1 and Complex 3 of the ETC respectively, causing a disruption in electron flow through the ETC and, consequently, a decreased OCR. By adding these compounds sequentially to the cells and measuring the OCR and ECAR, certain assay parameters associated with mitochondrial oxidative phosphorylation can be calculated as shown in Figure 5.

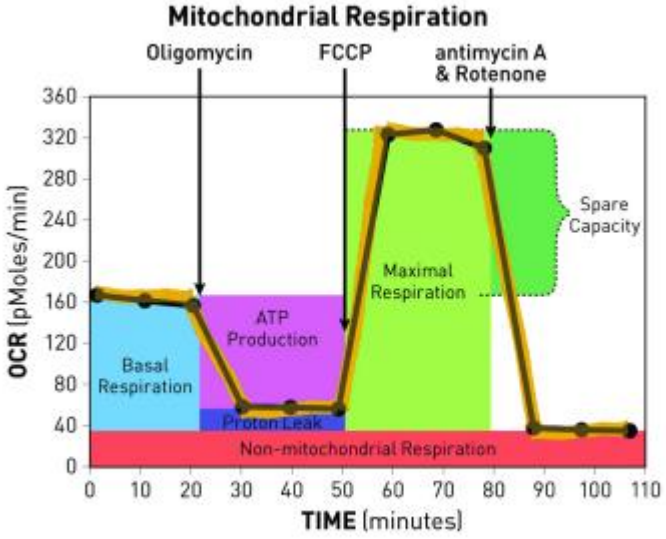

Figure 5: The calculation of mitochondrial respiration rate parameters, Seahorse Training Manual (Miller, 2018:10).

3.3.1 Cell treatment and seeding

A) RAW 264.7 cell line

Single-compound treatment at different glucose conditions

The cells were detached by cell scraping after three days in culture in the three different glucose concentrations. The cells were subjected to centrifugation (200 x g for 5 min), after which the supernatant was removed and the cell pellet resuspended in 1 mL corresponding medium (containing 5 mM, 11 mM, or 25 mM glucose). The cells were counted, and the viability tested. Cell suspensions of 4.8 mL containing 437 500 cells/mL were prepared for each glucose condition. The cell suspensions were then divided into four equal parts (1.2 mL for each treatment group) and 1.2 µL treatment compound (LPS, E2, or IL-4) was added as follows: (1) Group 1 (Control): No treatment; (2) Group 2: LPS (final concentration: 10 ng/mL); (3) Group 3: IL-4 (final concentration: 20 ng/mL); and (4) Group 4: E2 (final concentration: 0.1 nM). For each condition 35 000 cells (in 80 µL) were seeded per well in a Seahorse XF96 cell culture plate. Six to eight replicates were seeded per condition (see Figure A8 in Annexure A). The above-mentioned cell seeding density was optimised in a pilot study. The plate was incubated for 1 hour at room temperature to allow the cells to adhere and then for another 24 hours in a 5% CO_2, 37ºC environment. On the same day, a XF96 sensor cartridge was prepared by the addition of 200 µL sterile water to each well and incubation for 24 hours in a non-CO_2 environment.

Combined treatment at fixed glucose condition

The cells were cultured in 11 mM glucose for three days and detached for analysis. Cells were subject to centrifugation at 200 x g for 5 min, resuspended in 1 mL medium and counted and the viability tested. A 7.2 mL cell suspension was prepared containing 437 500 cell/mL and divided into 6 equal parts (1.2 mL each) and treated with 1.2 µL of the drugs (LPS, E2, or IL-4) as follows: (1) Group 1 (control): No treatment; (2) Group 2: LPS (final concentration: 10 ng/mL); (3) Group 3: IL-4 (final concentration: 20 ng/mL); (4) Group 4: E2 (final concentration: 0.1 nM); (5) Group 5: LPS (final concentration: 10 ng/mL) + E2 (final concentration: 0.1 nM) ; and (6) Group 6: IL-4 (final concentration: 20 ng/mL)+ E2 (final concentration: 0.1 nM). The treated cells were seeded at 35 000 cells (in a volume of 80 µL) per well in a Seahorse XF96 cell culture plate. Ten to twelve replicates were seeded per condition (refer to Figure A9 in Annexure A). The plate was incubated for 1 hour at room temperature to allow the cells to adhere and then for another 24 hours in a 5% CO_2, 37ºC environment. On the same day, a XF96 sensor cartridge was prepared by the addition of 200 µL sterile water to each well and incubation for 24 hours in a non-CO_2 environment.

B) BMDMs

Single-compound treatment at different glucose conditions

BMDMs (differentiated in 5 mM, 11 mM, or 25 mM glucose medium) were thawed at 37ºC, resuspended in 5 mL corresponding cultivation medium (containing 5 mM, 11 mM, or 25 mM glucose), and centrifuged at 200 x g for 5 min. The supernatants were discarded, and each pellet resuspended in 1 mL cultivation medium. The cells were counted, and the viability tested. Cell suspensions (4.8 mL) containing 625 000 cells/mL were prepared for each of the glucose conditions. The cell suspensions were then divided into four equal parts (1.2 mL for each treatment group) and 1.2 µL treatment compound (LPS, E2, or IL-4) was added as follows: (1) Group 1 (control): No treatment; (2) Group 2: LPS (final concentration: 10 ng/mL); (3) Group 3: IL-4 (final concentration: 20 ng/mL); and (4) Group 4: E2 (final concentration: 0.1 nM). For each condition 50 000 cells (in 80 µL) were seeded per well in a Seahorse XF96 cell culture plate. Six to eight replicates were seeded per condition (refer to Figure A8 in Annexure A). The above-mentioned cell-seeding density was optimised in a pilot study. The plate was incubated for 1 hour at room temperature to allow the cells to adhere and then for another 24 hours in a 5% CO_2, 37ºC environment. On the same day, a XF96 sensor cartridge was prepared by addition of 200 µL sterile water to each well and incubation for 24 hours in a non-CO_2 environment.

Combined treatment at fixed glucose condition

Bone marrow cells that were differentiated in 5 mM glucose were thawed, resuspended in the culture medium, centrifuged at 200 x g for 5 min, and the supernatant discarded. The cell pellet was resuspended in culture medium and a 7.2 mL cell suspension prepared containing 625 000 cells/mL. The cell suspension was then divided into 6 equal parts (1.2 mL each) and treated with 1.2 µL of the drugs (LPS, E2, or IL-4) as follow: (1) Group 1 (control): No treatment; (2) Group 2: LPS (final concentration: 10 ng/mL); (3) Group 3: E2 (final concentration: 0.1 nM); (4) Group 4: IL-4 (final concentration: 20 ng/mL); (5) Group 5: LPS (final concentration: 10 ng/mL) + E2 (final concentration: 0.1 nM); and (6) Group 6: IL-4 (final concentration: 20 ng/mL) + E2 (final concentration: 0.1nM). The treated cells were seeded at 50 000 cells (in a volume of 80 µL) per well in a Seahorse XF96 cell culture plate. Ten to twelve replicates were seeded per condition (see Figure A9 in Annexure A). The plate was incubated for 1 hour at room temperature to allow the cells to adhere and then for another 24 hours in a 5% CO_2, 37ºC environment. On the same day, a XF96 sensor cartridge was prepared by addition of 200 µL sterile water to each well and incubation for 24 hours in a non-CO_2 environment.

3.3.2 Flux analysis

The next day, an unbuffered assay medium for the Mitochondrial Stress test was prepared for each glucose condition, containing 1 mM sodium pyruvate and 2 mM L-glutamine in addition to the 5 mM, 11 mM, or 25 mM glucose, and made up with Seahorse base medium to a final volume of 37 mL per glucose condition. The assay media were warmed at 37ºC, and the pH adjusted to 7.4 with 0.5 M NaOH. Aliquots of the three-assay media (6 mL each) were set aside for the preparation of the injectable compounds. The cell culture medium (with or without LPS, E2, or IL-4) in the XF96 well plate was replaced with 175 µL of the respective assay media. The cells were incubated for 1 hour at 37°C in a non-CO_2 environment. The water in the Seahorse cartridge was replaced with 200 µL Seahorse calibration buffer. The injectable compounds (Oligomycin, FCCP, and rotenone/antimycin A) were prepared in assay medium for each of the glucose conditions as shown in Annexure A, Figure A10 and Figure A11. Each compound (25 µL) was loaded into the Seahorse cartridge and utility plate ports using loading guides. The cartridge and utility plate were loaded into the Seahorse XF Analyzer and calibrated. Once calibrated, the XF96 cell culture plate was loaded into the instrument and the protocol for the Mitochondrial Stress test was run. After analysis, the medium was discarded, and the cell culture plate was sealed with parafilm and stored at -20ºC for the normalisation assay.

3.3.3 Normalisation

In order to correct for any differences in cell density between the individual wells, the CyQUANT® GR cell proliferation kit was used to determine the cell density in each well. The CyQUANT® dye binds to cellular nucleic acid and produces fluorescence which directly correlates with cell numbers.

The CyQUANT® FR stock solution (in DMSO) and XF96 cell culture plates were allowed to thaw at room temperature. CyQUANT® GR dye/cell –lysis buffer mix was prepared as follows: 9.5 mL nuclease-free distilled water, 500 µL cell lysis buffer (20X), and 25 µL CyQUANT® GR (400X). CyQUANT® GR dye/cell –lysis buffer (100 µL) was added to each well of the XF96 cell culture plate containing RAW 264.7 cells or BMDMs and incubated for 5 min in the dark. Finally, 95 µL of the reaction mix from each well was transferred to a black spectrophotometer microplate to measure fluorescence at 480 nm excitation and 520 nm emission. The fluorescence value for each well was imported into the Wave software and used to adjust the OCR and ECAR data to that single fluorescence value (scale factor:50) and is reported as OCR/ECAR (pmol/min/cells).

3.4 Liquid chromatography tandem mass spectrometry (LC-MS/MS) analysis of estrogen metabolites

LC-MS/MS analyses are becoming increasingly popular to analyse metabolites, especially parent estrogens and estrogen metabolites (EM) in cell culture medium as compared to methods that are traditionally used for these matrices. Conventional methods such as immunoassays are often time-consuming, lack specificity for some EM structures (Caron *et al.*, 2015), display non-specific binding, and have poor reproducibility due to variation between different antibody lots (Huang *et al.*, 2011). LC-MS/MS analyses bypass these obstacles and provide rapid, highly specific quantification of estrogens and EM. The above-mentioned is particularly important in measuring these metabolites, which can undergo conjugation reactions and exist in multiple forms (Caron *et al.*, 2015). The basic principle on which an LC-MS/MS instrument operates is by separating the molecules in the injected sample by chromatography first. For example, in reversed phase chromatography the sample is passed via a polar mobile phase through a non-polar stationary phase. Hydrophobic non-polar molecules will interact with the stationary phase via hydrophobic interactions, whilst the more hydrophilic polar molecules will elute first from the stationary phase. The polarity of the mobile phase can be decreased in order to elute the non-polar metabolites from the stationary phase. This allows accurate separation of molecules in the sample. The separated molecules are then ionised by an ionisation source (such as electrospray ionisation [ESI]). The ions pass through a magnetic field in the mass spectrometer and are separated based

on the mass-to-charge ratio (m/z). In the case of tandem mass spectrometry (MS/MS), the first mass analyser detects precursor ions which are further fragmented into product ions in a collision cell and monitored by a second mass analyser. The tandem MS, therefore, further increases selectivity and sensitivity and together with chromatographic separation can distinguish between precursor ions which may have a similar m/z. The charged molecules can then be detected by a detector.

An in-house method for the analysis of EM in urine was validated and proven to be effective for the accurate detection and quantification of polar and non-polar estrogen metabolites (Jacobs, 2018), and was used as starting point for the analysis of EM in cell culture medium.

3.4.1 Preparation of analytical and internal standards

The use of standard samples (of which the exact concentration is known) is important in analysing matrix effects (Zhou *et al.*, 2017) and for the quantification of unknown samples (Jiang *et al.*, 2013). One hundred (100) ppm (0,1 mg/mL) stock standard solutions for the EM (estrone, estradiol alpha (17-α-estradiol), estradiol beta (17-β-estradiol), estriol, progesterone, testosterone, androstenedione, estriol-3-sulphate, estradiol-3-sulphate, estrone-3-sulphate, estrone-3-glucuronide, estradiol-3-glucuronide, estriol-16-glucuronide, 2-hydroxyestrone, 4-hydroxyestrone, 16α-hydroxyestrone, 2-methoxyestrone, 4-methoxyestrone, 2-hydroxyestradiol, 4-hydroxyestradiol, 2-hydroxyestrone-3-methyl ether, 2-methoxyestradiol, 4-methoxyestradiol, 16-epiestriol, 17-epiestriol, 16-keto-estradiol, estradiol-17-sulphate) were prepared in methanol (MeOH) and diluted to 1 ppm in MeOH which were dried under nitrogen gas and stored at -80°C until the preparation of standard samples and calibration standards.

The use of stable isotope-labelled internal standards (ILIS) is ideal in correcting for any sample loss during sample preparation and other variations during LC-MS/MS due to these compounds having very similar physical and chemical properties to the analytes of interest (Wang *et al.*, 2007). A 1 ppm internal standard stock solution was prepared in distilled water (dH_20) containing deuterated isotopes E1, E2, E3, 2-hydroxyestrone, 4-hydroxyestrone, testosterone, progesterone as well as 2-acetamidophenol (The internal standards used for each metabolite is shown in Annexure A, Table A2).

3.4.2 Instrumentation

A Phenomenex SPE column vacuum manifold with Phenomenex Strata C18-E SPE and Phenomenex Strata™ 33µm X Polymeric Reversed Phase SPE columns were used during SPE sample preparation. A Rotor Torque rotator and Buchi Switzerland Rotavapor R-215 (rotary

evaporator) with B-491 heating bath, V-700 vacuum pump, and V-850 vacuum controller (obtained from Labotech) were used during liquid-liquid extraction (LLE). An Abel Industries (AB2000) nitrogen evaporator from Stargate Scientific and a Virtis freeze dryer from United Scientific was used for the drying of samples. A Heraeus multifuge X3R centrifuge from Thermo Scientific and WX vortex was also used during sample preparation.

An Agilent 1290 Infinity series LC (equipped with a micro Vacuum Degasser [G1330B], binary pump SL [G4220A], autosampler HiP-ALS SL [G4226A] and column compartment SL [G1316C]) obtained from Agilent Technologies, SantaClara, CA, A Zorbax Eclipse plus rapid resolution high-definition (RRHD) C8-E column (959758-906) obtained from Agilent and Agilent 6460 triple quadrupole mass spectrometer (G6460A) with an ESI source was used for the analyses of EM.

3.4.3 LC-MS/MS conditions

Table 1: Conditions for polar and non-polar EM

LC Parameter	Condition
Autosampler temperature	4°C
Sample injection volume	10 µL
Column temperature	45°C
Mobile phase A composition	Ammonium formate (5 mM) with 5% acetonitrile (v/v) and formic acid (5 mM) in LC-grade water
Mobile phase B composition	100% Acetonitrile
Mobile phase flow rate	0.35 mL/min
Drying gas temperature	250°C
Drying gas flow rate	8 mL/min
Nebuliser pressure	50 psi
Sheath gas temperature	400°C
Sheath gas flow rate	12 mL/min
Ionisation mode	Negative for polar EM; Positive for non-polar EM
Capillary voltage	4000 V
Nozzle voltage	100 V

Table 2: Mobile phase gradients

Polar (conjugated) metabolites		
Time (min)	**Mobile phase A (%)**	**Mobile phase B (%)**
0.5	80	20
5	78	22
5.5	0	100
9	0	100
10	100	0
Non-polar (unconjugated) metabolites		
0.5	60	40
6	46	54
7	46	54
12	45	55
16	31	69
20	31	69
21	0	100
24	0	100
25	80	20

3.4.4 Sample-preparation optimisation

The method described by Jacobs (2018) is focused on the analysis of EM in urine. However, in this study EM in cell culture medium was analysed. Therefore, the sample preparation had to be optimised. Cell culture medium from RAW264.7 cells was used because these cells are easily cultured and cell stocks are readily available.

A) Evaluation of matrix effects

Matrix effects can be defined as a change in the response for the analyte of interest (visible as ion suppression or enhancement) because of components in the matrix that interfere with the analyte of interest. As a result matrix effects can obstruct the accurate detection and quantification of analytes of interest and should be reduced as far as possible (Zhou *et al.*, 2017).

The following three samples were prepared in triplicate as follows: Cell culture medium from RAW 264.7 cells (2 mL) and 2 mL dH_20 was each spiked with 100 µL of the 1 ppm standard stock solution prepared in *3.4.1* to a final concentration of 50 ng/mL. A medium only control (2 mL) which contained no EM was also included. Of the 1 ppm internal standard-stock solution prepared in *3.4.1*, 10 µL was added to all samples to obtain a final concentration of 50 ppb/200 µL. All three samples were further diluted to a final volume of 4 mL with dH_20.

i) SPE was used for sample clean-up. SPE is a valuable technique in which the analytes of interest can be separated from other components in the matrix based on the affinity of the analyte of interest to the column stationary phase. During SPE the liquid sample is passed through a column (choice based on physical and/or chemical properties).

The analytes of interest can then interact with the adsorbent and be eluted selectively by the addition of certain solvents. This allows the selective collection of certain analytes to reduce matrix effects. The Phenomenex Strata C18-E SPE columns were first prepared by washing with 6 mL acetone (100%). After this step it was ensured that the column sorbent was always just below the meniscus of the solvent before the addition of the following solvent unless specified otherwise. The columns were then washed with 6 mL of a 100% MeOH solution. At this stage a vacuum was applied to the SPE system and the flow rate adjusted to produce a steady droplet formation (about 3 mL/min), and the columns were washed with 6 mL dH_20 and equilibrated with 6 mL dH_20. Samples were loaded 2 mL at a time followed by a washing step with 6 mL MeOH (5%). Samples were eluted in 6 mL tubes with 6 mL MeOH (30%) that contained the polar EM. A wash step with 6 mL MeOH (45%) followed and the columns were allowed to dry under full vacuum for 5 min. The non-polar EM fraction was eluted in 6 mL tubes with 2 mL MeOH (100%) and 4 mL acetone (100%). Finally, the columns were washed with 4 mL MeOH (45%).

ii) The sample preparation for the polar fractions proceeded as follows: The samples were dried under nitrogen gas at 40°C until 30% of the MeOH had evaporated. Holes were pierced into the caps and the tubes were frozen at -80°C for at least 4 hours or until completely frozen. The samples were freeze-dried (at a negative temperature and about 200 milliTorr) for approximately 24 hours. The samples were centrifuged at 4000 rpm for 10 min. MeOH (45%; 200 µL) was added to each sample and dissolved by vortexing.

iii) The sample preparation for the non-polar fractions proceeded as follows: The samples were evaporated under nitrogen gas at 40°C until completely dry, and stored frozen at -20°C until further preparation. Derivatisation is the modification of a compound by changing a functional group in order to change the physical or chemical properties of that compound. This allows better separation or quantitation of the compound (Black & Muir, 2003). Moreover, derivatisation was found to improve the sensitivity of analysis of estrogens (Li & Franke, 2015). Dansylchloride was used as derivatisation agent in this study as it has been shown to improve ionisation (Anari *et al.*, 2002) and limit of detection (Nguyen, 2010), and is a fast and simple method (Hunter, 1998). Derivatisation further limits the competition between the analytes of interest and other compounds (which typically occur at lower masses) by increasing the molecular weight of the estrogens. The phenol ring of estrogens allows them to undergo derivatization.

During this derivatisation, there is a chemical reaction between the secondary amine group of the dansylchloride molecule and the hydroxyl group on the phenol ring of an estrogen (Faqehi *et al.*, 2016). Sodiumbicarbonate (100 mM dissolved in dH_20; 50 µL) and 50 µL dansylchloride (1 mg/mL dissolved in acetone) was added to each sample and vortexed. The samples were allowed to incubate at 50°C for 5 min. MeOH (100%; 100 µL) was added to each sample and followed by vortexing.

Samples (200 µL) of both the polar and non-polar fractions were transferred to Spin-X 0,22 µm nylon polypropylene filter tubes and centrifuged at 4000 rpm for 2 min. The samples were then transferred to 2 mL LC glass vials (with 400 µL flat-bottom glass inserts and 9 mM screw caps) and analysed with the LC-MS/MS under the conditions already specified.

B) Identification of component/s of cell culture medium that contribute to matrix effects

2 mL of each of the following samples were prepared in triplicate:

1. Complete culture medium (RPMI medium supplemented with 10% FBS).
2. Serum (FBS)-free culture medium.
3. Protein-precipitated culture medium prepared as follows: 67 µL of a 30% trichloroacetic acid (TCA) solution was added to each medium sample to a final concentration of 1%. The samples were allowed to incubate on ice for 30 min and centrifuged at 17 226 x g for 10 min to pellet proteins. The supernatant was collected in new tubes.
4. Complete culture medium containing 100 µL of the 1 ppm standard stock solution.
5. dH_20 containing 100 µL of the 1 ppm standard stock solution.
6. 10% FBS in MilliQ water.
7. Phenol-red free RPMI medium.
8. Culture medium from estrogen-treated RAW 264.7 cells: Cells were counted with the Guava® Muse® Cell Analyzer and seeded at 1 x 10^6 cells per well (2 mL) in a 6-well plate. Each well was treated with 2 µL E2 (100 nM) and the plate was allowed to incubate for 24 hours at 37°C at 5% CO_2. Medium samples were collected and centrifuged at 125 x g and 4°C for 5 min to pellet any cells. The supernatant was collected in new tubes.
9. One medium-only well was included to serve as control and contained 2 µL E2 (100 nM) but no cells.

10 µL of the 1 ppm internal standard solution was added to each sample and all samples were diluted with dH_20 to a final volume of 4 mL. Sample preparation and analysis for all samples proceeded as described in *3.4.4 A.*

C) Evaluation of the effect of different mobile phase gradients

Three different mobile phase gradients were tested by comparing 2 mL culture medium samples (diluted to 4 mL with dH_20 and spiked with 100 µL of the 1 ppm standard solution) with 2 mL water samples (diluted to 4 mL with dH_20 and spiked with 100 µL of the 1 ppm standard solution). The three gradients were composed as indicated in Table 3.

Table 3: Different mobile phase gradients

Gradient 1			Gradient 2			Gradient 3		
Time (min)	**Mobile phase A (%)**	**Mobile phase B (%)**	**Time (min)**	**Mobile phase A (%)**	**Mobile phase B (%)**	**Time (min)**	**Mobile phase A (%)**	**Mobile phase B (%)**
0	80	20	0	80	20	0	80	20
0,5	60	40	0,5	60	40	0,5	60	40
6	46	54	6	46	54	6	46	54
7	46	54	7	46	54	7	46	54
12	45	55	12	45	55	12	45	55
16	40	60	16	35	65	16	35	65
24	40	60	25	20	80	18	29	71
25	20	80	25	20	80	24	29	71
27	0	100	27	0	100	28	20	80
28	0	100	28	0	100	29	0	100
29	80	20	29	80	20	30	0	100
						31	80	20

D) Full scan analysis of cell culture medium

A full scan in which all ions (from smallest mass to largest) are scanned gives an overview of all the components in the sample. Culture medium (2 mL) was diluted to 4 mL with dH_20 and spiked with 100 µL of the 1 ppm standard solution. This sample was subject to LC-MS/MS full scan in positive ionisation from 100 to 1000 m/z with a scan time of 500 ms. All other parameters (source and ionisation conditions) were set as per final optimised method.

E) Double SPE on non-polar fractions

Culture medium from RAW 264.7 cells (n=6; 2 mL of each), which contained 5% FBS, were collected. TCA (30%; 67 µL) was added to a final concentration of 1% per sample and the samples were incubated on ice for 30 min, after which the samples were subjected to centrifugation at 17 226 x g for 10 min to precipitate proteins. The supernatant was then collected. The pH was adjusted to 7 with NaOH (0.5 M). Each sample was again diluted with 2 mL H_2O and spiked with 100 µL of the 1 ppm standard solution. Sample preparation proceeded as described in *3.4.4 A (i)*. A second SPE was then done on the non-polar fraction as follows: The columns were conditioned as before prior to sample loading. After sample loading, the columns were washed with 6 mL H_2O. Three samples were eluted with 6 mL of 40%, 50%, 60%, 70%, and 100% MeOH and each

fraction was collected. The other three samples were eluted with 6 mL of 80% and 100% MeOH and each fraction collected. Sample preparation then proceeded as described in *3.4.4 A (iii).* The non-polar fractions were transferred to Spin-X 0,22 µm nylon polypropylene filter tubes and centrifuged at 4000 rpm for 2 min. The samples were then transferred to 2 mL LC glass vials (with 400 µL flat-bottom glass inserts and 9 mM screw caps) and analysed with the LC-MS/MS under the conditions already specified.

F) Evaluating different SPE column volumes (2 mL and 15 mL) and liquid-liquid extraction (LLE)

Two volumes of culture medium were tested, namely 2 mL and 15 mL. Six 5% FBS medium samples were collected (3 x 2 mL and 3 x 15 mL) and three dH_20 samples. All samples were spiked with 100 µL of the 1 ppm standard mixture. SPE proceeded as already described in *3.4.4 A (i)*, sample preparation for the polar fractions then proceeded as described in *3.4.4 A (ii)* and sample preparation for the non-polar fractions proceeded as described in *3.4.4 A (iii).* The 15 mL samples were loaded without further dilution, and the 2 mL samples were diluted with dH_20 to a final volume of 15 mL before loading. Samples were stored at -20°C until further analysis.

Liquid-liquid extraction is a method used to separate analytes (in liquid matrix) by the addition of a second immiscible solvent. Separation occurs based on the solubility of the analytes in the solvents. This allows for the isolation of the analytes of interest from other compounds in the matrix. For the LLE, three culture medium samples (containing 5% FBS) and three water samples of 15 mL each were collected. The samples were spiked with 100 µL of the 1 ppm standard mixture. The samples were immediately extracted 3 times with 22.5 mL ethyl acetate (EA). After each EA addition the samples were mixed for 10 min on a Rotor Torque rotator and centrifuged for 1 min at 1000 rpm and 4°C. The organic layer was transferred to a Rotavapor flask and evaporated with a rotary evaporator until approximately 1 mL was left. The sample was then transferred to a Kimax tube and evaporated under nitrogen gas until dried out. Sodiumbicarbonate (0.1 M, dissolved in dH_20; 100 µL) and dansylchloride (1 mg/mL, dissolved in acetone) were added to each sample and incubated at 60°C for 15 min. The samples were dried again under nitrogen gas and stored at -20°C until further analysis.

The polar SPE fractions were resuspended and vialed for LC-MS/MS as already described (section *3.4.4 A (ii)*). The LLE non-polar fraction was resuspended in 200 µL dH_20 containing 10% MeOH and transferred to Spin-X 0,22 µm nylon polypropylene filter tubes and centrifuged at 4000 rpm for 2 min. The samples were then vialed for analysis with LC-MS/MS.

G) Liquid-liquid extraction: salt and pH test

Three dH_20 samples (15 mL) were spiked with 200 µL of the 1 ppm standard mixture and 2 M HCl was added dropwise to each sample until a pH of 1.0 was reached. The samples were salted out by the addition of 4.89 g NaCl. LLE, drying and vialing proceeded as already described in *3.4.4 F,* with the exception that the LC injection volume was set to 20 µL.

H) SPE column type and sample loading volume test

Culture medium from RAW 264.7 cells (n=4) was collected (two samples contained 5% FBS and two samples contained no FBS). Both samples were diluted with dH_20 to a final volume of 50 mL. The Phenomenex Strata™ 33 µm X Polymeric Reversed Phase SPE columns were prepared by washing with 15 mL acetone (100%) and 15 mL MeOH (100%), followed by 15 mL dH_20. The columns were equilibrated overnight with 30 mL dH_20. A sample (50 mL) was loaded and washed with 30 mL water, followed by a 30 mL MeOH (5%) wash step. One 5% FBS sample and one sample containing no FBS was washed with 18 mL MeOH (30%), and the fractions collected. A wash step with 18 mL MeOH (45%) followed and the fractions were collected. All samples were eluted with 6 mL MeOH (100%) and collected. Two elution steps with 6 mL acetone (100%) followed and each fraction was collected. The samples were dried and vialed, as described earlier in *3.4.4 A,* for LC-MS/MS analysis.

I) pH and ascorbic acid derivatisation test

Three medium samples (5% FBS) and three water samples of 2 mL each were spiked with 100 µL of the 1 ppm standard stock solution. The samples were dried under nitrogen. Two samples (one medium and one water) were derivatised as per normal protocol (50 µL sodiumbicarbonate and 50 µL dansylchloride, 5 min incubation at 50°C), after which 100 µL MeOH (100%) was added and the samples vialed for LC-MS/MS.

One medium and one water sample were derivatised as follows: One hundred (100) µL dansylchloride (1 mg/mL) and 100 µL sodiumbicarbonate (100 mM in water containing 0,04% w/v ascorbic acid, pH adjusted to 9.5 with 2 M HCl.). These samples were then vortexed and incubated at 70°C for 5 min and allowed to cool. The samples were vialed and analysed with LC-MS/MS.

One medium and one water sample were derivatised as follows: One hundred (100) µL dansylchloride (1 mg/mL) and 100 µL sodiumbicarbonate (100 mM in water, containing 0.04% w/v ascorbic acid, pH adjusted to 8.0). The samples were vortexed and incubated at 70°C for 5 min and allowed to cool. The samples were vialed and analysed with LC-MS/MS.

J) Standard series preparation and optimisation

For the preparation of the standard series a 4 ppm standard stock solution was prepared by resuspending one dried 1 ppm standard solution in 200 µL MeOH (100%) and mixed by vortexing. This solution was again transferred to a new dried 1 ppm stock solution (this was done two times more) for a final concentration of 4 ppm. A volume of 163.8 µL of the 4 ppm stock was diluted with MeOH to a final volume of 200 µL and a final concentration of 1 638 ng/mL. The standard series (ranging from 0.0125 ng/mL to 1 638 ng/mL) was prepared from this by preparation of a series dilution as described in Annexure A, Figure A12. The 1 ppm internal standard solution was diluted to a final concentration of 0.1 ppm in MeOH and 100 µL of this was added to each concentration. Standards were analysed directly on the LC-MS/MS without further drying or clean-up. Alternatively, the samples were dried under nitrogen and stored at -20°C until further SPE and analysis. For SPE, the Phenomenex Strata™ 33 µm X Polymeric Reversed Phase SPE columns were prepared the day before sample extraction (with SPE) by washing with 15 mL acetone and 15 mL MeOH. Thereafter, the columns were equilibrated overnight with 30 mL dH_20. On the day of SPE analysis each standard was resuspended in 15 mL RAW 264.7 culture medium (5% FBS). Each sample was diluted to a final volume of 50 mL with dH_20 and loaded onto the columns. The columns were washed with 30 mL dH_20 and then with 30 mL MeOH (5%). To elute the metabolites, different elution protocols were followed:

1. The polar metabolites were eluted with 18 mL MeOH (30%). The columns were washed with 18 mL MeOH (45%) and allowed to dry under full vacuum for 5 min. The non-polar metabolites were eluted with 6 mL MeOH (100%) and then with 12 mL acetone (100%). Polar fractions were pooled and non-polar fractions were pooled. The samples were dried, derivatised, vialed, and analysed on LC-MS/MS as per normal protocol.
2. Hereafter, the following fractions were collected after each of the following wash steps: water, 5% MeOH, 30% MeOH, and 45% MeOH. Sample drying, derivatisation, and vialing for LC-MS/MS analysis proceeded as per usual protocol.
3. The polar fractions were collected after both 30% and 45% MeOH elution. Non-polar metabolites were eluted as usual with 6 mL MeOH (100%) and 12 mL acetone (100%). Sample preparation and analysis proceeded as per usual protocol.

3.4.5 Final procedure

A) Cell culture and treatment

RAW 267.4 cells were cultivated (in 11 mM glucose) until a total of about 72 x 10^6 cells (6 x T75 flasks, each containing approximately 12 x 10^6 cells). The medium was removed, and fresh medium was added. The cells were detached via cell scraping, transferred to a 15 mL tube, and centrifuged at 125 x g for 5 min. The supernatant was discarded, and the cell pellet resuspended in 1 mL 5% FBS culture medium. The cells were counted and seeded at a density of 3,5 x 10^6 cells per flask for E2 and E2+IL4 treatment, or 5 x 10^6 cells per flask for E2+LPS treatment to compensate for the slower growth rate of cells in the presence of LPS. Cells were treated with 100 nM E2 (15 µL) alone or in combination with 20 µg/mL IL-4 (15 µL) or 10 µg/mL LPS (15 µL) in triplicate.

For each condition, one 5% FBS medium only control (i.e., without cells) were included: an E2 control, LPS + E2 control, and an IL-4 + E2 control. All flasks were allowed to incubate for 48 hours in a 5% CO_2, 37°C atmosphere. A medium sample (14 mL) was collected from each flask and centrifuged for 5 min at 180 x g and 4°C. The supernatants were collected and 10 µL of the 1 ppm internal standard was added to each. Proteins were precipitated by the addition of 460 µL TCA (1%) to each sample. The samples were incubated on ice for 30 min and centrifuged for 10 min at 17226 x g on ice. The supernatant was collected (13 mL) and stored at -20°C until further analysis. Medium (7.5 mL) was added to each T75 flask and the remaining cells were detached via cell scraping and counted on the Guava® Muse® Cell Analyzer for normalisation purposes.

B) SPE and LC-MS/MS analysis

The Phenomenex Strata™ 33 µm X Polymeric Reversed Phase SPE columns were prepared the day before SPE by washing with 15 mL acetone and 15 mL MeOH. Thereafter, the columns were equilibrated with 30 mL dH_20. On the day of SPE, the samples were allowed to thaw, and each was diluted with dH_20 to a final volume of 50 mL. This solution was loaded onto the columns. The columns were then washed with 30 mL water and then 30 mL MeOH (5%). The polar metabolites were eluted with 18 mL MeOH (30%) and 18 mL MeOH (45%). The columns were allowed to dry under vacuum for 5 min. The non-polar metabolites were then eluted with 6 mL MeOH (100%) and 12 mL acetone (100%). All fractions eluted with 30% MeOH were dried under nitrogen until 30% MeOH evaporated and pooled together before freezing at -80°C overnight. All fractions eluted with 45% MeOH were dried under nitrogen at 40°C until 45% MeOH evaporated and pooled together before freezing at -80°C overnight. All polar fractions (30% and 45% MeOH fractions) were freeze-dried (at a negative temperature and about 200 milliTorr) for approximately

24 hours. These samples were centrifuged at 1431 x g for 10 min. MeOH (45%; 200 µL) was added to each sample and dissolved by vortexing. The non-polar fractions (100% MeOH and 100% acetone fractions) were dried with nitrogen gas at 40°C until all non-polar fractions could be pooled and further evaporated under nitrogen until dry. These samples were stored at -20°C until further preparation. Sodiumbicarbonate (100 mM dissolved in H_20; 50 µL) and 50 µL dansylchloride (1 mg/mL dissolved in acetone) was added to each of the non-polar samples and vortexed. The samples were allowed to incubate at 50°C for 5 min. MeOH (100%; 100 µL) was added to each sample and dissolved by vortexing. Samples (200 µL of each) were transferred to Spin-X 0,22 µm nylon polypropylene filter tubes and centrifuged at 4000 rpm for 2 min. The samples were then transferred to 2 mL LC glass vials (with 400 µL flat bottom glass inserts and 9 mM screw caps) and analysed with the LC-MS/MS.

3.5 Data processing and statistical analyses

3.5.1 Bio-energetics analyses

After normalisation, the data from the Seahorse XF Analyzer was further processed with the Wave Software. Outliers were removed by visual inspection of the OCR and ECAR graphs obtained for each well in a treatment group. Assay parameters were calculated from these graphs as depicted in Figure 5. The OCR and ECAR values of the calculated assay parameters were imported into the GraphPad Prism 5 software. The means of the groups (as listed in Table 4) were compared using two-way analysis of variance (ANOVA) tests for analysing the data of the single compound treatment at different glucose conditions, and one-way ANOVA tests for analysing the data of the combined treatment at fixed glucose condition. Bonferroni post-tests (for comparing all groups) were used for the data. The significance threshold was set as $p < 0.05$ (95% confidence intervals). A p value of less than 0.05 is indicated with one star (*), less than 0.01 is indicated with two stars (**) and less than 0.001 is indicated with three stars (***).

Table 4: Group comparisons for statistical analyses

Single-compound treatment at different glucose conditions	
5 mM Control	5 mM E2
5 mM Control	5 mM LPS
5 mM Control	5 mM IL-4
11 mM Control	11 mM E2
11 mM Control	11 mM LPS
11 mM Control	11 mM IL-4
25 mM Control	25 mM E2
25 mM Control	25 mM LPS
25 mM Control	25 mM IL-4
5 mM Control	11 mM Control
5 mM Control	25 mM Control
11 mM Control	25 mM Control
5 mM E2	11 mM E2
5 mM E2	25 mM E2
11 mM E2	25 mM E2
5 mM LPS	11 mM LPS
5 mM LPS	25 mM LPS
11 mM LPS	25 mM LPS
5 mM IL-4	11 mM IL-4
5 mM IL-4	25 mM IL-4
11 mM IL-4	25 mM IL-4
Combined treatment at fixed glucose condition.	
Control	E2
Control	LPS
Control	IL-4
Control	LPS + E2
Control	IL-4 + E2
LPS	LPS +E2
IL-4	IL-4 + E2

3.5.2 LC-MS/MS analysis

The Agilent MassHunter Qualitative Analysis for QQQ software (B.06.00) was used to view peaks and the Agilent MassHunter Quantitative Analysis software (B.06.00) was used for quantifying peaks.

A) Relative response

The relative reponse for each metabolite was calculated using the following formula:

Relative response = Sample response/Standard response

B) Limit of detection (LOD) and limit of quantification (LOQ)

LOD refers to the lowest concentration of analyte that can be detected by the instrument, but not necessarily quantified. On the other hand, LOQ, is the lowest concentration of analyte that can be accurately and reliably quantified (Shrivastava & Gupta, 2011). Two methods of determining the LOD and LOQ was employed:

1. The linear regression method: The method is typically used when the standard curve is linear (R^2>0.99). Here the slope (S) and the standard deviation of the response (S_y) of the curve is calculated. The following formulas are used to calculate the LOD and LOQ (Shrivastava & Gupta, 2011):
   LOD = 3.3 (S_y/S)
   LOQ = 10 (S_y/S)

2. Signal-to-noise ratio (S/N) method: This method is typically used when there is background noise. The following formula was used to calculate the S/N (Baber, 1994):
   S/N = H/h
   Where the height of the peak (H) is measured from the base of the peak (at half-height of the background noise) to the top of the peak. The height of the background noise (h) is measured from base to top of the noise for a distance of 20 times the width of the peak at half-height.

C) Final analysis

The concentration of each metabolite for each treatment was calculated relative to their corresponding internal standard (Shown in Annexure A, Table A2): The sample response was divided by the response of the internal standard and multiplied by the IS concentration (50 ng/mL). This value was divided by the response factor for the metabolite (the slope of the standard series). This concentration was then divided by 13 (volume of sample after protein precipitation) to obtain a concentration in ng/mL.

A fold change was calculated between the treatment and control groups as listed in Table 5 by subtracting the average concentration of the treatment from the control, and dividing this value by the control. A fold change of 1.5 and higher was used to identify a possible increase or decrease in concentration of the treatment groups compared to the controls.

Table 5: Group comparisons for fold change calculations.

Treatment	Control
LPS+E2	Control LPS+E2
IL-4+E2	Control IL-4+E2
E2	Control E2

CHAPTER 4 RESULTS AND DISCUSSION

4.1 Isolation of mouse bone marrow cells and differentiation into macrophages.

The health, confluency, and the number of cells were determined after the differentiation of BM cells from different mice, at different glucose conditions (Table 6). The number of differentiated cells obtained was more or less the same for all three glucose conditions (~2-3 million cells). The confluency of the cells cultured with 25 mM glucose tended to be higher compared to the other glucose conditions (80%-90% confluent). The colour of the cell culture medium for this high glucose condition was an orange-red colour, which is indicative of a lower pH and hence, a higher lactic acid production and cellular proliferation. Although we did not assess the degree of differentiation through the measurement of cell differentiation markers, medium glucose concentration did not seem to have a significant influence on the number of differentiated BM cells obtained.

Table 6: Cell count and confluency of BMDMs at different glucose concentrations

Mouse	Glucose concentration								
	5 mM			11 mM			25 mM		
	Confluency (%)	Cellcount (cells/mL)	Differentiation	Confluency (%)	Cellcount (cells/mL)	Differentiation	Confluency (%)	Cellcount (cells/mL)	Differentiation
1	80	3.01 x 10^6	Cellular attachment, amoeboid shape	80	2.26 x 10^6	Cellular attachment, amoeboid shape	90	3.29 x 10^6	Cellular attachme amoeboid shape
2	80	2.94 x 10^6	Cellular attachment, amoeboid shape	80	2.85 x 10^6	Cellular attachment, amoeboid shape	80	2.26 x 10^6	Cellular attachment, amoeboid shape
3	70	2.49 x 10^6	Cellular attachment, amoeboid shape	80	2.57 x 10^6	Cellular attachment, amoeboid shape	80	2.71 x 10^6	Cellular attachment, amoeboid shape

4.2 THP-1 culturing and differentiation optimisation

The PMA differentiation protocol according to (Starr *et al.*, 2018) was chosen as a starting point for optimisation, since this group tested different PMA concentrations, differentiation incubation periods, and sensitivity towards LPS treatment. The researchers found a PMA concentration of 20 ng/mL and differentiation of three days to be sufficient for THP-1 differentiation with little effect of LPS treatment on the health of the cells. However, after recreating those conditions in our lab (Annexure A, Figure A1) it was found that this low PMA concentration was not sufficient for THP-1 differentiation since cells were still in suspension and displayed a round morphology. Guided by the work of others (Baxter *et al.*, 2020; Biriken *et al.*, 2018; Starr *et al.*, 2018), different PMA concentrations (0 ng/mL (control), 50 ng/mL, 100 ng/mL, and 200 ng/mL PMA) and incubation times (24 hours, 48 hours and 72 hours) were tested next. Table 7 portrays the difference in differentiation between cells treated with 50 ng/mL, 100 ng/mL, and 200 ng/mL PMA after 24 hr incubation. After PMA removal the cells that were treated with 50 ng/mL PMA for 24 hours showed very little attachment and a small number of cellular debris. Cells treated with 100 ng/mL and 200 ng/mL PMA showed slightly more attached cells compared to the lower PMA concentration, however more dead and dying cells were also present. The cells were then left to rest in PMA-free medium for 24 hours. After the 24-hour rest in a PMA-free medium, the cells were detached, counted, and the viability determined with the Muse Cell Analyzer to assess the impact of the respective PMA concentrations and incubation times on the health of the cells. Although a higher PMA concentration increased the number of differentiated cells, it also increased the number of cellular debris, and therefore, decreased overall cell viability (from 98% to 86%; Table 7). The detached cells were then seeded in 12 well plates and treated with or without LPS (final concentration of 10 ng/mL) for 24 hours to evaluate the effect of this endotoxin on the health of the differentiated cells. The morphology and number of cellular debris of LPS-treated cells were similar to the cells that were not subjected to LPS treatment at 50 ng/ml PMA. However, it was again apparent that the health of the LPS-treated cells was compromised as PMA concentration increased. Although this short incubation period with PMA and LPS treatment did not decrease the viability of the cells significantly, the number of differentiated cells obtained (10%-40%) was not sufficient for downstream applications.

Table 7: 24-Hour differentiation of THP-1 cells at different PMA concentrations

	PMA concentration (ng/mL)	Percentage differentiated cells	Cell count and viability	Effect of LPS treatment on cell health
24-hr plate	50	10%-20%	4,2 x 10^4 cells/mL 91 % Viability	Similar to LPS-free control
	100	30%-40%	1.02 x 10^5 cells/mL 90 % Viability	Similar to LPS-free control
	200	30%-40%	8,87 x 10^5 cells/mL 86,14% Viability	Similar to LPS-free control
	No PMA control	0%	1.6 x 10^6 cells/mL Viability 98%	Similar to LPS-free control

Table 8 portrays the difference in differentiation between cells treated with 50 ng/mL, 100 ng/mL, and 200 ng/mL PMA at 48 hours. After PMA removal the cells treated with 50 ng/mL PMA for 48 hours showed more attachment and cluster formation, but also more cellular debris compared to the 24-hour group. Cells treated with 100 ng/mL and 200 ng/mL PMA also showed more attachment overnight, yet a significant number of cellular debris was visible. After a 24-hour rest in a PMA-free medium the cells were detached, counted, and the viability was determined again. Similar to the cells that were incubated for 24 hours in PMA, PMA concentration appeared to increase the number of differentiated cells and also the number of cellular debris. Therefore, overall cell viability seemed to have been compromised at high PMA concentrations (from 96% viability to 79%). Further treatment of the cells with LPS (final concentration of 10 ng/mL) resulted in slightly more cellular debris compared to the cells that were not subject to LPS treatment. However, it was again apparent that the health of the LPS-treated cells deteriorated more when the PMA concentration increased. Although the longer incubation time with PMA increased the number of differentiated cells somewhat (up to 50%), it hurt the health of the cells—an effect that was worsened by further incubation with LPS.

Table 8: 48-Hour differentiation of THP-1 cells at different PMA concentrations

	PMA concentration (ng/mL)	Percentage differentiated cells	Cell count and viability	Effect of LPS treatment on cell health
48-hr plate	50	30%–40%	8,24 x 10^4 cells/mL 86, 20% Viability	A slight increase in cellular debris in LPS-treated cells compared to LPS- free control
	100	40%–50%	1,27 x 10^5 cells/mL 82% Viability	A slight increase in cellular debris in LPS-treated cells compared to LPS- free control
	200	40%–50%	1,64 x 10^5 cells/mL 79% Viability	A slight increase in cellular debris in LPS-treated cells compared to LPS- free control
	No PMA control	0%	5,61 x 10^6 cells/mL 96,3% Viability	Similar to LPS-free control

Table 9 portrays the difference in differentiation between cells treated with 50 ng/mL, 100 ng/mL, and 200 ng/mL PMA for 72 hours. Although the percentage of differentiated cells was comparable with the 48-hour incubation at all three PMA concentrations, the adherent cells showed characteristic macrophage cluster formation after 72 hours additionally and a few cells displayed the typical elongated amoeboid-like macrophage morphology. However, a significant number of cellular debris were visible, which again increased at high PMA concentrations. Cell viability assessment after the 24-hour rest in a PMA-free medium again confirmed the decrease in overall cell viability with increasing PMA concentration (viability decreased from 96% to 77%). Further incubation of the differentiated cells with LPS (final concentration of 10 ng/mL) resulted in a change in morphology (cell shrinkage) but also an increase in the number of cellular debris floating in the medium compared to the cells that were not subject to LPS treatment. It was again apparent that the health of the LPS-treated cells was more impaired as the PMA concentration increased. Although the 72-hour differentiation with PMA appeared to induce around 50% differentiation, it compromised the health of the cells drastically. This brings the suitability and reliability of the cells for downstream cell biological investigations under question since it is not known to what extent their metabolism and overall function would be affected. For this reason, we decided to exclude these cells from further analyses and proceeded with only the RAW 264.7 and BMDMs.

Table 9: 72-Hour differentiation of THP-1 cells at different PMA concentrations

	PMA concentration (ng/mL)	Percentage differentiated cells	Cell count and viability	Effect of LPS treatment on cell health
72-hr plate	50	30%–40%	2.15 x 10^5 cells/mL 86% Viability	LPS treatment results in more dying cells than LPS- free control
	100	50%	2,90 x 10^5 cells/mL 88% Viability	LPS treatment results in more dying cells than LPS- free control
	200	50%	3,73 x 10^5 cells/mL 77% Viability	LPS treatment results in more dying cells than LPS- free control
	No PMA control	0%	4,13 x 10^6 cells/mL 96% Viability	Similar to LPS-free control

4.3 Determining the optimal glucose concentration for *in vitro* metabolic studies of macrophages

4.3.1 Glucose consumption measurement

The importance of choosing a suitable cell culture medium was stressed in a recent paper published by Lagziel *et al.* (2020) since it was found that variation in medium components can affect the soundness and reproducibility of metabolic data. There is a large variation in the type of culturing medium used in previous macrophage studies. The glucose concentration in each medium often differs and does not always correspond with the physiological glucose condition, which may potentially affect the experimental outcome. Physiological glucose concentrations for mice are between 4 mM and 6 mM. Using high glucose concentrations of 25 mM (4.5 g/L) for *in vitro* culturing of macrophages is, therefore, not corresponding with physiological conditions at all. However, when working with highly glycolytic cell lines like RAW 264.7 cells the use of lower glucose concentrations may result in glucose depletion of the medium and starvation of the cells. To determine if glucose concentrations closer to physiological concentrations could be used without starving the cells of glucose, we assessed the glucose consumption of RAW 264.7 cells and BMDMs in RPMI medium containing different glucose concentrations. Cell culture medium was collected from these cells in culture and analysed with the Amplex Red Glucose Oxidase Assay as per section *3.2.2*.

A) RAW 264.7 cells

An incubation period of 72 hours was chosen for this cell line since this is the time required for the cells to reach a confluency of about 80% (which is the minimum confluency to ensure full recovery from cryopreservation/passaging and that the cells are in the log phase of growth). The extracellular glucose concentration of the RAW 264.7 cells that were cultured in medium with 5 mM glucose decreased over the 72-hour incubation period. A significant drop in glucose concentration happened between 48 hours and 72 hours, probably due to the exponential rate at which these cells proliferate in culture. The fast increase in cells would have resulted in more glucose being consumed from the medium. The end glucose concentration after 72 hours was around 1 mM (Figure 6A) which is below the 2.3 mM hypoglycaemic cut-off for mice (Burcelin *et al.*, 2000). This hypoglycaemic state can affect the metabolism and function of these cells. For example, low glucose concentrations were shown to polarize monocytes towards a pro-inflammatory state (Piarulli *et al.*, 2017). The glucose concentration of the RAW 264.7 cells cultured with 11 mM glucose also decreased, especially after 48 hours, to a concentration of around 8 mM at the end of the 72-hour incubation period (Figure 6B). Although this concentration is still above the physiological range of 4 mM-6 mM in mice, the impact on cellular metabolism and function may not be as pronounced as that of a hypoglycaemic state. The cells cultured with high glucose (25 mM) showed a drop in glucose concentration to about 20 mM, again with the largest decrease occurring after 48 hours of incubation (Figure 6C). This concentration is well above physiological conditions and our results indicate that these cells are in a constant hyperglycaemic state. Similar to low glucose concentrations, hyperglycaemia has been shown to affect inflammation. High glucose concentrations increase the polarization of pro-inflammatory macrophages and the expression of acyl-Coenzyme A synthetase (ASCL 1) in peritoneal macrophages and BMDMs (Kanter *et al.*, 2012). The increase in glucose concentration observed for the control group shown in blue (Figure 6B and 6C) could be the result of medium evaporation during incubation or other variations that may occur during pipetting, medium collection etc.

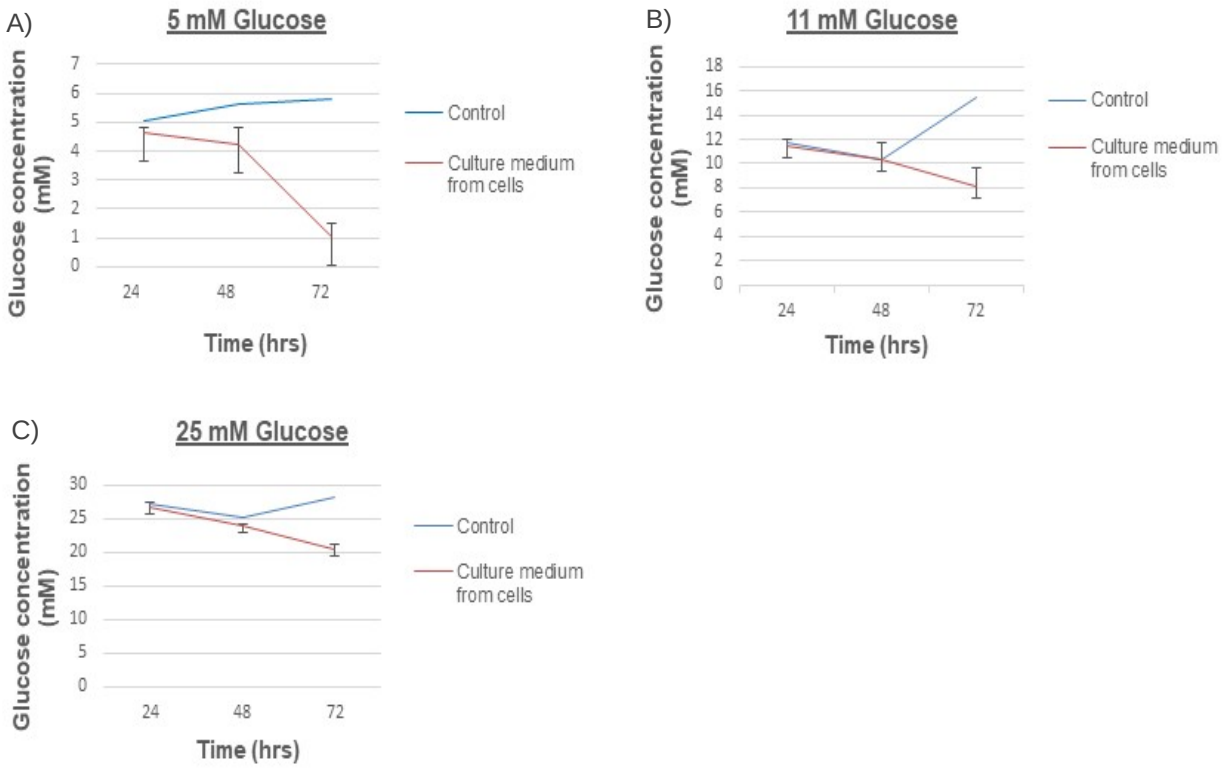

Figure 6: Extracellular glucose concentration (measured with the Amplex Red Glucose test) of RAW 264.7 cells cultured for 72 hours in RPMI medium containing either (A) 5 mM, (B) 11 mM, or (C) 25 mM glucose. Blue line represents glucose concentration of the cell culture medium from control flasks without cells, red line indicates glucose concentration of the cell culture medium from RAW 264.7 cells. Error bars represent standard deviation of replicate measurements of samples (n=3)

Figure 7A depicts the cumulative glucose consumption (calculated by subtracting the glucose concentration at 24 hours from the control at 24 hours, the concentration at 48 hours from the concentration at 24 hours, etc.) of the RAW 264.7 cells cultured with different glucose concentrations over the 72-hour incubation period. The amount of glucose consumed by the cells increased over time. This increase is especially visible for all glucose conditions after 48 hours of incubation. According to Assanga and Lujan (2013) cells typically exit the lag phase of the cell-growth curve (in which the cells are still recovering from cryopreservation or sub-culturing) after 48 hours, after which they enter an exponential growth phase where cell numbers increase exponentially. This may result in more cells consuming glucose after this period. The cumulative glucose consumption per cell at 72 hours was calculated by dividing the glucose consumed by the number of cells at 72 hours of incubation which is shown in Figure 7B. The cells that were cultured with higher glucose concentrations (11 mM and 25 mM) consumed more glucose in total compared to the cells that were cultured with low glucose (5 mM) at 72 hours. This is interesting

since it could indicate that the cells that have a limited supply of glucose may be in a starvation state, in which certain metabolic pathways such as glycolysis are slowed down to conserve energy. In contrast, the cells that had glucose readily available to them (11 mM and 25 mM group) had no need to compensate for a lack of energy resources. An alternative explanation is that the cells cultured with low glucose (5 mM) consumed less glucose, because less glucose is available to be consumed.

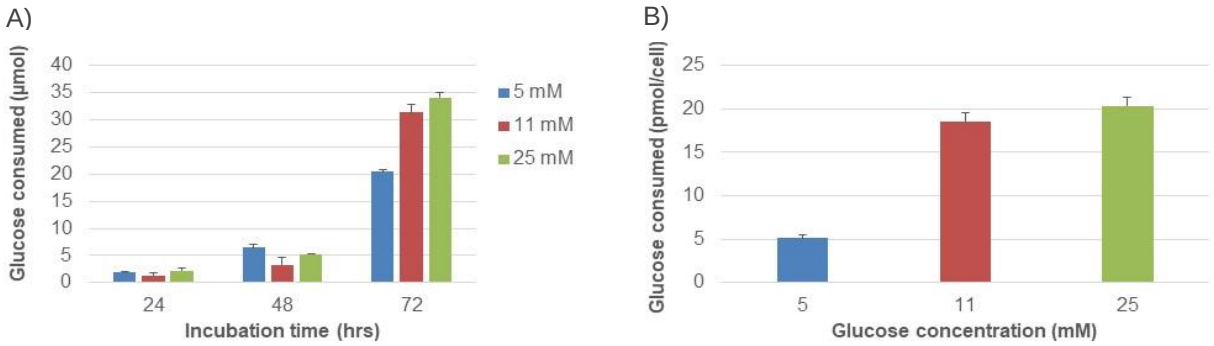

Figure 7: (A) Cumulative glucose consumption by RAW 264.7 cells cultured with either 5 mM, 11 mM, or 25 mM glucose over the course of 72 hours. (B) Cumulative glucose consumption per cell cultured with either 5 mM, 11 mM, or 25 mM glucose at 72 hours. Error bars represent standard deviation of replicate measurements of samples (n=3).

B) BMDMs

The glucose concentration of the cell culture media collected from BMDMs during days four to seven of the differentiation period are shown in Figure 8. From these graphs, it is clear that the actual glucose concentration of the 5 mM and 25 mM glucose medium differed from the theoretical concentration. We suspect that the L929-conditioned medium that was used to prepare the differentiation medium still had a significant glucose content. This may have resulted in the increase in glucose concentration in the 5 mM glucose medium, while having a dilution effect in the 25 mM glucose medium. To confirm this, we measured the glucose concentration in the L929-conditioned medium using the Amplex Red assay. Indeed, the conditioned medium was found to have a glucose concentration of around 11 mM, explaining the elevation of glucose concentration in the 5 mM glucose medium to ~8 mM, and the reduction in glucose concentration to ~18 mM in what was meant to be the 25 mM glucose medium. The extracellular glucose concentration for the cells differentiated in 5 mM glucose medium was close to physiological conditions (about 5 mM) at the end of the seven-day differentiation period (Figure 8A). The glucose concentration of the cells that were differentiated in 11 mM glucose medium was around 9 mM (Figure 8B) at the

end of the differentiation period, while that of the highest glucose condition was also about 9 mM (Figure 8C).

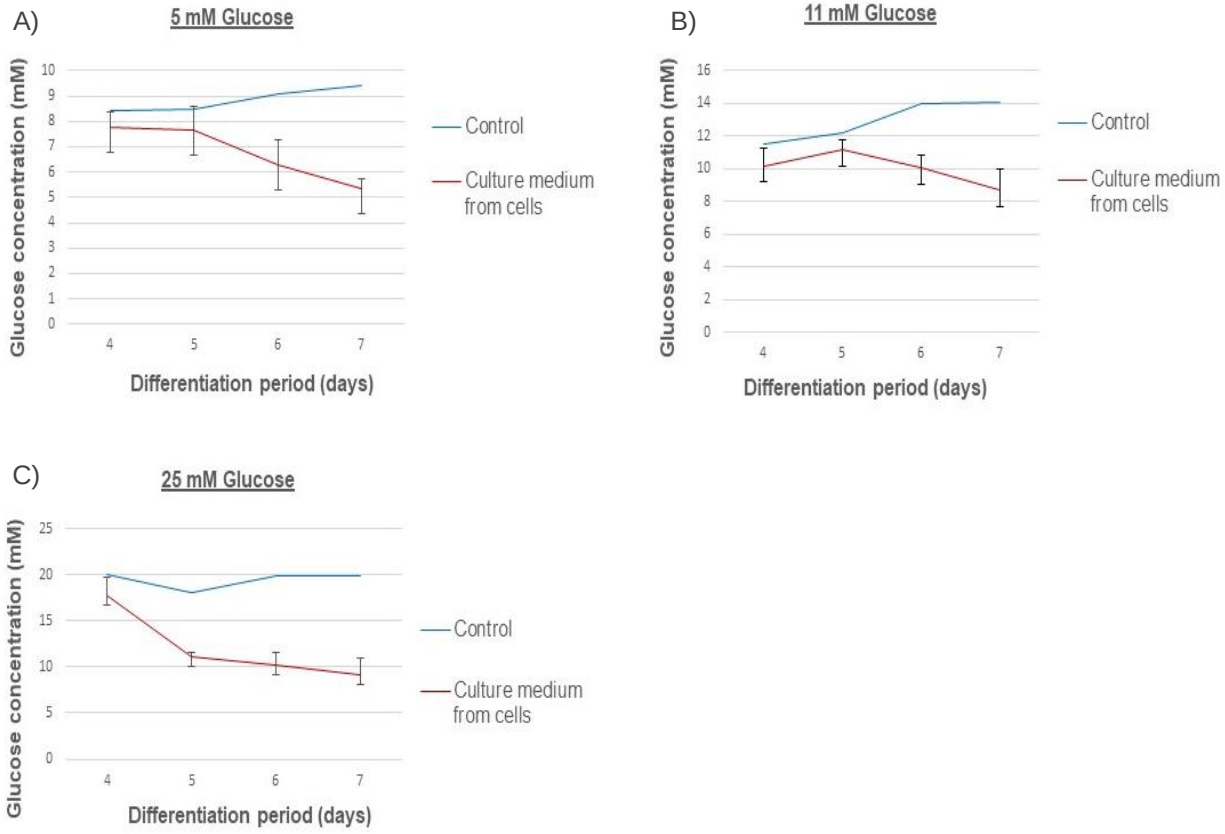

Figure 8: Extracellular glucose concentration (measured with the Amplex Red Glucose test) of BM cells differentiated in RPMI medium containing either (A) 5 mM, (B) 11 mM, or (C) 25 mM glucose during days four to seven of the differentiation period. Blue line represents glucose concentration of medium from control flasks without cells, red line indicates glucose concentration of the cell culture medium from BMDMs. Error bars represent standard deviation of replicate measurements of samples (n=3).

The cumulative glucose consumption of the BMDMs (calculated by subtracting the glucose concentration on day four from the concentration of the control on day four, the concentration on day six from the concentration on day five, and so forth) is shown in Figure 9A. Like the RAW 264.7 cells, the glucose consumption for all glucose conditions increased over time. Since it is possible that differentiated cells have an enhanced mitochondrial and glycolytic ability as compared to undifferentiated cells, as proven in neuronal cells (Li *et al.*, 2020), it may be that bone-marrow cells also increase metabolism and glucose consumption to fulfil their specialised roles as differentiated cells, which could explain the increase in glucose consumption for these cells during differentiation. The proliferation capacity of fully differentiated BMDMs is limited (Botnick *et al.*, 1982), therefore the contribution of increased cell numbers to the increase in

glucose consumption would be minimal. The cumulative glucose consumption per cell at day seven was calculated by dividing the glucose consumed by the number of cells at day seven of incubation which is shown in Figure 9B. The BMDMs differentiated at higher glucose concentrations (11 mM and 25 mM glucose) consumed more glucose in total compared to the 5 mM glucose group at day seven of differentiation. The glucose consumption for the cells differentiated in 25 mM glucose appeared to increase the most after only four days of differentiation, whereas the glucose consumption of the 5 mM and 11 mM glucose groups increased mostly after five days. It is possible that the high glucose concentration stimulated BMDM differentiation (as has been shown for adipocyte differentiation from mouse bone marrow cells (Hankamolsiri *et al.*, 2016)) since the confluency of differentiatied cells was slightly higher compared to the cells cultured with lower glucose concentrations. This, in turn, could have led to an increase in glucose consumption, as explained above.

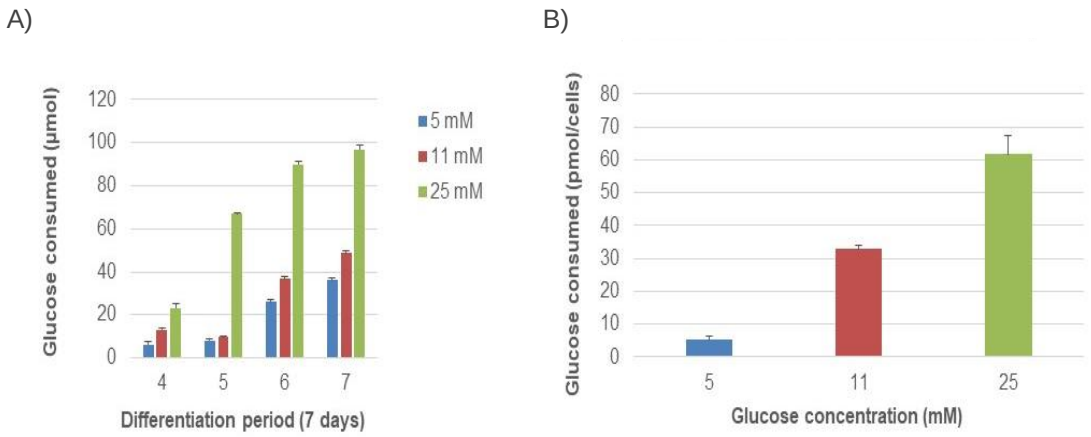

Figure 9: (A) Cumulative glucose consumption by BMDMs cultured either 5 mM,11 mM, or 25 mM glucose during days 4-7 of differentiation (B) Cumulative glucose consumption per cell cultured with either 5 mM, 11 mM, or 25 mM glucose at day 7. Error bars represent standard deviation of replicate measurements of samples (n=3).

4.3.2 Bio-energetics flux analysis of macrophages stimulated with LPS, IL-4, and 17-β-estradiol at different medium glucose concentrations

The second phase in determining the most appropriate glucose concentration for macrophage studies, entailed the bio-energetics analyses of cells cultured at different glucose concentrations to determine whether and how different glucose concentrations affected the bio-energetic metabolism of these cells. Since it is known that macrophage metabolism is regulated by

polarization state (Sun *et al.*, 2022) we additionally stimulated the macrophages either with LPS, IL-4, or E2 to see whether the different culturing glucose concentrations would alter the effect of these stimuli on macrophage metabolism.

The Mito Stress test results for the RAW 264.7 cells and BMDMs cultured with 5 mM, 11 mM, and 25 mM glucose medium are shown in Figures 10 and 11, respectively. At glucose conditions 5 mM and 11 mM, the RAW 264.7 cells treated with IL-4 had the highest oxygen consumption, followed by the E2-treated cells. BMDMs, on the other hand, that were treated with E2 displayed the highest OCR, followed by IL-4. At a glucose concentration of 25 mM, the differences in OXPHOS between the control and IL-4 or E2 became less apparent for both cell lines. Furthermore, both cell lines displayed decreased OCR upon LPS stimulation at all three glucose concentrations. These results are consistent with previous literature on macrophages that indicated that IL-4 and E2 treatment increase mitochondrial OXPHOS, while LPS-treated cells display decreased mitochondrial OXPHOS (Keselman *et al.*, 2017; Viola *et al.*, 2019). An interesting finding was that the overall OCR of the RAW 264.7 cells in 25 mM glucose medium was markedly lower (ranging between 300 pmol/min/cell and 700 pmol/min/cell; Figure 10C) compared to that of the cells in 5 mM and 11 mM glucose medium (ranging from 450 pmol/min/cells to 1300 pmol/min/cell; Figure 10A and Figure B) for all treatment conditions. High glucose concentrations induce glycolysis (Lund *et al.*, 2019) which will result in more ATP production from glycolysis. If sufficient energy can be produced via glycolysis the cell will rely less on mitochondrial OXPHOS which will result in the downregulation of this pathway. This may explain the lower OCR observed for the RAW264.7 cells in 25 mM glucose medium. Comparison of the OCR of BMDMs with RAW 264.7 cells revealed that the OCR of the RAW 264.7 cells were remarkably (~10x) higher than the BMDMs. Considering the high proliferation rate of the RAW 264.7 cells (Chamberlain *et al.*, 2015), it is plausible that the respiration rate also increases to keep up with the energy demands of this high proliferation rate. This is in accordance with Venter *et al.* (2014) who found that the proliferation rate of RAW 264.7 cells was significantly reduced in the presence of the OXPHOS inhibitor oligomycin. Similar to the RAW 264.7 cells the basal respiration of the BMDMs decreased as glucose concentration increased.

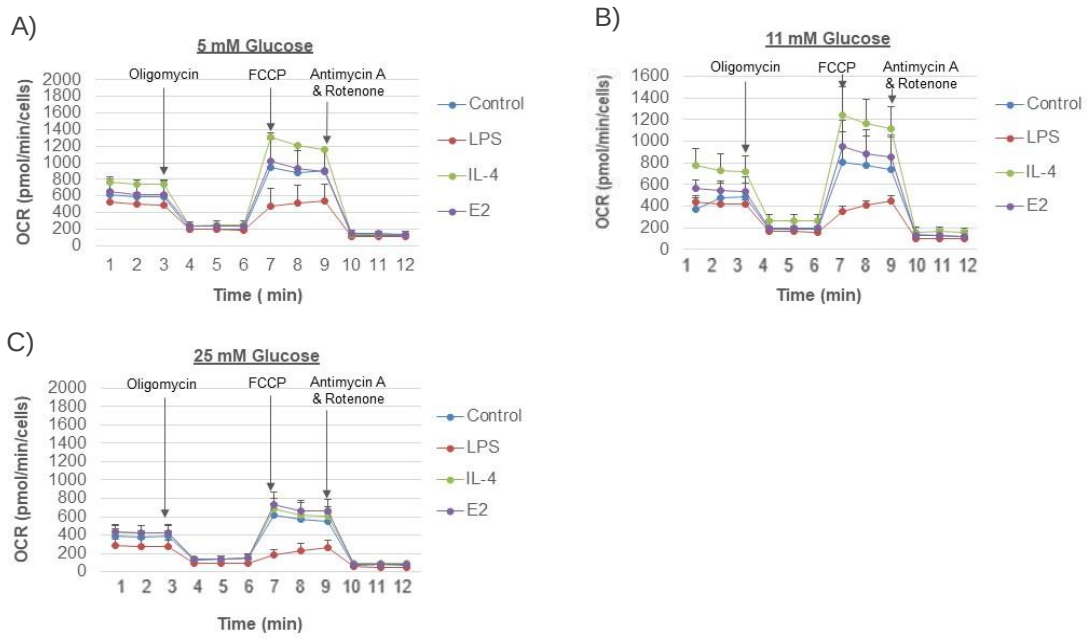

Figure 10: Oxygen consumption rate associated with mitochondrial OXPHOS (measured with the Seahorse XF Analyzer) of RAW 264.7 cells (in the presence and absence of 10 ng/mL LPS, 20 ng/mL IL-4, or 0.1 nM E2 for 24 hours) cultured with (A) 5 mM, (B) 11 mM, or (C) 25 mM glucose medium before and after the injection of ETC inhibitors (Oligomycin, Antimycin A and Rotenone) or uncoupler (FCCP) over a course of 12 min. Error bars represent standard deviation of replicate measurements of control (n=6) and treated samples (n=8).

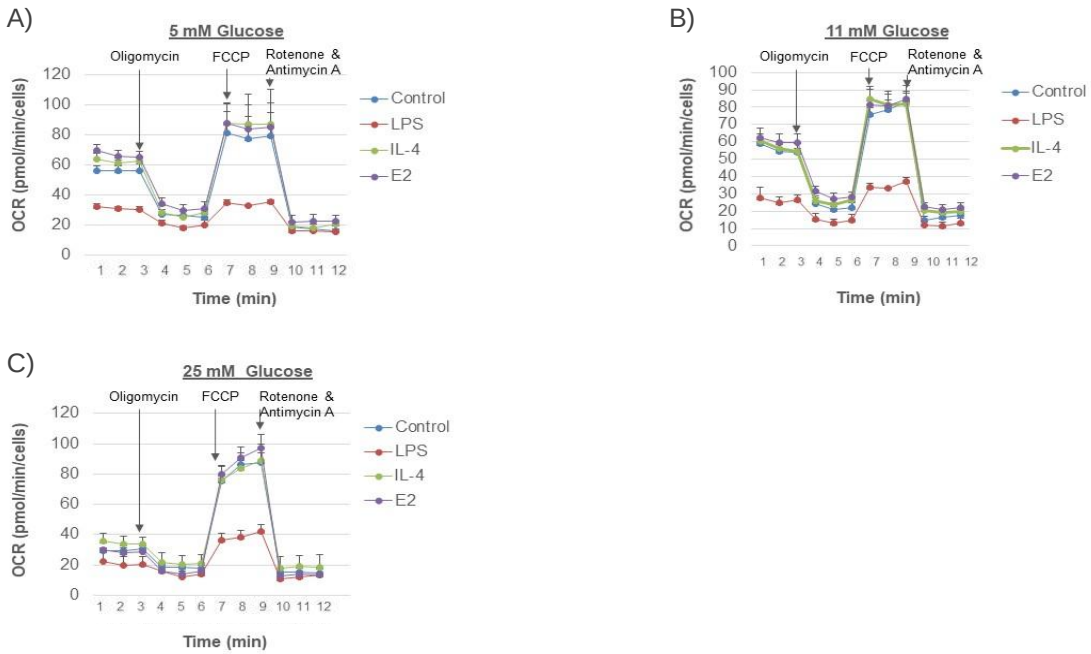

Figure 11: Oxygen consumption rate associated with mitochondrial OXPHOS (measured with the Seahorse XF Analyzer) of BMDMs (in the presence and absence of 10 ng/mL LPS, 20 ng/mL IL-4, or 0.1 nM E2 for 24 hours) cultured with (A) 5 mM, (B) 11 mM, (C) or 25 mM glucose medium before and after the injection of ETC inhibitors (Oligomycin, Antimycin A and Rotenone) or uncoupler (FCCP) over a course of 12 min. Error bars represent standard deviation of replicate measurements of control (n=6) and treated (n=8) samples.

From the results presented in Figure 10 and Figure 11 the following assay parameters were calculated as explained in the materials and methods, section *3.3* and in Figure 5: (i) non-mitochondrial oxygen consumption, which is related to oxygen consumed in processes other than mitochondrial metabolism; (ii) basal respiration, which refers to the oxygen consumed to meet energy demands at baseline; (iii) maximal respiration, which is the maximum respiration that can be attained by the ETC during increased energy demands; (iv) proton leak, which is an indication of the basal respiration not linked to ATP production and can indicate mitochondrial impairment but can also be a way to regulate ATP production in cells with intact mitochondria; (v) OCR associated with ATP production, which is the percentage of basal respiration used to produce ATP; (vi) spare respiratory capacity, which is a measurement of how well the cell can respond to energy demands and also indicates how close the cell's respiration is to the theoretical maximum; and (vii) coupling efficiency, which refers to the portion of consumed oxygen used for ATP production (ATP-associated OCR/basal OCR).

Non-mitochondrial oxygen consumption

The assay parameters for the RAW 264.7 cells cultured with either 5 mM, 11 mM, or 25 mM glucose are shown in Figure 12 and that of the BMDMs in Figure 13. The OCR associated with non-mitochondrial respiration (Figure 12A and Figure 13A) did not significantly differ between the control and treatment groups, however, a high glucose concentration (25 mM) resulted in a decreased non-mitochondrial oxygen consumption of all polarized RAW 264.7 cells (treated with LPS, IL-4, or E2) and M2 polarized BMDMs (treated with E2 or IL-4) compared to the 5 mM and/or 11 mM glucose conditions. Other oxygen consuming processes besides mitochondrial OXPHOS may include cell-surface oxygen consumption. A study conducted by Herst and Berridge (2007) proved that cell surface oxygen consumption (via a NADH:oxidoreductase system in which electrons move from intracellular NADH to extracellular oxygen) in RAW 264.7 and transformed mouse macrophage cells (J774) may constitute a considerable part of total oxygen consumption (between 30% and 80%). Since high glucose may stimulate glycolysis and thereby increase lactate dehydrogenase (LDH) activity which oxidises NADH to NAD^+, it is possible that less NADH was available for cell surface oxygen consumption via the NADH: oxidoreductase system in the RAW264.7 cells in our study.

Basal respiration

Significant changes in the OCR for basal respiration (Figure 12B and Figure 13B) between the control and treatments were only observed for the RAW 264.7 cells cultured with 11 mM glucose and for the BMDMs cultured with 5 mM glucose: The basal respiration of the LPS-treated cells was significantly decreased compared to the control. This parameter was significantly increased

in IL-4-treated cells compared to the control. This corresponds with previous literature on macrophages (de Paula Assis *et al.*, 2022; Van den Bossche *et al.*, 2015). The E2-treated cells' basal respiration was also significantly increased compared to the control. Previous studies have also found an increase in mitochondrial oxygen consumption at baseline in E2-treated MCF-7 (mammary endothelial tumor) cells (Radde *et al.*, 2015). The same trends were observed for the RAW 264.7 cells cultured with 5 mM and 25 mM glucose and the BMDMs cultured with 11 mM and 25 mM glucose although the differences were not statistically significant. Furthermore, the reducing effect of both LPS and high (25 mM) glucose on basal respiration was more severe in the BMDMs than what was seen in the RAW 264.7 cells. For the IL-4 and E2 treatments a reduced basal respiration in BMDMs was also seen for the 11 mM compared to the 5 mM glucose group which may indicate that elevating the glucose to only 11 mM already induces a shift in the metabolic wiring of BMDMs.

OCR for ATP production

The results presented in Figure 12C and Figure 13C show that both high (25 mM) glucose conditions and treatment with LPS clearly reduced the OCR coupled to ATP production. This effect was much more prominent in the BMDMs compared to the RAW 264.7 cells. In RAW 264.7 cells significant changes in OCR between the control and treatments were only observed for the cells cultured with 11 mM glucose: the OCR of the LPS-treated cells was significantly decreased compared to the control. In the BMDMs, the OCR coupled to ATP production was significantly reduced in LPS-treated cells at all glucose concentrations. These results, again, are consistent with previous literature (Van den Bossche *et al.*, 2015). IL-4 and E2 treatment resulted in significant increases in this parameter at 11 mM glucose for RAW 264.7 cells and at 5 mM glucose for BMDMs, as has been shown previously in THP-1 macrophages in the presence of IL-4 (de Paula Assis *et al.*, 2022)) and MCF-7 breast cancer cells in the presence of E2 (Radde *et al.*, 2015).

Maximal respiration

The OCR values for maximal respiration in RAW 264.7 cells are shown in Figure 12D and that of BMDMs in Figure 13D. In this instance, significant reductions in the maximal respiration of LPS-treated cells compared to the control were visible for all three glucose conditions. The lower maximal respiration in LPS-treated macrophages was also previously observed (Van den Bossche *et al.*, 2015). On the other hand, the maximal respiration of the IL-4 cells was increased compared to the control, although this was only significant in the 5 mM and 11 mM glucose group (for the RAW 264.7 cells) and the 5 mM group (for the BMDMs). Furthermore, the OCR for this parameter was increased in the E2-treated cells, and this change was significant in the 11 mM

glucose group (for the RAW 264.7 cells) and the 5 mM group (for the BMDMs). These results agree with the work by Van den Bossche *et al.* (2015) on IL-4-treated macrophages and that of Yao *et al.* (2011) on E2-treated neuronal cells. This increased maximal respiration may indicate that the expression of genes involved in OXPHOS was upregulated in the cells treated with IL-4 and E2, thereby increasing their capacity to make use of mitochondrial OXPHOS during increased energy demands. In contrast with the RAW 264.7 results, a higher glucose concentration seemed to increase the maximal respiration of some treatments in the BMDMs: (i) The OCR of the 25 mM control was higher than the 5 mM; (ii) the OCR for the LPS-treated cells increased as glucose concentration increased; and (iii) the E2-treated cells cultured with 25 mM glucose was increased compared to the 11 mM glucose group. This is interesting since a group has previously found an increase in oxygen consumption in non-diabetic BMDMs under high glucose conditions (Ayala *et al.*, 2019), whereas another study which show that high glucose stimulates glycolysis was done on RAW 264.7 cells (Wang *et al.*, 2018). A possible explanation for a higher OCR in some OXPHOS parameters under high glucose conditions in BMDMs as opposed to a decreased OCR seen in RAW 264.7 cells is that RAW 264.7 cells are more dependent on glycolysis for ATP production than BMDMs (Németh *et al.*, 2016), and in order to recycle NADH back to NAD^+ to sustain glycolysis, pyruvate is converted to lactate instead of being oxidised via the TCA cycle. In support of this, we found that the basal ECAR of the RAW 264.7 cells (ranging from 160 pmol/min/cells-380 pmol/min/cells) was higher compared to that of the BMDMs which ranged from 35 pmol/min/cells-80 pmol/min/cells (refer to Annexure B, Figure B1 and Figure B2), while glucose consumption per cell appeared to be either the same or higher in BMDMs compared to RAW 264.7 cells (Figure 7B and Figure 9B). This may mean that in BMDMs proportionally more pyruvate is oxidised via the TCA cycle to generate NADH and FADH that drive OXPHOS compared to RAW 264.7 cells, meaning that glycolysis and OXPHOS are better coupled in BMDMs and therefore OXPHOS capacity is not downregulated under high glucose conditions in BMDMs.

Spare respiratory capacity

The spare respiratory capacity is shown for the RAW 264.7 cells in Figure 12E and that of the BMDMs in Figure 13E. This parameter was significantly reduced in LPS-treated BMDMs and RAW 264.7 cells compared to the control groups for all glucose conditions. In RAW 264.7 cells a high glucose concentration (25 mM) also resulted in a decreased spare respiratory capacity. This is in accordance with another study that found that hyperglycaemia leads to decreased spare respiratory capacity in renal cells (Czajka & Malik, 2016). In contrast, high glucose (25 mM) significantly increased the spare respiratory capacity of the control, LPS, IL-4, and E2-treated BMDMs compared to the 5 mM and 11 mM glucose conditions. This further supports the notion

that glycolysis is better coupled to OXPHOS in BMDMs and that BMDMs retain their capacity to use mitochondrial OXPHOS in times of high energy demands even at high glucose concentrations.

Proton leak

The OCR associated with proton leak in the RAW 264.7 cells and BMDMs are shown in Figure 12F and Figure 13F respectively. High glucose resulted in a lower proton leak for both the RAW 264.7 cells and BMDMs—an effect seen especially in LPS-treated BMDMs. These results correspond to previous work on macrophages in which it was found that LPS decreased the proton leak of these cells (Wang *et al.*, 2020). Low glucose has previously been shown to be associated with increased ROS production in aortic endothelial cells (Kajihara *et al.*, 2017). In turn, increased ROS production can increase proton leak (Brookes, 2005; Cheng *et al.*, 2017). This is considered a protective feedback loop through which further ROS production is limited. This may explain why the proton leak of cells at a lower glucose concentration is higher compared to a higher glucose condition.

Coupling efficiency

The coupling efficiency results for RAW 264.7 cells shown in Figure 12G indicate that 11 mM glucose was the only condition that did not result in any significant change in coupling efficiency for any of the treatments. At 5 mM glucose the coupling efficiency of both LPS-treated and E2-treated cells was impaired compared to the control. Low coupling efficiency can be due to oxygen not being used for oxidative phosphorylation and instead for processes such as ROS or heat production. This may indeed be the case for the LPS-treated cells, since these cells are known to produce ROS and heat as part of their inflammatory role to fight invading cells (More & Makola, 2020). Some studies such as that of Felty *et al.* (2005) state that estrogen stimulates ROS production, however, others mention that estrogen has anti-oxidative effects (Terrazas *et al.*, 2018). Furthermore, low glucose concentrations have been associated with an increase in mitochondrial reactive oxygen species (Kajihara *et al.*, 2017) due to the upregulation of mitochondrial metabolism (e.g. FA oxidation). Together, this may contribute to the reduced coupling efficiency observed. High glucose conditions seemed to increase coupling efficiency in the polarized (i.e., LPS-, IL-4-, and E2-treated) RAW 264.7 cells. This corresponds with a decreased proton leak compared to 5 mM and 11 mM glucose (Figure 11F) (Brown *et al.*, 2010). No significant changes in the coupling efficiency of the BMDMs were observed (Figure 13G) which correlated with what was seen for the RAW 264.7 cells at 11 mM glucose.

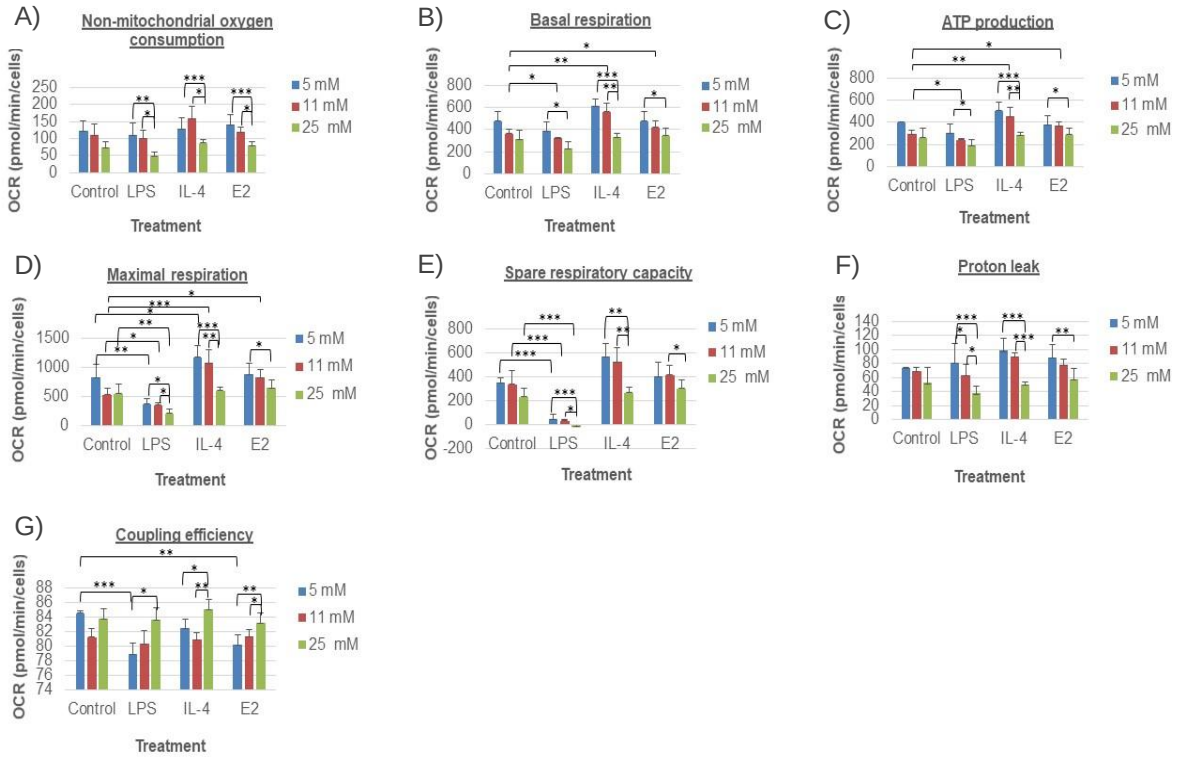

Figure 12: Mitochondrial respiration assay parameters associated with mitochondrial OXPHOS of RAW 264.7 cells cultured with 5 mM, 11 mM, or 25 mM (treated with or without 10 ng/mL LPS, 20 ng/mL IL-4, or 0.1 nM E2 for 24 hours). Error bars represent standard deviation of replicate measurements of control (n=6) and treated (n=8) samples. Two-way ANOVA with Bonferroni post-test was applied. Significant differences are indicated with stars (one star indicates a p<0.05; two stars indicate a p<0.01; three stars indicate a p<0.001).

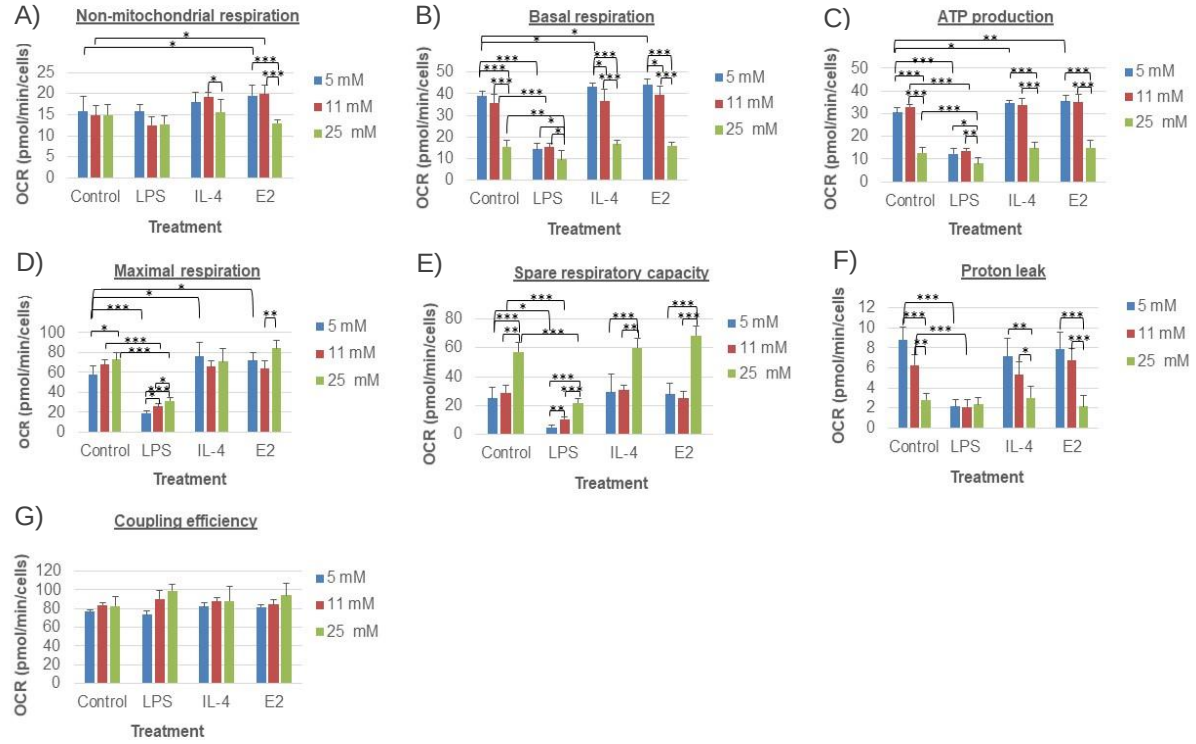

Figure 13: Mitochondrial respiration assay parameters associated with mitochondrial OXPHOS of BMDMs cultured with 5 mM, 11 mM, or 25 mM (treated with or without 10 ng/mL LPS, 20 ng/mL IL-4, or 0.1 nM E2 for 24 hours). Error bars represent standard deviation of replicate measurements of control (n=6) and treated (n=8) samples. Two-way ANOVA with Bonferroni post-test was applied. Significant differences are indicated with stars (one star indicates a p<0.05; two stars indicate a p<0.01; three stars indicate a p<0.001).

The following can be deduced from these results:

1. The mitochondrial OXPHOS may differ between cell lines (such as RAW 264.7 cells) and primary cells (such as BMDMs) since the mitochondrial OXPHOS of RAW 264.7 cells is higher than BMDMs.
2. The mitochondrial OXPHOS of LPS-treated (pro-inflammatory) cells is decreased in both RAW 264.7 cells and BMDMs and at all glucose concentrations (5 mM,11 mM, and 25 mM). On the other hand, the mitochondrial OXPHOS of IL-4-treated (anti-inflammatory) cells is increased in both RAW 264.7 cells and BMDMs and at all glucose concentrations (5 mM,11 mM and 25 mM). E2 treatment resulted in a bio-energetic profile more comparable to the IL-4-treated cells in both RAW 264.7 cells and BMDMs and at all glucose concentrations. However, most significant changes were observed at 11 mM glucose for RAW 264.7 cells and 5 mM for BMDMs.
3. Glucose concentration affects the bio-energetics of both RAW 264.7 cells and BMDMs. In polarized RAW 264.7 cells, a high glucose concentration decreases the mitochondrial OXPHOS parameters such as non-mitochondrial oxygen consumption, basal respiration, maximal respiration, OCR for ATP production, proton leak and spare respiratory capacity, but it increases coupling efficiency. In BMDMs (both naïve and polarized), a high glucose concentration decreases mitochondrial OXPHOS parameters such as non-mitochondrial oxygen consumption, basal respiration, OCR for ATP production, and proton leak, while maximal respiration and spare respiratory capacity is increased for a majority of treatments at a high glucose concentration.
4. Between the three glucose concentrations tested, a concentration of 11 mM appeared to be the optimal condition to use for RAW 264.7 cells since this concentration did not deviate too much from the physiological condition during the culturing period. The lowest (5 mM) and highest (25 mM) glucose conditions were considered not ideal conditions, since the cells are at risk of being in either a hypo- or hyperglycaemic state, respectively, during incubation. Moreover, the bio-energetics of the cells cultured with 11 mM glucose was also more comparable to previous literature on macrophages (de Paula Assis *et al.*, 2022; Van den Bossche *et al.*, 2015) and more distinctive differences between the treatment groups and the control were visible. Although the cells cultured with 5 mM glucose displayed high mitochondrial OXPHOS in general the proton leak of these cells were also the highest which could be an indication of mitochondrial damage due to the low glucose concentration. To prevent starvation of the cells one could consider refreshing growth medium daily when culturing RAW 264.7 cells in 5 mM glucose. However, this may also not be ideal since this might result in the loss of valuable growth factors (secreted by the

cells) which are important for cell health and proliferation. Moreover, as already described, the cells that were cultured with 5 mM glucose (which received fresh medium every day during the bio-energetics analysis) still displayed some parameters such as an increased proton leak and decreased coupling efficiency. On the other hand, although the cells cultured with the highest glucose (25 mM) had the lowest proton leak these cells' spare respiratory capacity was drastically impaired, especially when treated with LPS. The cells cultured with 11 mM glucose displayed a bio-energetic metabolism between these two extremes and was used for the remainder of the study.

5. A glucose concentration of 5 mM was chosen as the optimal condition to use for BMDMs since this concentration was the closest to physiological conditions during the differentiation period as compared to the other glucose conditions. The bio-energetics of the cells cultured with 5 mM glucose was also more comparable to previous literature on macrophages (de Paula Assis *et al.*, 2022; Van den Bossche *et al.*, 2015) and more discernible differences between the treatment groups and the control were visible. This glucose concentration was also most comparable to the results of the RAW 264.7 cells in terms of significant differences between the control and treatment groups.

4.4 Determining the effect of estrogen on the bio-energetic metabolism of pro- and anti-inflammatory macrophages using extracellular flux analyses.

As discussed in the literature review, macrophage phenotype and function are reciprocally coupled to its metabolic state. Although former studies have confirmed a role for E2 in macrophage function and polarization, little is known about how it affects the bio-energetic metabolism of macrophages, either in their naïve or their polarized state. In order to investigate this the cell lines were cultured at the chosen glucose condition and polarized to M1 (with LPS) and M2 (with IL-4) macrophages in the presence and absence of E2. The Mito Stress test results for the RAW 264.7 cells are depicted in Figure 14 and the BMDMs in Figure 15. The OCR values of the IL-4, E2, and IL-4+E2 groups were higher compared to the control for both cell types. In contrast, the LPS and LPS+E2 groups' overall OCR was lower than the control group.

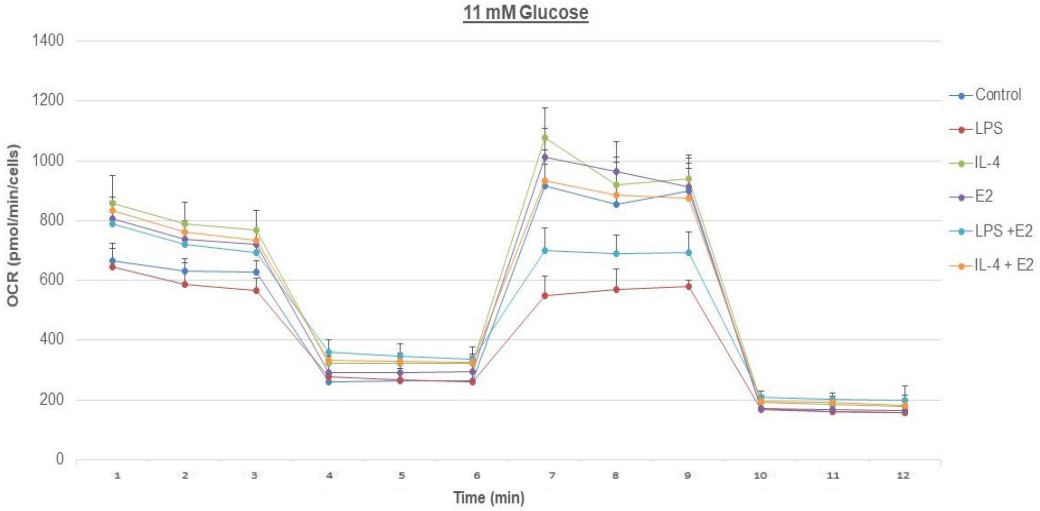

Figure 14: Oxygen consumption rate (measured with the Seahorse XF Analyzer) associated with mitochondrial OXPHOS of pro-inflammatory (treated with 10 ng/mL LPS) and anti-inflammatory (treated with 20 ng/mL IL-4) RAW 264.7 cells cultured with 11 mM glucose medium in the presence and absence of 0.1 nM E2 before and after the injection of ETC inhibitors (Oligomycin, Antimycin A and Rotenone) or uncoupler (FCCP) over a course of 12 min. Error bars represent standard deviation of replicate measurements of control (n=10) and treated (n=12) samples.

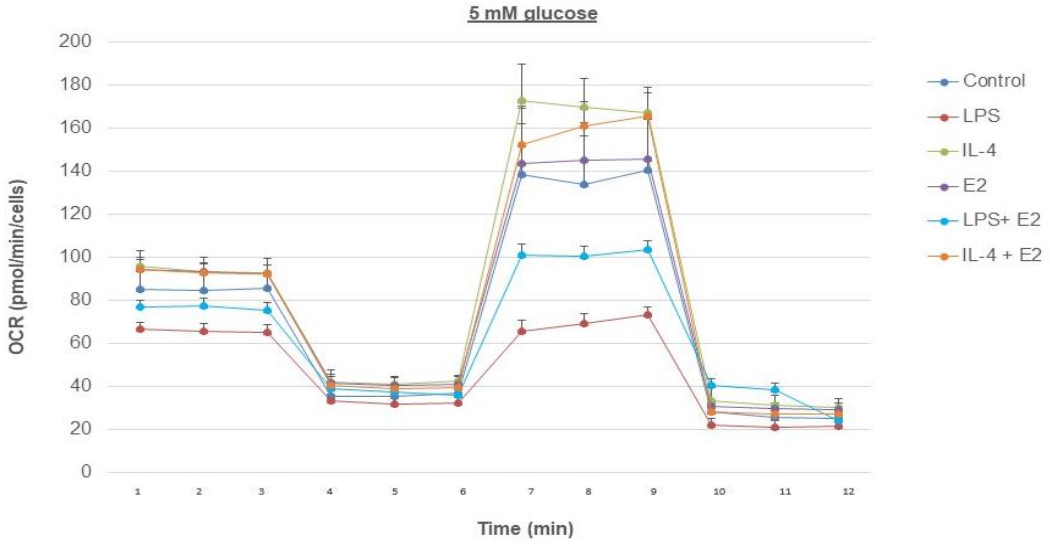

Figure 15: Oxygen consumption rate (measured with the Seahorse XF Analyzer) associated with mitochondrial OXPHOS of pro-inflammatory (treated with 10 ng/mL LPS) and anti-inflammatory (treated with 20 ng/mL IL-4) BMDMs cultured with 5 mM glucose medium in the presence and absence of 0.1 nM E2 before and after the injection of ETC inhibitors (Oligomycin, Antimycin A and Rotenone) or uncoupler (FCCP) over a course of 12 min. Error bars represent standard deviation of replicate measurements of control (n=10) and treated (n=12) samples.

The parameters associated with mitochondrial respiration were calculated for both cell lines. The OCR associated with basal respiration, maximal respiration, and ATP production of both cell lines treated with IL-4, E2, or a combination of the two were significantly increased compared to the control as well as an increase in spare respiratory capacity in BMDMs. Significant reductions in the OCR associated with basal respiration, maximal respiration, ATP production and spare respiratory capacity were observed for the LPS-treated cells in both cell lines. However, there was no significant difference in OCR for most parameters between the IL-4 group and IL-4+E2 group, suggesting that the anti-inflammatory effect of E2 does not further increase the OXPHOS activity of cells that are already in an anti-inflammatory state. Estrogen treatment did, however, significantly increase the OCR for basal respiration, maximal respiration, ATP production, and spare respiratory capacity of LPS-treated cells (Figure 16, turquoise bars) in both cell lines as well as an increase in coupling efficiency of BMDMs. E2, therefore, caused a metabolic shift towards a more oxidative metabolism in the inflammatory macrophages. This may indicate that estrogen can cause a shift in the polarization state of pro-inflammatory macrophages towards a phenotype more comparable to naïve cells (since no significant changes between control and LPS+E2 were visible for most parameters). This may imply that the activation of pro-inflammatory macrophages may be dampened in tissues (such as mammary tissue) where the cells are chronically exposed to E2. This may favour tumour development in these tissues since the number of pro-inflammatory macrophages, which fight cancer, is limited.

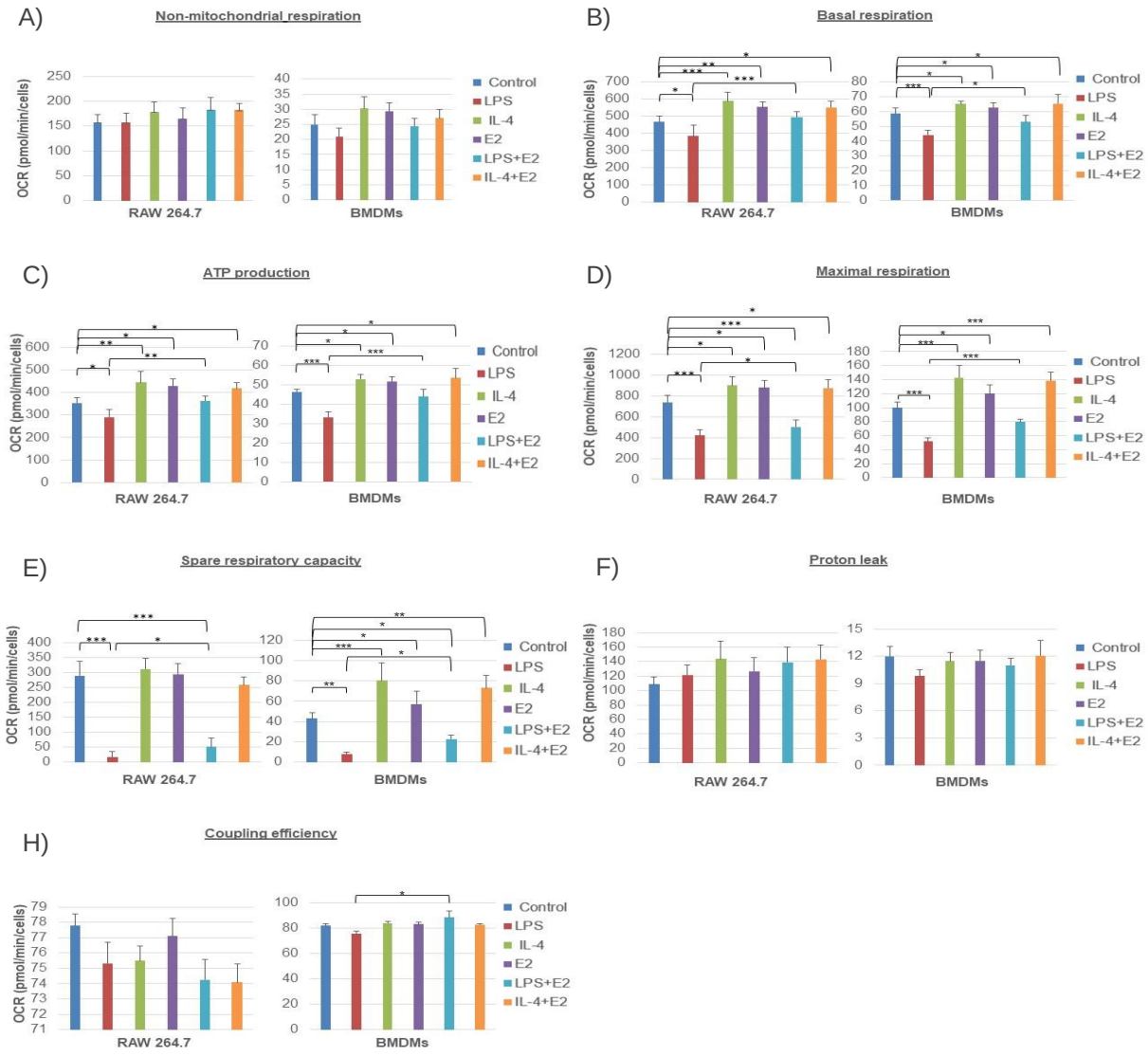

Figure 16: Mitochondrial respiration assay parameters associated with mitochondrial OXPHOS of RAW 264.7 cells and BMDMs cultured with 11 mM and 5 mM glucose, respectively (treated with or without 10 ng/mL LPS, 20 ng/mL IL-4, 0.1 nM E2, LPS (10 ng/mL)+E2 (0.1 nM) or IL-4 (20 ng/mL) +E2 (0.1 nM) for 24 hours). Error bars represent standard deviation of replicate measurements of control (n=10) and treated (n=12) samples. One-way ANOVA with Bonferroni post-test was applied. Significant differences are indicated with stars (one star indicates a p<0.05; two stars indicate a p<0.01; three stars indicate a p<0.001).

4.5.1 LC-MS/MS sample preparation optimisation

The method described by Jacobs (2018) focuses on the analysis of EM in urine. In this study, EM in cell culture medium was analysed. Therefore, the sample preparation had to be optimised. Cell culture medium from RAW264.7 cells (and not BMDMs) was used for optimisation since these cells are easily cultured and cell stocks are readily available.

Matrix effect evaluation

In order to determine whether there were any matrix effects, the response of the metabolites of interest (listed in Table 10) in control and spiked cell culture medium was compared to that in spiked water samples. The results are shown in Table 11 where increased responses (relative to water-spiked samples) are indicated in red and decreased responses in blue. The media that contained no standards displayed high background responses for some of the polar metabolites (estradiol-3-sulphate, estradiol-17 sulphate, and estrone-3-sulphate). The spiked media yielded increased responses for all the polar metabolites as well as the non-polar metabolite estrone-2-hydroxy-3-methyl ether which may indicate enhanced ionisation as a result of the cell culture medium matrix. On the contrary, the responses of the non-polar metabolites, estriol, 2- and 4-methoxyestrone, 2-methoxyestradiol, and 2- and 4-hydroxyestrone/estradiol metabolites in the spiked media were lower than the spiked water samples. This indicates possible interference of the matrix, leading to diminished ionisation of these metabolites.

Table 10: List of estrogen metabolites analysed

Polar conjugated metabolites (water-soluble)	Non-polar unconjugated metabolites (less water-soluble)
Estriol-3-sulfate Estradiol-3-sulfate Estradiol-17-sulfate Estrone-3-sulfate Estriol-16-glucuronide Estradiol-3-glucuronide Estrone-3-glucuronide	Testosterone Androstenedione Progesterone Estriol 16-Epiestriol 17-Epiestriol Estrone 16-Hydroxystrone Estrone-2-hydroxy-3-methyl ether 2-Methoxyestrone 4-Methoxyestrone 2-Hydroxyestrone 4-Hydroxyestrone Estradiol Alpha Estradiol Beta 16-Ketoestradiol 2-Methoxyestradiol 4-Methoxyestradiol 2-Hydroxyestradiol 4-Hydroxyestradiol

Table 11: A comparison of the relative response of the complete media samples and standard-spiked media samples as a ratio of the response of standard-spiked water samples

Metabolite	Complete media		Complete media +standard	
	Ratio	Stdev	Ratio	Stdev
Estriol-3-sulphate	ND	-	1.91	0.28
Estradiol-3-sulphate	0.32	0.11	13.83	2.08
Estradiol-17-sulphate	4.18	0.45	4.12	0.41
Estrone-3-sulphate	0.87	0.12	2.19	0.11
Estriol-16-glucuronide	0.10	0.02	2.04	0.04
Estradiol-3-glucuronide	ND	-	1.69	0.26
Estrone-3-glucuronide	0.05	0.02	1.52	0.14
Testosterone	ND	-	0.85	0.05
Androstenedione	ND	-	0.87	0.05
Progesterone	0.03	-	1.07	0.14
Estriol	ND	-	0.36	0.02
16-Epiestriol	ND	-	0.79	0.04
17-Epiestriol	ND	-	0.85	0.07
Estrone	ND	-	0.84	0.09
16-Hydroxyestrone	ND	-	0.80	0.05
Estrone-2-hydroxy-3-methyl ether	ND	-	4.5	1.66
2-Methoxyestrone	ND	-	0.34	0.20
4-Methoxyestrone	ND	-	0.54	0.19
2-Hydroxyestrone	ND	-	ND	-
4-Hydroxyestrone	ND	-	0.13	0.07
Estradiol Alpha	0.01	0.01	0.86	0.09
Estradiol Beta	ND	-	0.84	0.08
16-Ketoestradiol	ND	-	0.76	0.06
2-Methoxyestradiol	ND	-	0.48	0.24
4-Methoxyestradiol	ND	-	0.80	0.29
2-Hydroxyestradiol	0.03	0.01	0.42	0.11
4-Hydroxyestradiol	0.01	0.003	0.15	0.04

**Not detected (ND)*

Identification of component/components of cell culture medium that contribute to matrix effect

In order to eliminate the effect of the matrix on responses as far as possible the component/components in the cell culture medium that caused matrix effects had to be identified. Some components of cell culture medium such as FBS (which can contain low levels of estrogens), phenol-red (a weak estrogen) (De Faria *et al.*, 2016) and serum-proteins which can bind to estrogens (Chiu *et al.*, 2010) were identified as possible contributors to matrix effects. Therefore, the response of serum-free medium, phenol-red free medium, protein-precipitated medium, and 10% FBS in water was analysed and compared to complete culture media (containing 10% FBS, phenol-red, and proteins). Table 12 presents the response values of the seven conjugated metabolites (three of which gave increased responses, shown in red in Table 11) and the non-polar metabolite estrone-hydroxy-3-methyl ether relative to the complete media. From this data it was clear that the presence of 10% FBS contributed to the increased responses observed for these metabolites. This is evident from the high relative response values for the 10% FBS in water samples in Table 12 (shown in red) indicating comparable background responses, and the reduction in the relative response values of six of the seven conjugates in the serum-free medium samples (shown in blue) indicating reduced background responses. This suggests that FBS supplementation of the medium could be contributing to matrix effects seen for these metabolites. To determine to what extent the proteins that are present in FBS may contribute to the matrix effects, protein precipitation was also tested. This seemed to be a viable option to decrease matrix effects since the relative response for all seven of the conjugated metabolites and estrone-2-hydroxy-3-methyl ether was reduced (shown in green). It was, therefore, decided to use cell culture medium that contained less serum and of which the proteins were precipitated prior to SPE for the remainder of the study.

Table 12: A comparison of the relative response of phenol-red-free medium, serum-free medium, 10% FBS in water, and protein-precipitated media as a ratio of the response of medium only samples.

Metabolite	Phenol-red-free medium		Serum-free medium		Protein-precipitated medium		10% FBS in H_2O	
	Ratio	Stdev	Ratio	Stdev	Ratio	Stdev	Ratio	Stdev
Estriol-3-sulphate	0.01	0.02	0.15	0.09	ND	-	0.83	0.09
Estradiol-3-sulphate	ND	-	ND	-	0.06	0.10	0.66	0.16
Estradiol-17-sulphate	0.33	0.02	0.37	0.07	0.14	0.02	0.32	0.07
Estrone-3-sulphate	ND	-	ND	-	ND	-	2.5	1.50
Estriol-16-glucuronide	0.61	0.56	0.15	0.10	0.33	0.20	1	0.15
Estradiol-3-glucuronide	0.54	0.54	0.31	0.10	0.21	0.27	0.53	0.25
Estrone-3-glucuronide	0.11	0.10	ND	-	0.09	0.05	0.38	0.05
Estrone-2-hydroxy-3-methyl ether	0.28	0.14	0.26	0.04	0.04	0.07	1.23	1.74

**Not detected (ND)*

Evaluating the effect of different mobile phase gradients on response of quenched metabolites

Another observation made while evaluating matrix effects, was a quenched response (a reduced detector response because of matrix effects) of some non-polar metabolites (Estriol, 2- and 4-methoxyestrone, 2- and 4-hydroxyestrone,2-methoxyestradiol, and 2- and 4-hydroxyestradiol) in spiked medium samples compared to spiked water samples (shown in blue in Table 11). This could have been a result of other components in the cell culture medium entering the ionisation source along with these metabolites of interest, thereby reducing the ionisation efficiency and detection of the metabolites of interest. In an attempt to elute these impurities in another fraction from the column and prevent them from entering the ionisation source together with the metabolites of interest, the mobile phase gradients were adjusted as indicated in Table 3. However, none of the gradients proved to substantially increase the response of the above-mentioned metabolites (Annexure B, Table B1).

Full scan analysis of cell culture medium

A full scan of the cell culture medium was done to get an overview of all the components in the medium that enter the ionisation chamber along with the quenched metabolites (shown in blue in

Table 11) and that can possibly interfere with the ionisation of these metabolites. It was found that there were a lot of other impurities in the cell culture medium with similar m/z ratios to the metabolites of interest and it was clear that these had to be eliminated to reduce the quenching effect in the ionisation source.

Double SPE

Since adaptation of the mobile phase gradient did not resolve the issue of the quenching effect seen for the metabolites in blue in Table 11, a second strategy for eliminating these culture medium impurities was followed. This entailed a double SPE of the fractions which contained the non-polar metabolites (and quenched metabolites shown in blue in Table 11). Different elution concentrations (40%, 50%, 60%, 70%, 100% and then only 80% and 100%) of methanol were also evaluated to determine whether the problematic metabolites may elute in fractions that were not collected before. However, no detectable peaks for the metabolites in Table 11 were found in any of the gradients tested and the responses compared to the water-spiked samples were not improved.

SPE: Effect of column volume

Another troublesome observation was that only some of the metabolites of interest (shown in purple in Table 13) seemed to be elevated in culture medium from cells treated with E2 compared to a control medium that contained no cells. It could either be that most metabolites are not produced by RAW 264.7 cells or that the concentration of the metabolites in 2 mL cell culture medium is too low to be detected by the instrument. To rule out the latter and increase the metabolite concentration in the final samples, the volume of collected cell culture medium was increased. However, it is important to ensure that the SPE column is not overloaded when using high volumes, because the retention and separation of metabolites can be affected negatively. To test this, the metabolite responses of two spiked sample volumes (15 mL and 2 mL) were compared (Table 14). The responses for the higher volume (15 mL) did not drastically differ from the lower volume (2 mL) and, therefore, a higher volume of cell culture medium could be loaded on the SPE columns without overloading the column and affecting the response of the metabolites.

Table 13: A comparison of the relative response of the media collected from cells treated with E2 as a ratio of the media that contained no cells

Metabolite	Ratio	Stdev	Metabolite	Ratio	Stdev
Estriol-3-sulphate	0.8	2.9	16-Hydroxyestrone	0.95	0.59
Estradiol-3-sulphate	1.7	0.001	Estrone-2-hydroxy-3-methyl ether	0.99	0.59
Estradiol-17-sulphate	0.9	0.4	2-Methoxyestrone	0.003	0.002
Estrone-3-sulphate	1.0	0.5	4-Methoxyestrone	0.26	0.04
Estriol-16-glucuronide	0.8	0.2	2-Hydroxyestrone	0.74	0.16
Estradiol-3-glucuronide	3.8	1.2	4-Hydroxyestrone	0.85	0.47
Estrone-3-glucuronide	1.1	0.001	Estradiol Alpha	13.03	8.33
Testosterone	0.95	0.32	Estradiol Beta	1.26	0.99
Androstenedione	0.86	0.34	16-Ketoestradiol	1.24	0.75
Progesterone	1.22	0.19	2-Methoxyestradiol	0.56	0.51
Estriol	0.96	0.53	4-Methoxyestradiol	ND	-
16-Epiestriol	0.96	0.12	2-Hydroxyestradiol	0.03	0.03
17-Epiestriol	2.24	0.89	4-Hydroxyestradiol	0.11	0.09
Estrone	0.96	0.22			

**Not detected (ND)*

Table 14: A comparison of the relative response of the 2 mL standard-spiked media as a ratio of the response 15 mL standard-spiked media.

Metabolite	Ratio	Stdev	Metabolite	Ratio	Stdev
Estriol-3-sulphate	1	0.37	16-Hydroxyestrone	0.78	0.04
Estradiol-3-sulphate	0.99	0.023	Estrone-2-hydroxy-3-methyl ether	1.2	0.08
Estradiol-17-sulphate	1.27	0.30	2-Methoxyestrone	1.1	0.05
Estrone-3-sulphate	0.98	0.20	4-Methoxyestrone	1.1	0.05
Estriol-16-glucuronide	0.80	0.28	2-Hydroxyestrone	0.72	0.11
Estradiol-3-glucuronide	0.91	0.33	4-Hydroxyestrone	0.79	0.073
Estrone-3-glucuronide	0.93	0.31	Estradiol Alpha	1.2	0.03
Testosterone	0.56	0.05	Estradiol Beta	1.06	0.03
Androstenedione	0.73	0.005	16-Ketoestradiol	0.86	0.3
Progesterone	0.84	0.04	2-Methoxyestradiol	1.4	0.04
Estriol	0.95	0.12	4-Methoxyestradiol	1.2	0.13
16-Epiestriol	0.88	0.02	2-Hydroxyestradiol	1.05	0.25
17-Epiestriol	0.99	0.09	4-Hydroxyestradiol	0.91	0.14
Estrone	1.1	0.03			

**Not detected (ND)*

Liquid-liquid extraction

Although SPE appeared not to be an ideal clean-up method for the quenched metabolites in Table 11, it was efficient for most of the other metabolites. In order to determine whether a different clean-up method would result in better responses for the problematic metabolites, a combined clean-up method (SPE and LLE [for non-polar metabolites]) was then considered. An LLE clean-up was compared to the SPE clean-up method for the quenched metabolites and the relative responses compared in Annexure B, Table B2. The LLE method did not significantly improve the response of the metabolites in the water or medium samples. It was clear that the SPE method delivered better results.

LLE: Effect of salt and pH

To see whether a more acidic pH and salting out will improve the separation between the organic and water phase and better solubility of the quenched metabolites in the organic phase during LLE, the pH of the samples was then adjusted with 2 M HCl and NaCl added. However, the adjustment of the pH and addition of salt did not drastically improve the response of the metabolites in culture medium and it was clear that the SPE method still produced better results than the LLE method (Annexure B, Table B3).

SPE: Effect of column type and sample loading

In a further attempt to eliminate the culture medium impurities that can interfere with the ionisation of the quenched metabolites (shown in blue in Table 11) a different SPE column (with a bigger loading volume) and increased washing and elution volumes were tested (Table 15). Most of the quenched metabolites appeared to elute in the 100% methanol and 100% acetone fraction (after the column was washed with 30% and 45% methanol) for both medium containing FBS and medium without FBS. It was also interesting that the majority of quenched metabolites also appeared to elute in a second 100% acetone wash. This could mean that a great deal of these metabolites were not captured in the first SPE methods, which could have resulted in the low responses observed for these problem metabolites. By using a combination of a new column (Polymeric Reversed Phase), increased sample loading volume of 50 mL, and increased washing and elution volumes, the response of the quenched metabolites markedly increased to quantifiable levels compared to the response obtained with the original method. This adjusted method was, therefore, used for the remainder of the study.

Table 15: A comparison of the relative response of standard-spiked media (with or without FBS) extracted with different methanol concentrations to the standard-spiked media extracted with the original method.

	Spiked media (no FBS)					
Metabolite	**30% MeOH**	**45% MeOH**	**100% MeOH (with prior 30% and 45% MeOH wash)**	**100%Acetone (with prior 30% and 45% MeOH wash)**	**100% MeOH**	**2x 100% acetone**
	Ratio	**Ratio**	**Ratio**	**Ratio**	**Ratio**	**Ratio**
Estriol	ND	-	2.75	0.05	2.74	0.11
2-Methoxyestrone	ND	-	5.39	4.41	0.79	13.60
4-Methoxyestrone	0.006	0.008	19.23	4.63	0.13	32.59
2-Hydroxyestrone	0.01	0.01	21.50	2.85	3.64	37.05
4-Hydroxyestrone	0.02	0.02	41.64	15.68	27.72	66.20
2-Methoxyestradiol	0.001	0.002	20.97	0.20	15.20	2.69
2-Hydroxyestradiol	0.06	0.03	26.20	0.28	14.22	3.80
4-Hydroxyestradiol	0.16	0.47	38.81	0.92	26.20	13.57
	Spiked media (with FBS)					
Metabolite	**30% MeOH**	**45% MeOH**	**100% MeOH (with prior 30& and 45% MeOH wash)**	**100% Acetone (with prior 30% and 45% MeOH wash)**	**100% MeOH**	**2x 100% acetone**
	Ratio	**Ratio**	**Ratio**	**Ratio**	**Ratio**	**Ratio**
Estriol	ND	-	2.50	0.06	2.42	0.12
2-Methoxyestrone	ND	-	5.42	4.67	0.07	19.20
4-Methoxyestrone	0.008	0.009	19.19	3.90	0.02	34.81
2-Hydroxyestrone	ND	-	21.20	3.74	0.22	31.40
4-Hydroxyestrone	0.01	0.009	20.50	22.48	1.73	80.93
2-Methoxyestradiol	0.007	0.006	14.99	0.21	3.71	10.30
2-Hydroxyestradiol	0.10	0.05	17.46	0.32	1.47	17.80
4-Hydroxyestradiol	0.37	0.50	19.41	1.13	3.58	30.60

SPE: Effect of pH and ascorbic acid

As part of further optimisation of the method (described in the previous paragraph), for the quenched metabolites, modifications to the derivatisation procedure was evaluated to investigate whether this would further improve the method. Different volumes of dansylchloride, sodium bicarbonate, pH of sodiumbicarbonate as well as the addition of ascorbic acid were evaluated. The difference in response between the original derivatisation method and the adjusted methods are shown in Annexure B, Table B4. No apparent improvement of response was visible upon adjusting the pH and addition of ascorbic acid for both water and medium samples. The original derivatisation method still proved to deliver the best results and was, therefore, used for the remainder of the study.

4.5.2 Linearity, limits of detection and limits of quantification

After optimising the sample preparation steps, a standard curve was prepared for the quantification of the estrogen metabolites in cell culture medium and the determination of the LOD and LOQ. However, the method displayed poor linearity for all the polar metabolites (r^2<0,99), whereas the non-polar metabolites displayed good linearity as shown in Table 16 and Annexure B (Figure B3).

Table 16: R^2 Values of metabolites with clean-up

Metabolite	R^2 value	Metabolite	R^2 value
Estriol-3-sulphate	0.87	16-Hydroxyestrone	0.99
Estradiol-3-sulphate	0.01	Estrone-2-hydroxy-3-methyl ether	0.99
Estradiol-17-sulphate	0.02	2-Methoxyestrone	0.99
Estrone-3-sulphate	0.01	4-Methoxyestrone	0.99
Estriol-16-glucuronide	0.07	2-Hydroxyestrone	0.99
Estradiol-3-glucuronide	0.5	4-Hydroxyestrone	0.99
Estrone-3-glucuronide	0.01	Estradiol Alpha	0.99
Testosterone	0.99	Estradiol Beta	0.99
Androstenedione	0.99	16-Ketoestradiol	0.99
Progesterone	0.99	2-Methoxyestradiol	0.99
Estriol	0.99	4-Methoxyestradiol	0.99
16-Epiestriol	0.99	2-Hydroxyestradiol	0.99
17-Epiestriol	0.99	4-Hydroxyestradiol	0.98
Estrone	0.99		

A second standard series, which did not undergo SPE, was prepared, to determine if the clean-up process resulted in non-linearity of the polar metabolites. The standard curves of most of the polar metabolites were linear (Table 17 and Annexure B, Figure B4) and it was evident that the SPE clean-up for the polar metabolites had to be optimised to ensure linearity of the polar metabolites with clean-up as well.

Table 17: R^2 values of metabolites without clean-up

Metabolite	R^2 value
Estriol-3-sulphate	0.99
Estradiol-3-sulphate	0.99
Estradiol-17-sulphate	0.99
Estrone-3-sulphate	0.99
Estriol-16-glucuronide	0.99
Estradiol-3-glucuronide	0.99
Estrone-3-glucuronide	0.98

In order to determine whether the polar metabolites may elute in earlier wash steps, fractions were collected after the water, 5%, 30% and 45% MeOH wash steps. These fractions were analysed with LC-MS/MS and the relative responses compared (Table 18). Most metabolites appeared to elute in both 30% and 45% methanol and, therefore, both these concentrations were used for the elution of the polar metabolites and both fractions were analysed.

Table 18: Comparison of the relative response of metabolites in standard-spiked media samples eluted with different solvents and concentrations

Metabolite	H_20	5% MeOH	30% MeOH	45% MeOH
Estriol-3-sulphate	ND	ND	0.06	0.74
Estradiol-3-sulphate	0.01	0.01	0.05	0.80
Estradiol-17-sulphate	ND	ND	ND	0.19
Estrone-3-sulphate	ND	ND	0.44	0.43
Estriol-16-glucuronide	0.05	0.03	0.03	0.75
Estradiol-3-glucuronide	ND	ND	ND	0.86
Estrone-3-glucuronide	ND	ND	0.12	0.25

**Not detected (ND)*

After the above-mentioned modification to the method, standard curves for three out of the seven polar metabolites (namely estriol-3-sulphate, estriol-16-glucuronide, and estradiol-3-glucuronide) along with all the non-polar metabolites were obtained with good linearity (r^2>0.99). However, the following metabolites still showed poor linearity and could, therefore, not be accurately quantified in this study: Estrone-3-glucuronide, estradiol-3-sulphate, estrone-3-sulphate and estradiol-17-sulphate (Table 19 and Annexure B, Figure B5).

Table 19: R^2 values of final standard curve

Metabolite	R^2 value	Metabolite	R^2 value
Estriol-3-sulphate	0.99	16-Hydroxyestrone	0.99
Estradiol-3-sulphate	0.001	Estrone-2-hydroxy-3-methyl ether	0.99
Estradiol-17-sulphate	0.003	2-Methoxyestrone	0.99
Estrone-3-sulphate	0.005	4-Methoxyestrone	0.99
Estriol-16-glucuronide	0.99	2-Hydroxyestrone	0.99
Estradiol-3-glucuronide	0.99	4-Hydroxyestrone	0.99
Estrone-3-glucuronide	0.006	Estradiol Alpha	0.99
Testosterone	0.99	Estradiol Beta	0.99
Androstenedione	0.99	16-Ketoestradiol	0.99
Progesterone	0.99	2-Methoxyestradiol	0.99
Estriol	0.99	4-Methoxyestradiol	0.99
16-Epiestriol	0.99	2-Hydroxyestradiol	0.99
17-Epiestriol	0.99	4-Hydroxyestradiol	0.99
Estrone	0.99		

The LOD and LOQ were then determined with the linear regression method for each of the quantifiable metabolites (see Table 19) and are presented in Table 20.

Table 20: LOD and LOQ of the different metabolites

Metabolite	LOD (ng/mL)	LOQ (ng/mL)	Metabolite	LOD (ng/mL)	LOQ (ng/mL)
Estriol-3-sulphate	2.28	6.91	2-Methoxyestrone	1.61	4.87
Estriol-16-glucuronide	1.47	4.47	4-Methoxyestrone	1.50	4.54
Estradiol-3-glucuronide	2.40	7.28	2-Hydroxyestrone	2.02	6.12
Testosterone	1.17	3.54	4-Hydroxyestrone	0.63	1.91
Androstenedione	1.62	4.90	Estradiol Alpha	2.57	7.79
Progesterone	1.53	4.65	Estradiol Beta	0.47	1.43
Estriol	1.56	4.73	16-Ketoestradiol	2.21	6.69
16-Epiestriol	2.38	7.20	2-Methoxyestradiol	1.04	3.15
17-Epiestriol	0.96	2.90	4-Methoxyestradiol	0.87	2.62
Estrone	1.76	5.34	2-Hydroxyestradiol	2.72	8.26
16-Hydroxyestrone	1.63	4.95	4-Hydroxyestradiol	2.89	8.76
Estrone-2-hydroxy-3-methyl ether	2.16	6.65			

4.5.3 Final LC-MS/MS analysis of estrogen metabolites in cell culture medium

After completing all the optimisation steps described in *3.4.4*, cell culture medium from RAW 264.7 cells treated with LPS and IL-4, respectively in the presence of E2 were collected and analysed for the presence of estrogen biotransformation metabolites and precursors. Out of the 27 metabolites analysed, only the concentration of estradiol alpha in the treatments was above the LOD (Annexure B, Table B5) when the linear regression method was used to determine LOD and LOQ. Therefore, a second method to estimate LOD and LOQ, namely, the S/N ratio method was applied (Annexure B, Table B6). The S/N ratio of the following metabolites were above three (sufficient for estimating LOD) and above ten (sufficient for estimating LOQ): 17-epiestriol, estrone, estradiol alpha, and estradiol beta. The concentrations of these metabolites in the medium of the treated cells are shown as a fold change of the control medium without cells in Figure 17. A fold change of at least 1,5 (which shows a possible increase/decrease) was seen for estradiol beta in LPS-treated cells and estradiol alpha in all of the treatments. It therefore appears as if the RAW 264.7 cells are able to synthesise estrogen (for e.g. from cholesterol but not to biotransform this steroid since no phase I or II metabolites could be detected. It is also clear that considerably more estradiol alpha (~15-20X) was present in the cell culture medium compared with estradiol beta. Estradiol alpha and estradiol beta are enantiomers (Stout *et al.*, 2017) and

Toran-Allerand *et al.* (2005) has shown that interconversion between the two is possible as 17-β-estradiol can be converted to estrone which then, in turn, can be converted to 17-α-estradiol (Figure 18). However, estradiol alpha production has not been studied thoroughly yet. It is, therefore, possible that the majority of estradiol beta formed by macrophages are converted to the less biologically active estradiol alpha. Although estradiol beta is the most well-known enantiomer involved in tumourigenesis, work by Edwards and McGuire (1980) showed that estradiol alpha is also active in breast tumour cells and can reverse the inhibition of proliferation. It is possible, then, that the estradiol alpha produced by macrophages may play a role in tumourigenesis of estrogen dependent tissues (such as mammary tissue). However, more research is needed on this to get a full picture of the estrogen biotransformation pathways that are active in macrophages before their role in tumourigenesis can be established.

To determine whether production of the four detectable metabolites is influenced by polarization state, the concentrations were normalised to cell number (Figure 19). The concentrations of all four of the metabolites in LPS+E2 cells was increased compared to the IL-4+E2 and E2 treatments. A study by Ferranti *et al.* (2018) demonstrated that LPS treatment increased estrogen levels in the ovaria of heifers through the modulation of aromatase expression via beta-catenin signaling. Furthermore, pro-inflammatory macrophages are known to produce pro-inflammatory cytokines such as TNF-α which, in turn, activates aromatase which produce estradiol and estrone (further metabolised to 17-epiestriol) (Mercogliano *et al.*, 2020). Further research is, however, needed to elucidate the biochemical pathways that may be involved here.

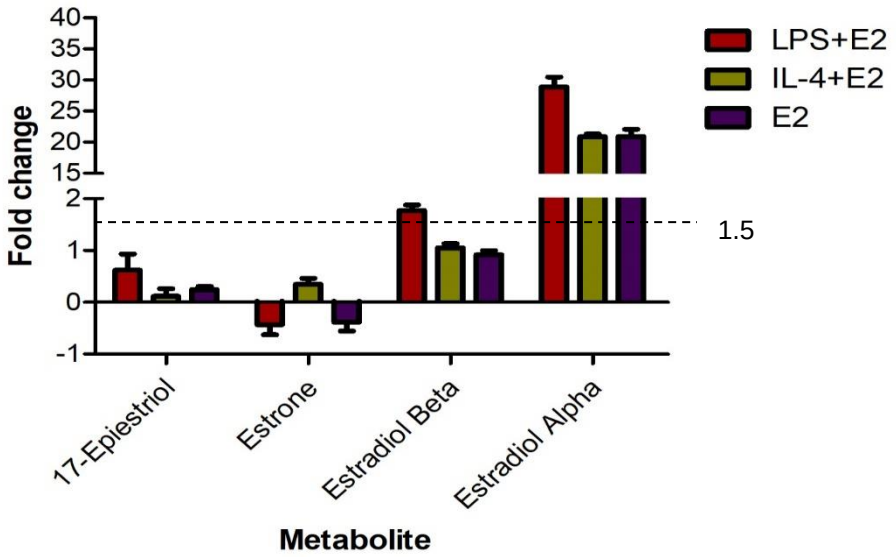

Figure 17: The concentrations of the estrogen metabolites detected with LC-MS/MS in cell culture medium collected from RAW 264.7 cells (treated with LPS (10 ng/mL) + E2 (0.1 nM), IL-4 (20 ng/mL) + E2 (0.1 nM) or E2 (0.1 nM) for 48 hours) shown as a fold change of the control that contained no cells. Error bars represent standard deviation of replicate measurements.

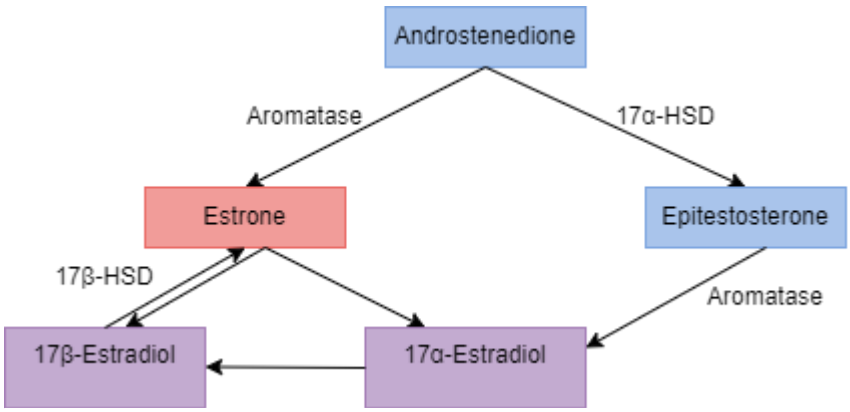

Figure 18: Schematic representation of estradiol alpha production (Reconstructed from Toran-Allerand et al., 2005).

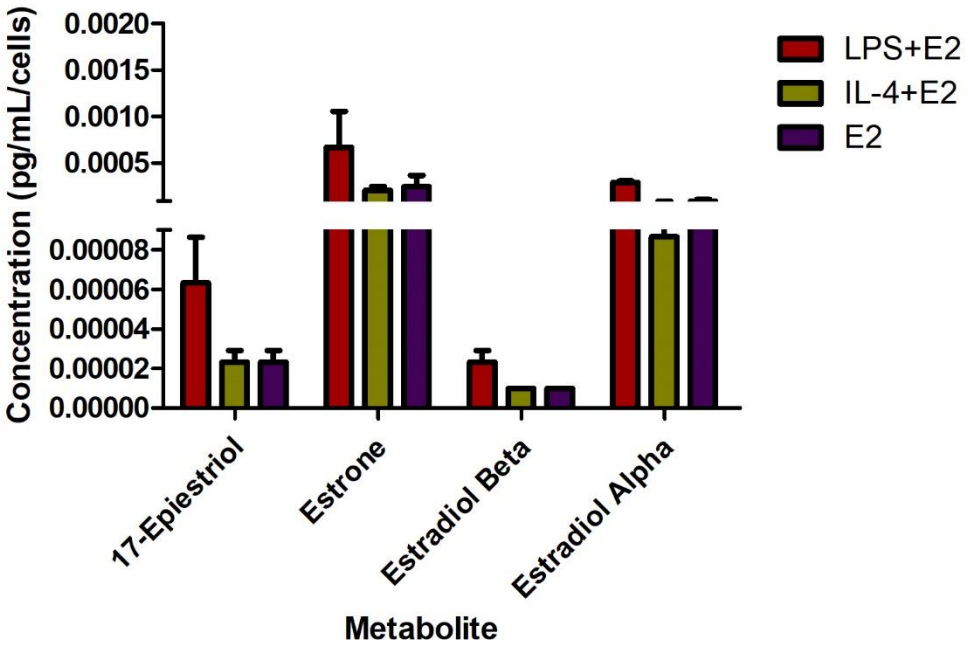

Figure 19: A comparison of the concentrations (normalised to cell number) of estrogen metabolites (detected with LC-MS/MS) in cell culture medium between different treatments (LPS+E2, IL-4+E2, and E2). Error bars represent standard deviation of replicate measurements.

CHAPTER 5 CONCLUSION

Breast cancer is a complex disease, influenced by a variety of factors including components in the TME. These components may include metabolites, hormones, and different cell types. Estrogen and macrophages form part of the breast TME and both are known to play a role in tumour development and progression. It is therefore necessary to understand the fundamental biology of estrogen and macrophages and the possible interaction between these two components (i.e., influence of estrogen on macrophage metabolism and estrogen metabolism in macrophages) to understand their role in tumourigenesis and tumour progression, and ultimately their potential as treatment targets. Some aspects such as macrophage bio-energetics and the effect of estrogen on macrophage activation have been investigated before, yet the influence of estrogen on the bio-energetics of already polarized macrophages and estrogen metabolism in macrophages has not been studied. This study therefore addressed these gaps in the literature by evaluation of the following:

1) *The influence of estrogen on the bio-energetic metabolism in different macrophage cell lines and activation states.* The results from the bio-energetics analyses of RAW264.7 cells and BMDMs in the presence of three different glucose concentrations indicate that glucose concentration affects macrophage bio-energetics (high glucose concentration decreased most OXPHOS parameters in both cell lines), and also influences (by enhancing or diminishing) the effect of other compounds (e.g., LPS, IL-4, and E2 in this study) on macrophage bio-energetics. Therefore, careful consideration must be taken when choosing a suitable glucose concentration for studies on macrophages. From this study, we concluded that 11 mM for RAW 264.7 cells and 5 mM for BMDMs were the optimal medium glucose concentrations to use. Despite the decrease in most OXPHOS parameters observed at a high glucose concentration in BMDMs, it is evident that some mitochondrial OXPHOS parameters such as maximal respiration are not downregulated to the same extent in BMDMs as compared to RAW 264.7 cells. Instead, it seems as if glycolysis and mitochondrial OXPHOS are more efficiently coupled in BMDMs than in RAW264.7 cells, since ECAR was lower but glucose consumption rate appeared to be similar (or even higher) in BMDMs compared to RAW 264.7 cells. Although previous literature has shown that estrogen can activate macrophages to an anti-inflammatory state and increase parameters associated with mitochondrial OXPHOS in other cell lines (such as tumour cells), this study now showed that estrogen treatment also increases some OXPHOS parameters (such as basal respiration, OCR for ATP production, and maximal

respiration) in macrophages, and that E2-stimulated macrophages, therefore, display a bio-energetic profile similar to anti-inflammatory macrophages. The bio-energetics analyses of polarized macrophages treated with estrogen showed that estrogen treatment does not further affect the mitochondrial OXPHOS of anti-inflammatory macrophages. However, estrogen treatment does cause a shift in the bioenergetic metabolism of pro-inflammatory macrophages by increasing the mitochondrial OXPHOS activity towards a phenotype comparable to naïve cells. It is, therefore, possible that estrogen may limit the number of pro-inflammatory macrophages in the TME or dampen their tumouricidal activity.

2) *Estrogen metabolism in macrophages.* Since only parent estrogens 17-α-/17-β-estradiol (and not other phase I and phase II metabolites) appear to be produced by RAW 264.7 cells, it suggests that these macrophages can synthesise but not biotransform this steroid extensively. Macrophages may, therefore, contribute to estrogen production in the tissues they populate, such as mammary tissue. Furthermore, 17-α-estradiol (a less biologically active estrogen) was found to be the predominant metabolite in these cells. Although a possible role of 17-α-estradiol in tumourigenesis have been proposed, 17-β-estradiol is still considered the parent estrogen with the greatest carcinogenic potency (Acconcia & Marino, 2011). Estrogen metabolism in macrophages may, therefore, still play a role in tumourigenesis but not via the direct production of genotoxic estrogen quinones. The effect of estrogen on macrophage activity in the TME may, therefore, play a bigger role. Pro-inflammatory macrophages that were treated with estrogen also seemed to produce more 17-α-estradiol and 17-β-estradiol as compared to the anti-inflammatory macrophages. This may be possible due to the involvement of LPS in the regulation of aromatase expression.

Taken together, this study sheds light on the complex interplay between two prominent components of the breast TME (estrogen and macrophages) and demonstrated that this interplay can be influenced by other factors as well (e.g., extracellular glucose concentration) and possibly alter tumour dynamics. For example, E2 present in the TME may polarise macrophages toward an anti-inflammatory, cancer-promoting type and may also polarise pro-inflammatory, cancer-killing macrophages toward a naïve state. This may disturb the balance between pro- and anti-inflammatory macrophages in the TME by limiting the amount of cancer-killing macrophages and increasing cancer-promoting macrophages, which can increase cancer progression and worsen the prognosis. However, the following limitations of the study must be addressed before a comprehensive picture of the role of estrogen and macrophages in the TME can be obtained:

1. This study evaluated bio-energetics only in RAW 264.7 cells and mouse BMDMs, and estrogen metabolism only in RAW 264.7 cells. The metabolome between immortalised cell lines and primary cells as well as between species can differ. Thus, the inclusion of other human monocytic/macrophage cell lines such as THP-1, U937, and J774 may offer a more accurate depiction of macrophages in humans. The method for THP-1 differentiation can be optimised by considering the use of a lower PMA concentration (or a less toxic alternative such as PHA-P) and/or LPS concentration as well as the use of cell-bind plates for improved cell adherence. Culturing without antibiotics can also be considered, since antibiotics may further impact the health of the cells (Ryu *et al.*, 2017).
2. Macrophage differentiation and activation was not confirmed by analysis of differentiation markers. Phase contrast microscopy and the analysis of cytokines and cell signalling pathways associated with macrophage activation/differentiation via RT-PCR or western blot can be included in future studies to confirm the shift in polarization state in the presence of E2.
3. Focus was placed on assessing the mitochondrial OXPHOS in macrophages, however, analysing the glycolytic rate as well will provide a more comprehensive representation of bio-energetic activity in macrophages.
4. The LC-MS/MS method used in this study was only suitable for the determination of non-polar metabolites and the polar metabolites estriol-3-sulphate, estriol-16-glucuronide, and estradiol-3-glucuronide. Further optimisation of the method is required to accurately analyse all 27 metabolites. The use of charcoal-stripped FBS can be considered to decrease matrix effects. The use of two separate SPE clean-up methods can also be investigated, for example the use of both a C18 column for the retention of hydrophobic compounds and a polymeric reverse phase for the retention of neutral and aromatic compounds.
5. The number of replicates for the control groups during LC-MS/MS analyses was not sufficient for the use of more powerful statistical tools. Increasing the number of replicates in treatment and control groups will allow for more accurate assumptions. Furthermore, the inclusion of untreated control cells will allow a more accurate determination of the effect of different treatments on metabolite production.
6. Gene expression analyses can also be done, which may provide insight regarding the expression of genes involved in estrogen metabolism in macrophages.

The study of the TME remains a promising field of topic as the manipulation of estrogen metabolism and macrophage activity in the TME can potentially be used as a treatment option for breast cancer. In this study we showed that factors such as glucose and estrogen can affect macrophage bio-energetics. In addition, macrophages appear to be able to synthesise estrogen. All of these factors may influence tumour dynamics and, therefore, need to be taken into consideration when exploring hormone manipulation and immune engineering as options for breast cancer treatment.

ANNEXURES

Annexure A: Supplementary methods and materials

Table A1: Chemicals and kits

Cell culture and Bio-energetics analyses		
Supplier	**Material/Reagent**	**Details**
Invitrogen	Amplex Red reagent (2,56 µg/mL)	CAT: A12222
	CyQUANT GR Cell Proliferation Assay Kit	REF: C7206 LOT: 190236
Gibco Life Technologies	Fetal Bovine Serum (FBS)	CAT:10499-044 LOT:2021576K
	Sodium pyruvate (100 nM)	REF:11360-039 LOT:2010382
	Penicillin (100 U/mL) Streptomycin (100 µg/mL)	REF: 15140122 LOT:2051354
	Phosphate buffered saline (PBS)	REF: 18912014 LOT:2078385
Sigma Aldrich Life Science, now ©Merck KGaA, Darmstadt, Germany	Antimycin A (2.5 mM)i	CAT:1397-94-0
	D-Glucose (100 g/L)	REF: G8644-100ML LOT:RNBJ2222
	DMSO (Dimethyl sulfoxide)	CAT: D2650-100mL LOT: RNBH3210
	FCCP (2.5 mM)	CAT: 370-86-5
	Glucose oxidase from *Aspergillus Niger* (100 U/mL)	CAT: 9001-37-0 LOT:G7141
	Horseradish peroxidase (10 U/mL)	CAT: 9003-99-0 LOT: P8125
	IL-4 (20 µg/mL)	CAT: I1020-5UG
	L-Glutamine (200 mM)	G-3126 LOT: 45H0246
	NaOH powder	CAT: 1310732 LOT:SZBC1290V
	Oligomycin (2.5 mM)	CAT: 579-13-5
	17 β-estradiol (100 nM)	CAT: E2758-1G
	Tris-HCl (1 M)	CAT: T2194
	DMEM powder	CAT: D5030
	PMA (2000 ng/mL)	P8139-1MG
	RPMI 1640 medium powder (No Glucose)	REF: R1383-10X1L LOT: SLBZ1756
	Rotenone (2.5 mM)	CAT: 83-79-4
	LPS (10 µg/ML)	Cat: L4391-1MG
Cellonex	L929 cells	CAT: #CL929-C
	RAW 264.7 cells	CAT:CRAW-264.7-C
Amresco	NaCl powder	CAT: 1310-73-2 LOT: 02415500G
Agilent	Seahorse calibrant	pH 7.4 LOT: 08418001 Part: 100840-000

	Seahorse XF 96 sensor cartridge & utility plate	LOT: W053190
	Seahorse XF 96 cell culture plate	LOT: 09218 Part: 101085-004
Biocom Africa	Muse Count and Viability Kit	CAT: MCH100102
LC-MS/MS analyses		
Sigma Aldrich Life Science, now ©Merck KGaA, Darmstadt, Germany: Analytical standards:	E1 (Estrone)	CAT: 46573
	17 α -E2 (Estradiol)	CAT: 46542
	17 β -E2	CAT: E1132
	Progesterone	CAT: 1568007
	Androstenedione	CAT: 46033
	Testosterone	CAT: 46923
	Dehydroepiandrosterone	CAT: D4000
	dehydroepiandrosterone sulphate	CAT: D5297
	E3 (Estriol)-3-sulphate	CAT: E6375
	E2-3-sulphate	CAT: E9505
	E1-3-sulphate	CAT: E0251
	E1-3-glucuronide	CAT: E1752
	E2-3-glucuronide	CAT: E2127
	E3-16-glucuronide	CAT: E1877
Sigma Aldrich Life Science, now ©Merck KGaA, Darmstadt, Germany	Formic acid	CAT: 94318
	Ammonium formate	CAT: 70221
	Dansyl chloride	CAT: 03641
Honeywell, Burdick & Jackson, supplied by Anatech(South Africa)	LC-grade water	CAT: 365-4
	Methanol	CAT: 230-4
	Acetonitrile	CAT: 017-4
	Acetone	CAT: 010-4
Steraloids Inc., Newport United States via distributor Stargate scientific: Isotopes:	E1	CAT: E2300-010
	E2	CAT: E0950-014
	E3	CAT: E2600-016
	Progesterone	CAT: Q2600-014
	DHEA	CAT: A8500-009
Toronto research chemicals (TRC), Ontaria, via Industrial analytics	2&4-OHE1	CAT: E889061
Separations (South Africa)	Phenomenex SPE column vacuum manifold	AHO-6024
	Phenomenex Strata C18 SPE cartridges	8B–S002-FBJ

THP-1 optimisation

The differentiation protocol according to Starr *et al.* (2018) was followed and THP-1 cells were seeded at a density of 500 000 cells/well (2 mL) and incubated with 20 ng/mL PMA for three days in two 6-well plates as shown in Figure A1. A third 6-well plate (treated identically) was included as control that contained no cells. However, after three days of incubation, microscopic inspection of the cells showed that the cells incubated with PMA were not morphologically different compared to the control that contained no PMA. The cells remained in suspension and were therefore not fully differentiated. The cells were kept for another four days, after which, the PMA was replaced with PMA-free medium and 2 µL of each drug that will be used in this study (namely LPS, IL-4, and E2) was added to plate 1 as shown in Figure A1. The medium from each of the wells of plate 2 and 3 was replaced with PMA-free medium and treated similarly.

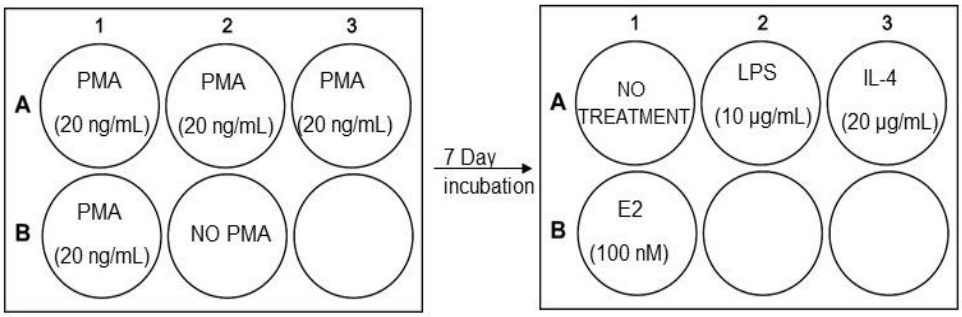

Figure A1: Plate layout (representative of the first two plates with cells and third plate with no cells) of THP-1 differentiation with 20 ng/mL PMA and treatment with LPS, IL-4 and E2.

The cells were incubated with the different drug treatments for 24 hours and inspected again. There was no difference between the various treatments and no significant difference between the PMA groups and No PMA control, with majority of the cells in the PMA groups still in suspension. It was clear that this low PMA concentration was not sufficient for THP-1 differentiation.

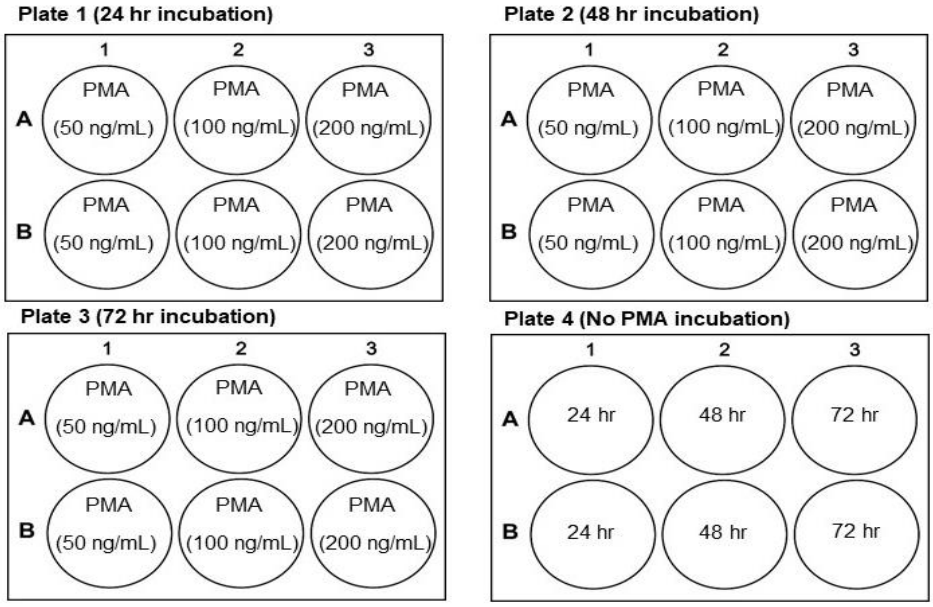

Figure A2: Optimisation of different PMA concentrations (20 ng/mL, 50 ng/mL, 100 ng/mL) and incubation times (24 hr, 48 hr, 72 hr) for THP-1 differentiation.

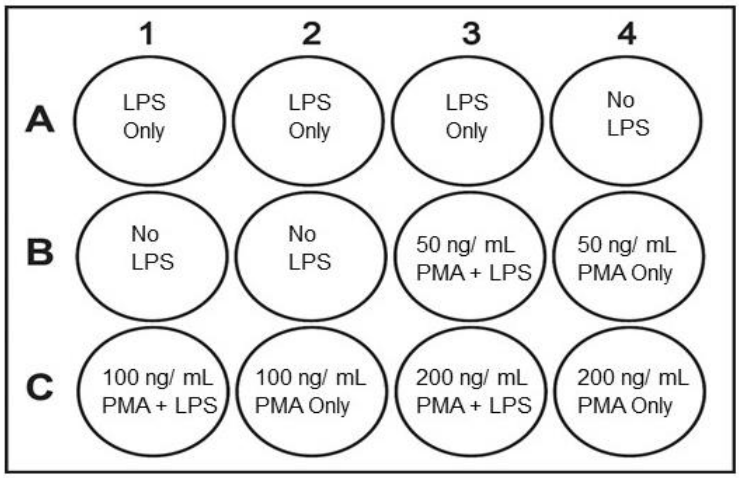

Figure A3: Optimisation of different PMA concentrations and incubation times: LPS treatment (10 ng/mL) of differentiated THP-1 cells.

Glucose measurement

Figure A4: Plate layout. Investigation of the optimal glucose concentration for *in vitro* metabolic studies of macrophages: Amplex Red Glucose assay of culture medium from RAW 264.7 cells on day one and two of incubation.

Figure A5: Plate layout. Investigation of the optimal glucose concentration for *in vitro* metabolic studies of macrophages: Amplex Red Glucose assay of culture medium from RAW 264.7 cells on day three of incubation

Figure A6: Plate layout. Investigation of the optimal glucose concentration for *in vitro* metabolic studies of macrophages: Amplex Red Glucose assay of culture medium from BMDMs on day four and five of differentiation.

Figure A7: Plate Layout 4. Investigation of the optimal glucose concentration for *in vitro* metabolic studies of macrophages: Amplex Red Glucose assay of culture medium from BMDMs on day six and seven of differentiation.

Bio-energetics analyses

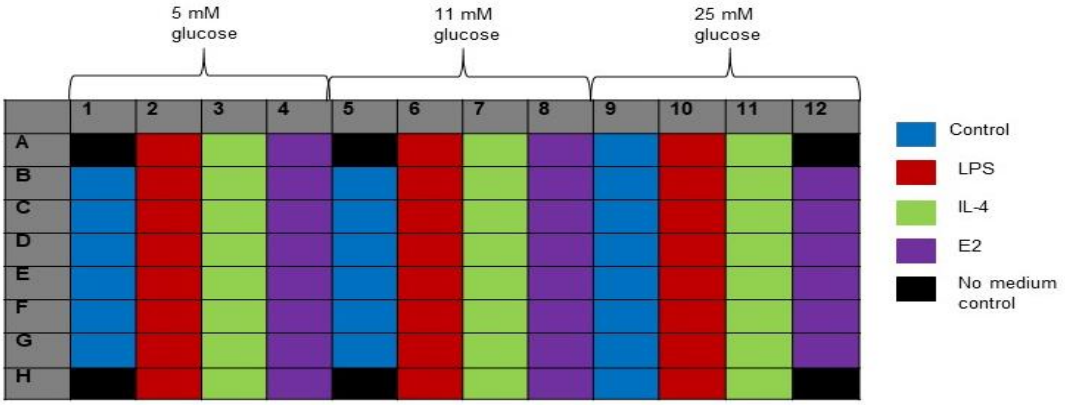

Figure A8: Plate Layout. Investigation of the optimal glucose concentration for *in vitro* metabolic studies of macrophages (RAW 264.7 cells and BMDMs).

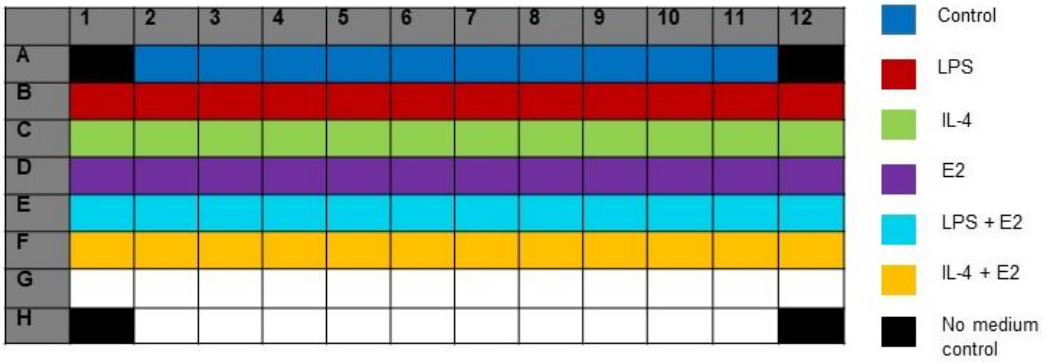

Figure A9: Plate Layout 6. Investigation of the effect of estrogen on the metabolism of pro- and anti-inflammatory macrophages (RAW 264.7 cells cultured with 11 mM glucose and BMDMs cultured with 5 mM glucose).

Compound A: Oligomycin (final concentration of 1 µM)	Compound B: FCCP (final concentration of 0.5 µM)	Compound C: Rotenone/Antimycin A (final concentration of 1 µM)
4.8 µL Oligomycin (2.5 mM) 1495 µL Assay medium (5 mM, 11 mM, or 25 mM glucose)	2.8 µL FCCP (2.5 mM) 1552.4 µL Assay medium (5 mM, 11 mM, or 25 mM glucose)	6 µL Rotenone (2.5 mM) 6 µL Antimycin A (2.5 mM) 1488 µL Assay medium (5 mM, 11 mM, or 25 mM glucose)

**Injectable compound concentrations were optimised in a pilot study.*

Figure A10: Mitochondrial Stress Test injectable compound preparation. Investigation of the optimal glucose concentration for *in vitro* metabolic studies of macrophages (RAW 264.7 and BMDMs).

Compound A: Oligomycin (final concentration of 1 µM)	Compound B: FCCP (final concentration of 0.5 µM)	Compound C: Rotenone/Antimycin A (final concentration of 1 µM)
9.6 µL Oligomycin (2.5 mM) 2990 µL Assay medium	5.6 µL FCCP (2.5 mM) 3104.8 µL Assay medium	12 µL Rotenone (2.5 mM) 12 µL Antimycin A (2.5 mM) 2976 µL Assay medium

**Injectable compound concentrations were optimised in a pilot study.*

Figure A11: Mitochondrial Stress Test injectable compound preparation. Bio-energetics investigation of the effect of estrogen on the metabolism of pro- and anti-inflammatory macrophages (RAW 264.7 cells cultured with 11 mM glucose and BMDMs cultured with 5 mM glucose).

LC-MS/MS Analyses

Table A2: Internal standards

Internal standard	Metabolite
Progesterone-D4	Testosterone
	Androstenedione
	Progesterone
Estriol-D4	Estriol
	16-Ketoestradiol
	16-Epiestriol
	17-Epiestriol
	16-Hydroxyestrone
Estrone-D4	Estrone
Estradiol-D4	Estrone-2-hydroxy-3-methylether
	2-Methoxyestrone
	4-Methoxyestrone
	2-Methoxyestradiol
	4-Methoxyestradiol
	Estradiol Alpha
	Estradiol Beta
2-Hydroxyestradiol-D4	2-Hydroxyestrone
	2-Hydroxyestradiol
4-Hydroxyestradiol-D4	4-Hydroxyestrone
	4-Hydroxyestradiol
2-Asetamidophenol	Estriol-3 sulphate
	Estradiol-3 sulphate
	Estradiol-17 sulphate
	Estrone-3 sulphate
	Estriol-16 glucuronide
	Estradiol-3 glucuronide
	Estrone-3 glucuronide

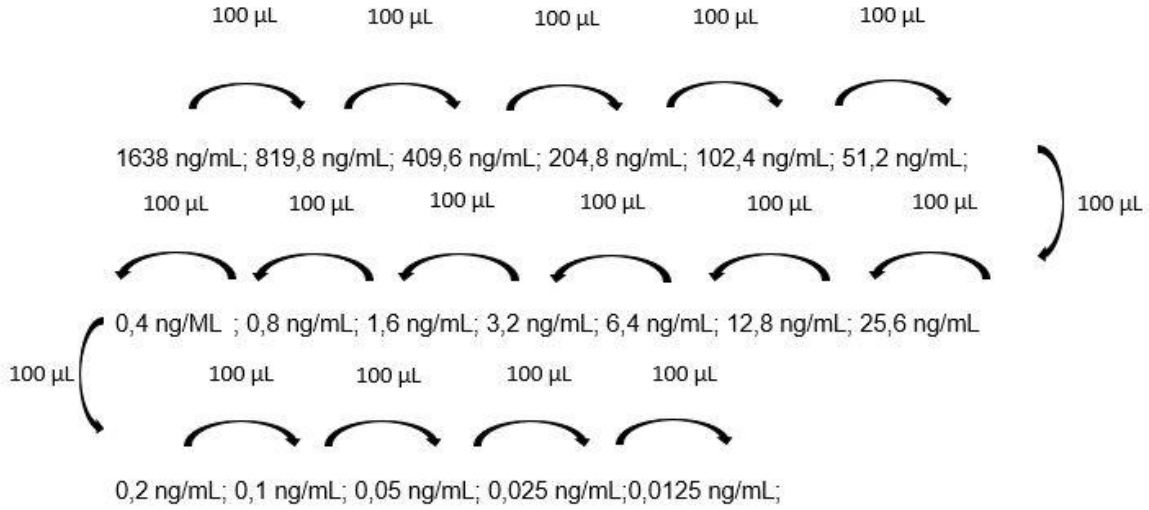

Figure A12: Series dilution for standard series.

Annexure B: Supplementary Results

Bio-energetics analyses

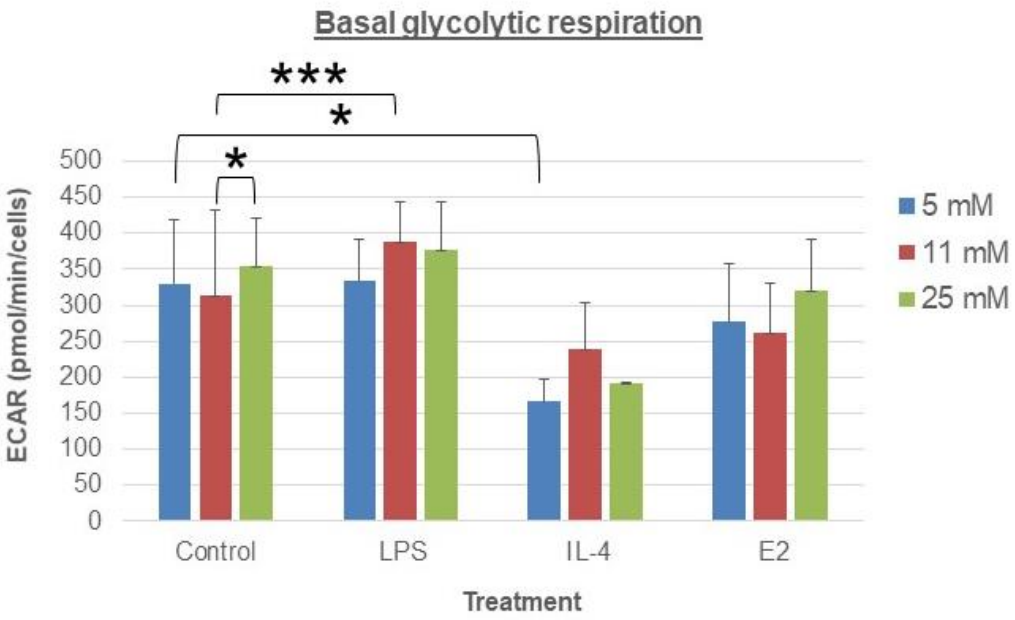

Figure B1: Basal glycolytic respiration of RAW 264.7 cells cultured with either 5 mM, 11 mM or 25 mM glucose. Error bars indicate standard deviation of replicate measurements of control (n=6) and treated (n=8) samples. Two-way ANOVA with Bonferroni post-test was applied. Significant differences are indicated with stars (one star indicates a $p<0.05$; two stars indicate a $p<0.01$; three stars indicate a $p<0.001$).

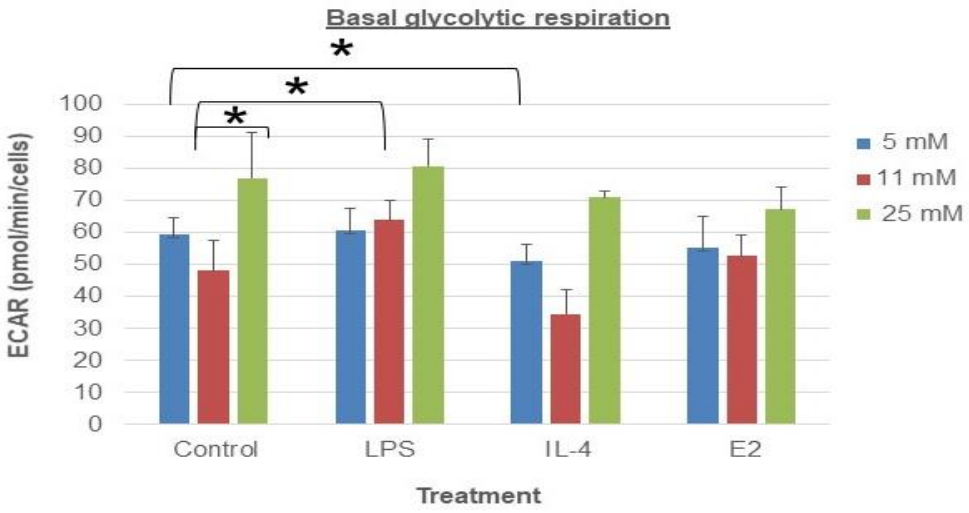

Figure B2: Basal glycolytic respiration of BMDMs cultured with either 5 mM, 11 mM, or 25 mM glucose. Error bars indicate standard deviation of replicate measurements of control (n=6) and treated (n=8) samples. Two-way ANOVA with Bonferroni post-test was applied. Significant differences are indicated with stars (one star indicates a $p<0.05$; two stars indicate a $p<0.01$; three stars indicate a $p<0.001$).

LC-MS/MS analyses

Table B1: A comparison of the relative response of metabolites in spiked media samples as a ratio of spiked water samples at different mobile phase gradients.

Metabolite	Gradient 1	Gradient 2	Gradient 3
Estriol	ND	0.06	0.26
2-Methoxyestrone	0.01	0.01	0.05
4-Methoxyestrone	0.03	0.03	0.13
2-Hydroxyestrone	ND	0.16	0.09
4-Hydroxyestrone	ND	0.12	0.08
2-Methoxyestradiol	0.03	0.03	0.01
2-Hydroxyestradiol	ND	0.0002	0.0002
4-Hydroxyestradiol	ND	0.15	0.9

**Not detected (ND)*

Table B2: A comparison of the relative response of spiked water and media samples from liquid-liquid extraction (LLE) clean-up to spiked water and media samples from SPE clean-up

Metabolite	Spiked water		Spiked medium	
	Ratio	**Stdev**	**Ratio**	**Stdev**
Estriol	0.01	0.007	0.23	0.07
2-Methoxyestrone	ND	-	0.13	0.008
4-Methoxyestrone	ND	-	ND	-
2-Hydroxyestrone	ND	-	ND	-
4-Hydroxyestrone	ND	-	ND	-
2-Methoxyestradiol	0.0007	0.0003	ND	-
2-Hydroxyestradiol	0.005	0.004	1.1	0.55
4-Hydroxyestradiol	0.06	0.05	0.88	0.035

**Not detected (ND)*

Table B3: A comparison of the relative response of spiked media samples (extracted with LLE) with or without pH adjustment and salt addition to spiked water samples extracted with SPE

Metabolite	pH adjusted		pH adjusted and salt added	
	Ratio	**Stdev**	**Ratio**	**Stdev**
Estriol	0.02	0.03	ND	-
2-Methoxyestrone	ND	-	ND	-
4-Methoxyestrone	0.002	0.001	0.13	0.09
2-Hydroxyestrone	ND	-	ND	-
4-Hydroxyestrone	ND	-	ND	-
2-Methoxyestradiol	0.0037	0.005	0.0002	0.0002
2-Hydroxyestradiol	0.0009	0.0001	0.0005	0.00005
4-Hydroxyestradiol	0.002	0.0004	0.0009	0.0002

**Not detected (ND)*

Table B4: A comparison of the relative response of different derivatisation methods of spiked water and media samples to the original derivatisation method.

Metabolite	Water samples		Medium samples	
	pH 9.5 and 0.04% w/v ascorbic acid	pH 8.0 and 0,04% w/v ascorbic acid	pH 9.5 and 0.04% w/v ascorbic acid	pH 8.0 and 0,04% w/v ascorbic acid
	Ratio	Ratio	Ratio	Ratio
Estriol	0.69	0.50	0.54	0.44
2-Methoxyestrone	0.58	0.10	0.40	0.68
4-Methoxyestrone	0.675	0.114	0.426	0.521
2-Hydroxyestrone	2.10	0.005	0.60	0.43
4-Hydroxyestrone	2.30	0.003	0.51	0.40
2-Methoxyestradiol	0.58	0.04	1.2	0.43
2-Hydroxyestradiol	0.96	0.26	0.6	0.35
4-Hydroxyestradiol	0.16	0.02	0.84	0.25

**Not detected (ND)*

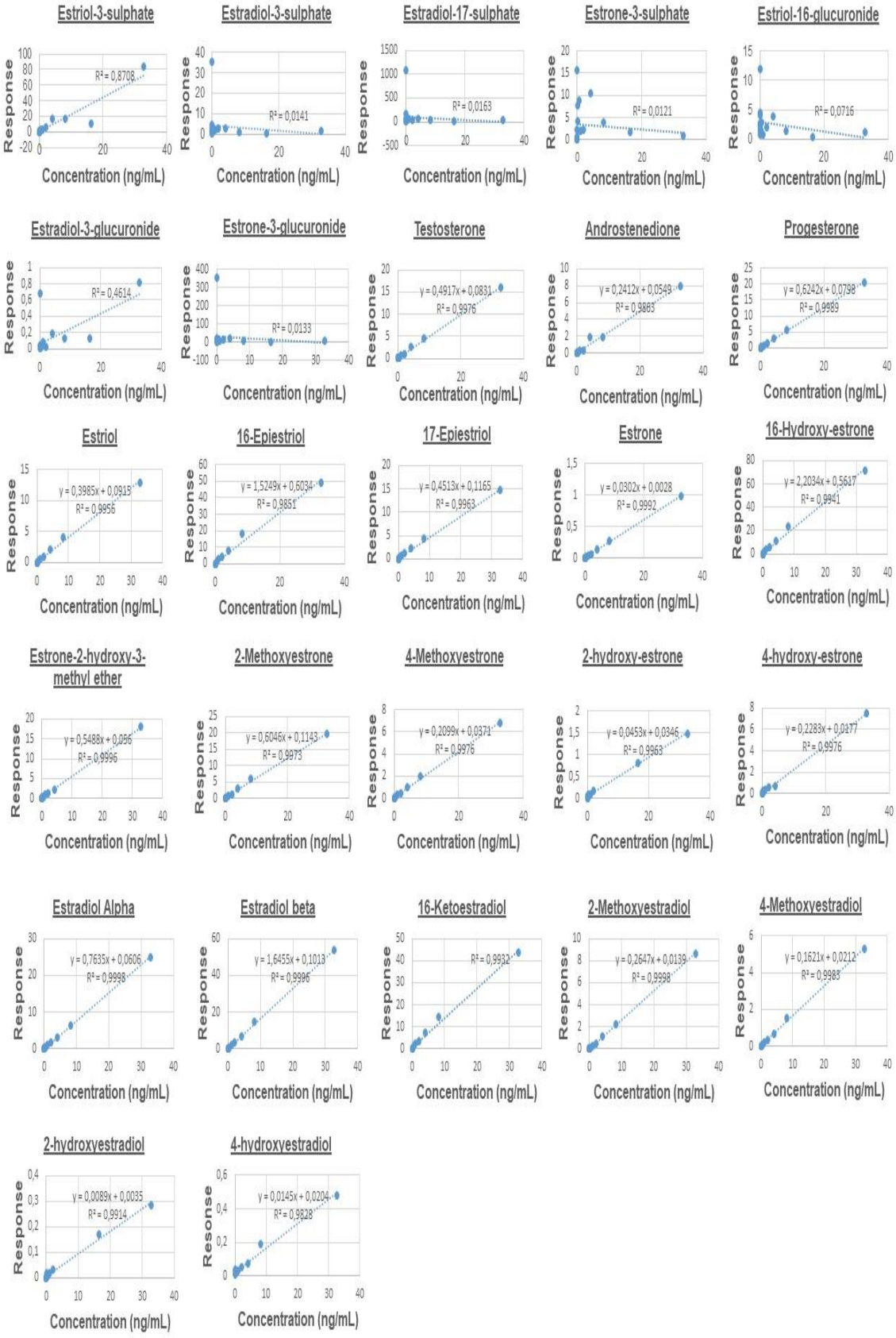

Figure B3: Graphs showing the linearity of the standard series prepared in cell culture medium with prior clean-up (polar metabolites eluted with 45% MeOH and non-polar metabolites eluted with 100% MeOH and Acetone).

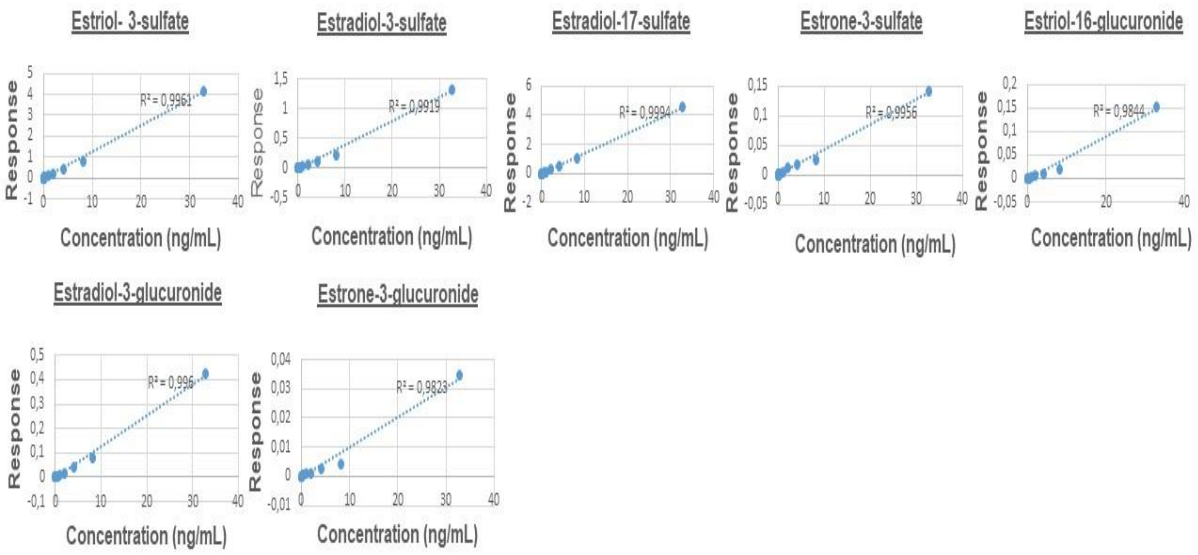

Figure B4: Graphs showing improved linearity of the standard series prepared in cell culture medium without prior clean-up.

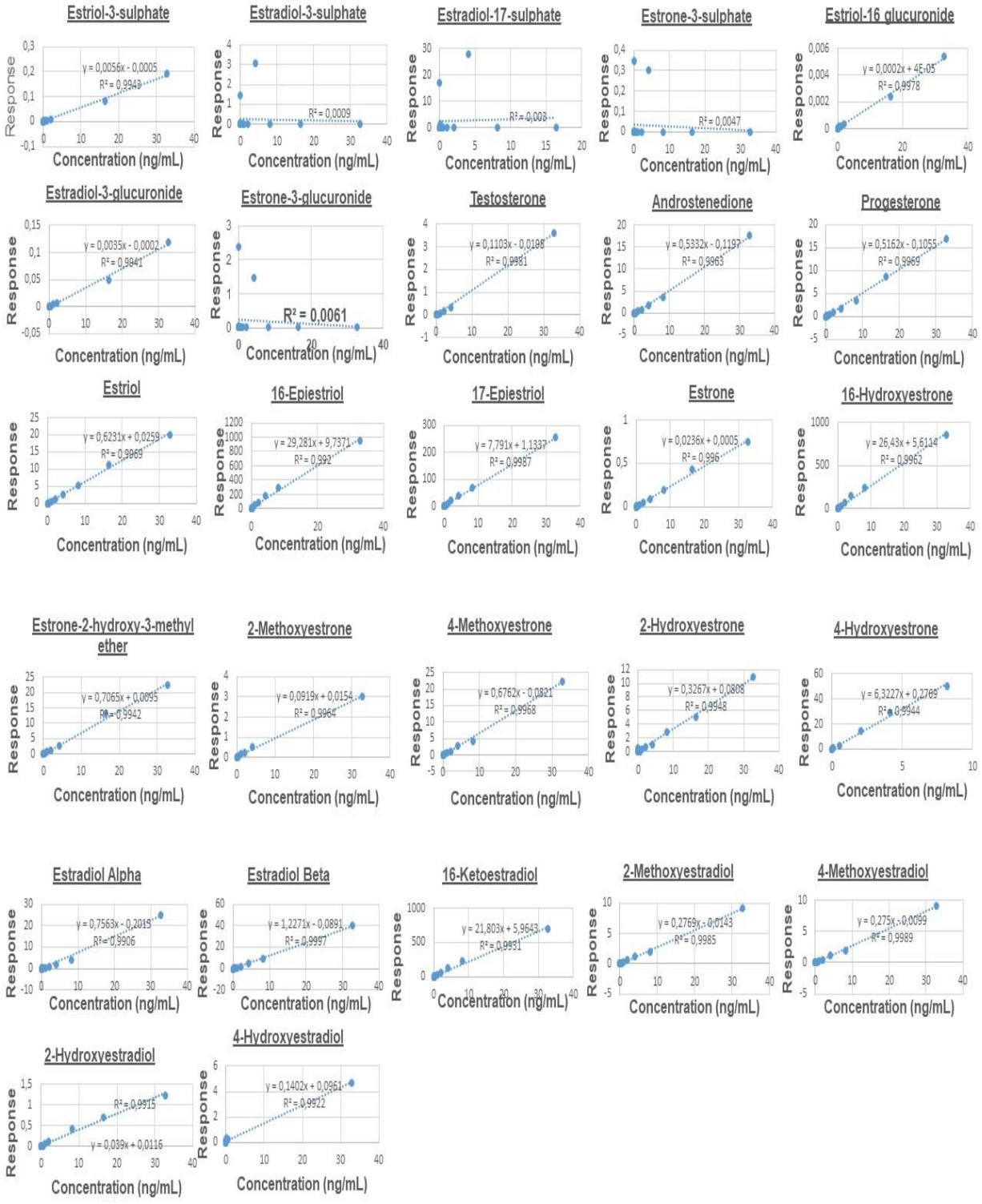

Figure B5: Graphs showing the linearity of the final standard series prepared in cell culture medium with clean-up (polar metabolites eluted with 30% and 45% MeOH and non-polar metabolites eluted with 100% MeOH and Acetone).

Table B5: Average concentration (ng/mL) of the estrogen metabolites (with good linearity) as measured in control samples and the medium of treated cells.

Metabolite	Treatment					
	Control LPS+E2	Control IL-4+E2	Control E2	LPS+E2	IL-4+E2	E2
Estriol-3-sulphate	0.06	0.01	0.03	0.05	0.04	0.05
Estriol-16-glucuronide	1.55	0.38	0.81	1.27	1.13	1.37
Estradiol-3-glucuronide	0.02	0.01	0.02	0.03	0.01	0.03
Testosterone	0.42	0.34	0.33	0.67	0.79	0.87
Androstenedione	0.02	0.03	0.02	0.05	0.08	0.07
Progesterone	0.04	0.07	0.05	0.12	0.14	0.10
Estriol	0.004	0.01	0.01	0.01	0.01	0.004
16-Epiestriol	ND	ND	ND	ND	ND	ND
17-Epiestriol	0.05	0.07	0.06	0.09	0.08	0.07
Estrone	1.41	0.48	1.05	0.92	0.75	0.74
16-Hydroxyestrone	ND	ND	ND	ND	ND	ND
Estrone-2-hydroxy-3-methyl ether	0.002	0.01	0.003	0.004	0.01	0.002
2-Methoxyestrone	0.001	0.002	0.001	0.001	0.001	0.001
4-Methoxyestrone	0.01	0.01	0.01	0.01	0.01	0.01
2-Hydroxyestrone	ND	ND	ND	ND	ND	ND
4-Hydroxyestrone	ND	ND	ND	ND	ND	ND
Estradiol Alpha	0.12	0.12	0.11	4.02	3.01	2.89
Estradiol Beta	0.13	0.14	0.14	0.35	0.28	0.26
16-Ketoestradiol	ND	ND	ND	ND	ND	ND
2-Methoxyestradiol	0.01	0.02	0.01	0.01	0.01	0.01
4-Methoxyestradiol	0.01	0.01	0.01	0.02	0.02	0.01
2-Hydroxyestradiol	1.25	1.36	1.38	1.96	1.72	2.25
4-Hydroxyestradiol	0.90	0.55	0.83	1.28	1.54	0.42

**Not detected*

Table B6: Signal to noise ratio of the different estrogen metabolites

Metabolite	S/N	Metabolite	S/N
Estriol-3-sulphate	<3	16-Hydroxyestrone	<3
Estradiol-3-sulphate	<3	Estrone-2-hydroxy-3-methyl ether	<3
Estradiol-17-sulphate	<3	2-Methoxyestrone	<3
Estrone-3-sulphate	<3	4-Methoxyestrone	<3
Estriol-16-glucuronide	<3	Estradiol Alpha	>10
Estradiol-3-glucuronide	<3	Estradiol Beta	>10
Estrone-3-glucuronide	<3	16-Ketoestradiol	<3
Testosterone	<3	2- Methoxyestradiol	<3
Androstenedione	<3	4-Methoxyestradiol	<3
Progesterone	<3	2-Hydroxyestrone	<3
Estriol	<3	4-Hydroxyestrone	<3
16-Epiestriol	<3	2-Hydroxyestradiol	<3
17-Epiestriol	>10	4-Hydroxyestradiol	<3
Estrone	>10		

REFERENCE LIST

Acconcia, F. & Marino, M. 2011. The effects of 17β-estradiol in cancer are mediated by estrogen receptor signaling at the plasma membrane. *Frontiers in Physiology*, 2:30.

Aitcheson, S.M., Frentiu, F.D., Hurn, S.E., Edwards, K. & Murray, R.Z. 2021. Skin wound healing: normal macrophage function and macrophage dysfunction in diabetic wounds. *Molecules and Cells*, 26(16):4917.

Amend, S.R., Valkenburg, K.C. & Pienta, K.J. 2016. Murine hind limb long bone dissection and bone marrow isolation. *JoVE*, (110):e53936. doi:10.3791/53936

Anari, M.R., Bakhtiar, R., Zhu, B., Huskey, S., Franklin, R.B. & Evans, D.C. 2002. Derivatization of ethinylestradiol with dansyl chloride to enhance electrospray ionization: application in trace analysis of ethinylestradiol in rhesus monkey plasma. *Analytical Chemistry Insights*, 74(16):4136-4144.

Anders, C. & Carey, L.A. 2008. Understanding and treating triple-negative breast cancer. *Oncology (Williston Park, N.Y.)*, 22(11):1233.

Anfray, C., Ummarino, A., Andón, F.T. & Allavena, P. 2020. Current Strategies to Target Tumor-Associated-Macrophages to Improve Anti-Tumor Immune Responses. *Cells Tissues Organs*, 9(1):46.

Aramini, B., Masciale, V., Grisendi, G., Banchelli, F., D'Amico, R., Maiorana, A., ... Haider, K.H. 2021. Cancer stem cells and macrophages: molecular connections and future perspectives against cancer. *OncoTargets and Therapy*, 12(3):230.

Argyle, D. & Kitamura, T. 2018. Targeting macrophage-recruiting chemokines as a novel therapeutic strategy to prevent the progression of solid tumors. *Frontiers in Immunology*, 9:2629.

Assanga, I. & Lujan, L. 2013. Cell growth curves for different cell lines and their relationship with biological activities. *International Journal of Biotechnology Molecular Biology Research*, 4(4):60-70.

Au, C.C., Docanto, M.M., Zahid, H., Raffaelli, F., Ferrero, R.L., Furness, J.B. & Brown, K.A. 2017. Des-acyl ghrelin inhibits the capacity of macrophages to stimulate the expression of aromatase in breast adipose stromal cells. *The Journal of Steroid Biochemistry Molecular Biology and Evolution*, 170:49-53.

Avagliano, A., Ruocco, M.R., Aliotta, F., Belviso, I., Accurso, A., Masone, S., ... Arcucci, A. 2019. Mitochondrial Flexibility of Breast Cancers: A Growth Advantage and a Therapeutic Opportunity. *Cells*, 8(5):401.

Ayala, T.S., Tessaro, F.H.G., Jannuzzi, G.P., Bella, L.M., Ferreira, K.S. & Martins, J.O. 2019. High glucose environments interfere with bone marrow-derived macrophage inflammatory mediator release, the TLR4 pathway and glucose metabolism. *Scientific Reports of the Istituto Superiore di Sanita*, 9(1):1-15.

Baber, N. 1994. International conference on harmonisation of technical requirements for registration of pharmaceuticals for human use (ICH). *British Journal of Clinical Pharmacology*, 37(5):401.

Barkhem, T., Carlsson, B., Nilsson, Y., Enmark, E., Gustafsson, J. & Nilsson, S. 1998. Differential response of estrogen receptor α and estrogen receptor β to partial estrogen agonists/antagonists. *Molecular Pharmacology*, 54(1):105-112.

Baron, J.M., Zwadlo-Klarwasser, G., Jugert, F., Hamann, W., Rübben, A., Mukhtar, H. & Merk, H.F. 1998. Cytochrome P450 1B1: a major P450 isoenzyme in human blood monocytes and macrophage subsets. *Biochemical Pharmacology*, 56(9):1105-1110.

Barros, R.P., Gabbi, C., Morani, A., Warner, M. & Gustafsson, J. 2009. Participation of ERα and ERβ in glucose homeostasis in skeletal muscle and white adipose tissue. *American Journal of Physiology Endocrinology Metabolism: Clinical and Experimental*, 297(1):E124-E133.

Baxter, E., Graham, A., Re, N., Carr, I., Robinson, J., Mackie, S. & Morgan, A. 2020. Standardized protocols for differentiation of THP-1 cells to macrophages with distinct M (IFNγ+ LPS), M (IL-4) and M (IL-10) phenotypes. *Journal of Immunological Methods*, 478:112721.

Beisecker, A.E., Cook, M.R., Ashworth, J., Hayes, J., Brecheisen, M., Helmig, L., ... Selenke, D. 1997. Side effects of adjuvant chemotherapy: perceptions of node-negative breast cancer patients. *Psycho-Oncology: Journal of the Psychological, Social Behavioral Dimensions of Cancer*, 6(2):85-93.

Belgiovine, C., Digifico, E., Anfray, C., Ummarino, A. & Torres Andón, F. 2020. Targeting tumor-associated macrophages in anti-cancer therapies: convincing the traitors to do the right thing. *Journal of Clinical Medicine Research*, 9(10):3226.

Bi, Y., Chen, J., Hu, F., Liu, J., Li, M. & Zhao, L. 2019. M2 macrophages as a potential target for antiatherosclerosis treatment. *Neural Plasticity*, 2019, 6724903. doi.org/10.1155/2019/6724903

Biriken, D., Yazıhan, N. & Yılmaz, Ş. 2018. Investigation of cytokine and midkine responses of human THP-1 leukemia cells induced by phorbol-12-Myristate-13-Acetate (PMA) at different concentrations and times. *Mikrobiyoloji Bulteni*, 52(2):147-155.

Black, R.M. & Muir, B. 2003. Derivatisation reactions in the chromatographic analysis of chemical warfare agents and their degradation products. *Journal of Chromatography A*, 1000(1-2):253-281.

Bolego, C., Cignarella, A., Staels, B. & Chinetti-Gbaguidi, G. 2013. Macrophage function and polarization in cardiovascular disease: a role of estrogen signaling? *Arteriosclerosis, thrombosis, vascular biology*, 33(6):1127-1134.

Botnick, L.E., Hannon, E.C., Obbagy, J. & Hellman, S. 1982. Decline in bone marrow proliferative capacity as a function of age. *Blood,* 60(1):245-252.

Boutilier, A.J. & Elsawa, S.F. 2021. Macrophage polarization states in the tumor microenvironment. *International Journal of Molecular Sciences*, 22(13):6995.

Bray, F., Ferlay, J., Soerjomataram, I., Siegel, R.L., Torre, L.A. & Jemal, A. 2018. Global cancer statistics 2018: GLOBOCAN estimates of incidence and mortality worldwide for 36 cancers in 185 countries. *CA: A Cancer Journal for Clinicians*, 68(6):394-424.

Brookes, P.S. 2005. Mitochondrial H+ leak and ROS generation: an odd couple. *Free Radical Biology Medicine & Health*, 38(1):12-23.

Brown, G.C., Murphy, M.P., Jastroch, M., Divakaruni, A.S., Mookerjee, S., Treberg, J.R. & Brand, M.D. 2010. Mitochondrial proton and electron leaks. *Essays in Biochemistry*, 47:53-67.

Burcelin, R., Dolci, W. & Thorens, B. 2000. Portal glucose infusion in the mouse induces hypoglycemia: evidence that the hepatoportal glucose sensor stimulates glucose utilization. *Diabetes & Metabolic Syndrome*, 49(10):1635-1642.

Burney, S., Caulfield, J.L., Niles, J.C., Wishnok, J.S. & Tannenbaum, S.R. 1999. The chemistry of DNA damage from nitric oxide and peroxynitrite. *Mutation Research/Fundamental and Molecular Mechanisms of Mutagenesis*, 424(1-2):37-49.

Callahan, R. & Hurvitz, S. 2011. HER2-positive breast cancer: current management of early, advanced, and recurrent disease. *Current Opinion in Obstetrics Gynecology*, 23(1):37.

Campbell, L., Emmerson, E., Williams, H., Saville, C.R., Krust, A., Chambon, P., ... Hardman, M.J. 2014. Estrogen receptor-alpha promotes alternative macrophage activation during cutaneous repair. *Journal of Investigative Dermatology*, 134(9):2447-2457.

Caron, P., Turcotte, V. & Guillemette, C. 2015. A chromatography/tandem mass spectrometry method for the simultaneous profiling of ten endogenous steroids, including progesterone, adrenal precursors, androgens and estrogens, using low serum volume. *Steroids*, 104:16-24.

Cavalieri, E., Chakravarti, D., Guttenplan, J., Hart, E., Ingle, J., Jankowiak, R., ... Santen, R. 2006. Catechol estrogen quinones as initiators of breast and other human cancers: implications for biomarkers of susceptibility and cancer prevention. *Biochimica et Biophysica Acta (BBA)-Reviews on Cancer*, 1766(1):63-78.

Chamberlain, L.M., Holt-Casper, D., Gonzalez-Juarrero, M. & Grainger, D.W. 2015. Extended culture of macrophages from different sources and maturation results in a common M2 phenotype. *Journal of Biomedical Materials Research Part A*, 103(9):2864-2874.

Chen, S.-H. & Li, C.-W. 2019. Detection and characterization of catechol quinone-derived protein adducts using biomolecular mass spectrometry. *Frontiers in Chemistry*, 7:571.

Chen, Y., Song, Y., Du, W., Gong, L., Chang, H. & Zou, Z. 2019. Tumor-associated macrophages: an accomplice in solid tumor progression. *Journal of Biomedical Science*, 26(1):1-13.

Cheng, J., Nanayakkara, G., Shao, Y., Cueto, R., Wang, L., Yang, W.Y., ... Yang, X. 2017. Mitochondrial proton leak plays a critical role in pathogenesis of cardiovascular diseases. *Mitochondrial Dynamics in Cardiovascular Medicine*:359-370.

Chiu, M.L., Lawi, W., Snyder, S.T., Wong, P.K., Liao, J.C. & Gau, V. 2010. Matrix effects—a challenge toward automation of molecular analysis. *JALA: Journal of the Association for Laboratory Automation*, 15(3):233-242.

Choi, S.Y., Lee, Y.J., Kim, J.M., Kang, H.J., Cho, S.H. & Chang, S.E. 2018. Epidermal growth factor relieves inflammatory signals in staphylococcus aureus-treated human epidermal keratinocytes and atopic dermatitis-like skin lesions in Nc/Nga mice. *BioMed Research International*, 2018, 9439182 doi.org/10.1155/2018/9439182

Colvin, E.K. 2014. Tumor-associated macrophages contribute to tumor progression in ovarian cancer. *Frontiers in Oncology*, 4:137.

Corliss, B.A., Azimi, M.S., Munson, J.M., Peirce, S.M. & Murfee, W.L. 2016. Macrophages: an inflammatory link between angiogenesis and lymphangiogenesis. *Microcirculation*, 23(2):95-121.

Cunningham, M.A., Wirth, J.R., Naga, O., Eudaly, J. & Gilkeson, G.S. 2014. Estrogen receptor alpha binding to ERE is required for full Tlr7-and Tlr9-induced inflammation. *SOJ Immunology*, 2(1):07.

Czajka, A. & Malik, A.N. 2016. Hyperglycemia induced damage to mitochondrial respiration in renal mesangial and tubular cells: Implications for diabetic nephropathy. *Redox Biology*, 10:100-107.

Dallal, C.M., Tice, J.A., Buist, D.S., Bauer, D.C., Lacey Jr, J.V., Cauley, J.A., ... Pfeiffer, R.M. 2014. Estrogen metabolism and breast cancer risk among postmenopausal women: a case–cohort study within B~ FIT. *Carcinogenesis*, 35(2):346-355.

De Faria, A., Zancanela, D., Ramos, A., Torqueti, M. & Ciancaglini, P. 2016. Estrogen and phenol red free medium for osteoblast culture: study of the mineralization ability. *Cytotechnology*, 68(4):1623-1632.

de la Cruz-López, K.G., Castro-Muñoz, L.J., Reyes-Hernández, D.O., García-Carrancá, A. & Manzo-Merino, J. 2019. Lactate in the regulation of tumor microenvironment and therapeutic approaches. *Frontiers in Oncology*, 9:1143.

de Paula Assis, L.H., de Gabriel Dorighello, G. & De Oliveira, H.C.F. 2022. Pro-inflammatory polarization of macrophages is associated with reduced endoplasmic reticulum-mitochondria interaction. *Biochemical Biophysical Research Communications*, 606:61-67.

Deimann, W. 1984. Endogenous peroxidase activity in mononuclear phagocytes. *Progress in Histochemistry Cytochemistry*, 15(2):III-56.

Deura, I., Harada, T., Taniguchi, F., Iwabe, T., Izawa, M. & Terakawa, N. 2005. Reduction of estrogen production by interleukin-6 in a human granulosa tumor cell line may have implications for endometriosis-associated infertility. *Fertility Sterility*, 83(4):1086-1092.

Diskin, C. & Pålsson-McDermott, E.M. 2018. Metabolic modulation in macrophage effector function. *Frontiers in Immunology*, 9:270.

Doak, G.R., Schwertfeger, K.L. & Wood, D.K. 2018. Distant relations: macrophage functions in the metastatic niche. *Trends in Cancer Research*, 4(6):445-459.

Dosi, R., Bhatt, N., Shah, P. & Patell, R. 2014. Cardiovascular disease and menopause. *Journal of Clinical Diagnostic Research: JCDR*, 8(2):62.

Edwards, D.P. & McGuire, W.L. 1980. 17α-Estradiol is a biologically active estrogen in human breast cancer cells in tissue culture. *Endocrinology and Metabolism Clinics of North America*, 107(4):884-891.

El-Kenawi, A., Gatenbee, C., Robertson-Tessi, M., Bravo, R., Dhillon, J., Balagurunathan, Y., ... Choi, J. 2019. Acidity promotes tumour progression by altering macrophage phenotype in prostate cancer. *British Journal of Cancer*:1-11.

Eliassen, A.H., Missmer, S.A., Tworoger, S.S. & Hankinson, S.E. 2008. Circulating 2-hydroxy- and 16α-hydroxy estrone levels and risk of breast cancer among postmenopausal women. *Cancer Epidemiology Prevention Biomarkers*, 17(8):2029-2035.

Elkabets, M., Gifford, A.M., Scheel, C., Nilsson, B., Reinhardt, F., Bray, M., ... Ebert, B. 2011. Human tumors instigate granulin-expressing hematopoietic cells that promote malignancy by activating stromal fibroblasts in mice. *The Journal of Clinical Investigation*, 121(2):784-799. doi.org/10.1371/journal.pone.0063967.

Epelman, S., Lavine, K.J. & Randolph, G.J. 2014. Origin and functions of tissue macrophages. *Immunity & Ageing*, 41(1):21-35.

Fadhil, M., Abdul-Rasheed, O. & Al-Naqqash, M.J. 2019. Clinical value of peripheral blood M2/M1 like monocyte ratio in the diagnosis of breast cancer and the differentiation between benign and malignant breast tumors. *Acta Biochimica Polonica*, 66(4):437-443.

Falah, N., Torday, J., Quinney, S.K. & Haas, D.M. 2015. Estriol review: clinical applications and potential biomedical importance. *Clinical Research and Trials*, 1(2):29-33.

Falcone, R., Roberto, M., D'Antonio, C., Romiti, A., Milano, A., Onesti, C.E., ... Fais, S.J. 2016. High-doses of proton pump inhibitors in refractory gastro-intestinal cancer: a case series and the state of art. *Digestive Liver Disease*, 48(12):1503-1505.

Faqehi, A.M., Cobice, D.F., Naredo, G., Mak, T.C., Upreti, R., Gibb, F.W., ... Andrew, R. 2016. Derivatization of estrogens enhances specificity and sensitivity of analysis of human plasma and serum by liquid chromatography tandem mass spectrometry. *Talanta*, 151:148-156.

Farhat, G.N., Parimi, N., Chlebowski, R.T., Manson, J.E., Anderson, G., Huang, A.J., ... Cauley, J.A. 2013. Sex hormone levels and risk of breast cancer with estrogen plus progestin. *Journal of the National Cancer Institute*, 105(19):1496-1503.

Feigelson, H.S., Jonas, C.R., Teras, L.R., Thun, M.J. & Calle, E.E. 2004. Weight gain, body mass index, hormone replacement therapy, and postmenopausal breast cancer in a large prospective study. *Cancer Epidemiology Prevention Biomarkers*, 13(2):220-224.

Felty, Q., Xiong, W., Sun, D., Sarkar, S., Singh, K.P., Parkash, J. & Roy, D. 2005. Estrogen-induced mitochondrial reactive oxygen species as signal-transducing messengers. *Biochemistry (Mosc.)*, 44(18):6900-6909.

Ferranti, E.M., Aloqaily, B.H., Gifford, C.A., Löest, C.A., Wenzel, J.C. & Hernandez Gifford, J.A. 2018. Lipopolysaccharide modulation of ovarian hormonal profile. *Translational Animal Science*, 2(suppl_1):S31-S34.

Frazier-Jessen, M. & Kovacs, E. 1995. Estrogen modulation of JE/monocyte chemoattractant protein-1 mRNA expression in murine macrophages. *The Journal of Immunology*, 154(4):1838-1845.

Freemerman, A.J., Johnson, A.R., Sacks, G.N., Milner, J.J., Kirk, E.L., Troester, M.A., ... Makowski, L. 2014. Metabolic reprogramming of macrophages glucose transporter 1 (GLUT1)-mediated glucose metabolism drives a proinflammatory phenotype. *Journal of Biological Chemistry*, 289(11):7884-7896.

Friedrich, E.B., Clever, Y.P., Wassmann, S., Hess, C. & Nickenig, G. 2006. 17β-estradiol inhibits monocyte adhesion via down-regulation of Rac1 GTPase. *Journal of Molecular Cellular Cardiology*, 40(1):87-95.

Gaikwad, N.W., Yang, L., Pruthi, S., Ingle, J.N., Sandhu, N., Rogan, E.G. & Cavalieri, E.L. 2009. Urine biomarkers of risk in the molecular etiology of breast cancer. *Breast Cancer: Basic Clinical Research and Regulatory Affairs*, 3:BCBCR. S2112.

Gál, P., Varinská, L., Fáber, L., Novák, Š., Szabo, P., Mitrengová, P., ... Smetana, K. 2017. How signaling molecules regulate tumor microenvironment: parallels to wound repair. *Molecules and Cells*, 22(11):1818.

Gatson, J.W., Liu, M.-M., Abdelfattah, K., Wigginton, J.G., Smith, S., Wolf, S., ... Minei, J.P. 2012. Estrone is neuroprotective in rats after traumatic brain injury. *Journal of Neurotrauma*, 29(12):2209-2219.

Geeraerts, X., Bolli, E., Fendt, S. & Van Ginderachter, J.A. 2017. Macrophage metabolism as therapeutic target for cancer, atherosclerosis, and obesity. *Frontiers in Immunology*, 8:289.

Gray, J.S., Birmingham, J.M. & Fenton, J.I. 2010. Got black swimming dots in your cell culture? Identification of Achromobacter as a novel cell culture contaminant. *Biologicals*, 38(2):273-277.

Grosick, R., Alvarado-Vazquez, P.A., Messersmith, A.R. & Romero-Sandoval, E.A. 2018. High glucose induces a priming effect in macrophages and exacerbates the production of pro-inflammatory cytokines after a challenge. *Journal of Pain Research*, 11:1769.

Güemes, M., Rahman, S.A. & Hussain, K. 2016. What is a normal blood glucose? *Archives of Disease in Childhood*, 101(6):569-574.

Gül, N. & van Egmond, M. 2015. Antibody-dependent phagocytosis of tumor cells by macrophages: a potent effector mechanism of monoclonal antibody therapy of cancer. *Cancer Research*, 75(23):5008-5013.

Gupte, A.A., Pownall, H.J. & Hamilton, D.J. 2015. Estrogen: an emerging regulator of insulin action and mitochondrial function. *Journal of Diabetes Research*, 2015, 916585. doi.org/10.1155/2015/916585

Hamilton, K.J., Hewitt, S.C., Arao, Y. & Korach, K.S. 2017. Estrogen hormone biology. In. *Current Topics in Developmental Biology*. 125: Elsevier. pp. 109-146.

Han, C., Zhang, P., Xu, W., Li, R., Xu, J. & Liu, W. 2017. Polarization of macrophages in the blood after decompression in mice. *Medical Gas Research*, 7(4):236.

Hankamolsiri, W., Manochantr, S., Tantrawatpan, C., Tantikanlayaporn, D., Tapanadechopone, P. & Kheolamai, P. 2016. The effects of high glucose on adipogenic and osteogenic differentiation of gestational tissue-derived MSCs. *Stem Cells International*, 2016, 9674614 doi.org/10.1155/2016/9674614

Hariri, L. & Rehman, A. 2019. *Estradiol*. https://www.ncbi.nlm.nih.gov/books/NBK549797/ Date of access: 18 Apr.

Harrison, D.G., Guzik, T.J., Lob, H.E., Madhur, M.S., Marvar, P.J., Thabet, S.R., ... Weyand, C.M. 2011. Inflammation, immunity, and hypertension. *Hypertension in Pregnancy*, 57(2):132-140.

Hart, M.L., Lauer, J.C., Selig, M., Hanak, M., Walters, B. & Rolauffs, B. 2018. Shaping the cell and the future: Recent advancements in biophysical aspects relevant to regenerative medicine. *Journal of Functional Morphology Kinesiology*, 3(1):2.

Herculano-Houzel, S., von Bartheld, C.S., Miller, D.J. & Kaas, J.H. 2015. How to count cells: the advantages and disadvantages of the isotropic fractionator compared with stereology. *Cell Tissue Research*, 360(1):29-42.

Herst, P.M. & Berridge, M.V. 2007. Cell surface oxygen consumption: a major contributor to cellular oxygen consumption in glycolytic cancer cell lines. *Biochimica et Biophysica Acta - Bioenergetics,* 1767(2):170-177.

Hirayama, D., Iida, T. & Nakase, H. 2018. The phagocytic function of macrophage-enforcing innate immunity and tissue homeostasis. *International Journal of Molecular Sciences*, 19(1):92.

Huang, H., Chiang, P. & Chen, S. 2011. Quantitative analysis of estrogens and estrogen metabolites in endogenous MCF-7 breast cancer cells by liquid chromatography–tandem mass spectrometry. *Journal of Chromatography B*, 879(20):1748-1756.

Hunter, K.J. 1998. A dansyl chloride-HPLC method for the determination of polyamines. In. *Polyamine protocols*: Springer. pp. 119-123.

Ioannidou, A., Goulielmaki, E. & Garinis, G.A. 2016. DNA damage: from chronic inflammation to age-related deterioration. *Frontiers in Genetics*, 7:187.

Jablonski, K.A., Amici, S.A., Webb, L.M., de Dios Ruiz-Rosado, J., Popovich, P.G., Partida-Sanchez, S. & Guerau-de-Arellano, M. 2015. Novel markers to delineate murine M1 and M2 macrophages. *PloS One*, 10(12), e0145342. doi.org/10.1371/journal.pone.0145342

Jacobs, C. 2018. *An analytical method to investigate the estrogen metabolism in women taking combined oral contraceptives.* Potchefstroom: North-West University. (Thesis-MSc).

Jarosz-Biej, M., Kamińska, N., Matuszczak, S., Cichoń, T., Pamuła-Piłat, J., Czapla, J., ... Szala, S.J. 2018. M1-like macrophages change tumor blood vessels and microenvironment in murine melanoma. *PloS One*, 13(1), e0191012. doi.org/10.1371/journal.pone.0191012

Jiang, H., Hsu, F., Farmer, M.S., Peterson, L.R., Schaffer, J.E., Ory, D.S. & Jiang, X. 2013. Development and validation of LC-MS/MS method for determination of very long acyl chain (C22: 0 and C24: 0) ceramides in human plasma. *Analytical Bioanalytical Chemistry*, 405(23):7357-7365.

Kajihara, N., Kukidome, D., Sada, K., Motoshima, H., Furukawa, N., Matsumura, T., ... Araki, E. 2017. Low glucose induces mitochondrial reactive oxygen species via fatty acid oxidation in bovine aortic endothelial cells. *Journal of Diabetes Investigation*, 8(6):750-761.

Kamel, M., Shouman, S., El-Merzebany, M., Kilic, G., Veenstra, T., Saeed, M., ... Salama, S.J. 2012. Effect of tumour necrosis factor-alpha on estrogen metabolic pathways in breast cancer cells. *Journal of Cancer Education*, 3:310.

Kanter, J.E., Kramer, F., Barnhart, S., Averill, M.M., Vivekanandan-Giri, A., Vickery, T., ... Chait, A. 2012. Diabetes promotes an inflammatory macrophage phenotype and atherosclerosis through acyl-CoA synthetase 1. *Proceedings of the National Academy of Sciences of the United States of America*, 109(12):E715-E724.

Kaplan, M., Kerry, R., Aviram, M. & Hayek, T. 2008. High glucose concentration increases macrophage cholesterol biosynthesis in diabetes through activation of the sterol regulatory element binding protein 1 (SREBP1): inhibitory effect of insulin. *Journal of Cardiovascular Pharmacology and Therapeutics*, 52(4):324-332.

Keselman, A., Fang, X., White, P.B. & Heller, N.M. 2017. Estrogen signaling contributes to sex differences in macrophage polarization during asthma. *The Journal of Immunology*, 199(5):1573-1583.

Khan, W.A. & Khan, M.W.A. 2013. Cancer morbidity in rheumatoid arthritis: role of estrogen metabolites. *BioMed research international*, 2013, 748178. doi.org/10.1155/2013/748178

Klinge, C.M. 2008. Estrogenic control of mitochondrial function and biogenesis. *Biochemical Journal*, 105(6):1342-1351.

Koo, S. & Garg, N.J. 2019. Metabolic programming of macrophage functions and pathogens control. *Redox Biology*, 24:101198.

Kou, X., Li, C., He, D., Wang, X., Hao, T., Meng, Z., ... Gan, Y. 2015. Estradiol promotes M1-like macrophage activation through cadherin-11 to aggravate temporomandibular joint inflammation in rats. *The Journal of Immunology*, 194(6):2810-2818.

Kovats, S. 2015. Estrogen receptors regulate innate immune cells and signaling pathways. *Cellular Immunology*, 294(2):63-69.

Lagziel, S., Gottlieb, E. & Shlomi, T. 2020. Mind your media. *Nature Metabolism*, 2(12):1369-1372.

Lam, R.S., O'Brien-Simpson, N.M., Holden, J.A., Lenzo, J.C., Fong, S.B. & Reynolds, E.C. 2016. Unprimed, M1 and M2 macrophages differentially interact with Porphyromonas gingivalis. *PloS One*, 11(7), e0158629. doi: 10.1371/journal.pone.0158629

Langston, P.K., Shibata, M. & Horng, T. 2017. Metabolism supports macrophage activation. *Frontiers in Immunology*, 8:61.

Larionova, I., Cherdyntseva, N., Liu, T., Patysheva, M., Rakina, M. & Kzhyshkowska, J. 2019. Interaction of tumor-associated macrophages and cancer chemotherapy. *Oncoimmunology*, 8(7), e1596004. doi: 10.1080/2162402X.2019

Lee, H., Kim, T. & Choi, K. 2012. Functions and physiological roles of two types of estrogen receptors, ERα and ERβ, identified by estrogen receptor knockout mouse. 28(2):71-76.

Lee, H., Stachelek, S.J., Tomczyk, N., Finley, M.J., Composto, R.J. & Eckmann, D.M. 2013. Correlating macrophage morphology and cytokine production resulting from biomaterial contact. *Journal of Biomedical Materials Research Part A*, 101(1):203-212.

Levenson, E.A., Martens, C., Kanakabandi, K., Turner, C.V., Virtaneva, K., Paneru, M., ... Porcella, S.F. 2018. Comparative transcriptomic response of primary and immortalized macrophages to murine norovirus infection. *The Journal of Immunology*, 200(12):4157-4169.

Li, D., Ding, Z., Gui, M., Hou, Y. & Xie, K. 2020. Metabolic enhancement of glycolysis and mitochondrial respiration are essential for neuronal differentiation. *Cellular Reprogramming*, 22(6):291-299.

Li, J., Hsu, H.-C. & Mountz, J.D. 2013. The Dynamic Duo–Inflammatory M1 macrophages and Th17 cells in Rheumatic Diseases. *Journal of Orthopedics & Rheumatology*, 1(1):4.

Li, X. & Franke, A.A. 2015. Improved profiling of estrogen metabolites by orbitrap LC/MS. *Steroids and Lipids Research*, 99:84-90.

Li, Z., Jia, Y., Han, S., Wang, X., Han, F., Zhang, J., ... Hu, D. 2018. Klf4 alleviates lipopolysaccharide-induced inflammation by inducing expression of MCP-1 induced protein 1 to deubiquitinate TRAF6. *Cellular Physiology and Biochemistry*, 47(6):2278-2290.

Lim, S.K., Won, Y.J., Lee, J.H., Kwon, S.H., Lee, E.J., Kim, K.R., ... Chung, B.C. 1997. Altered hydroxylation of estrogen in patients with postmenopausal osteopenia. *The Journal of Clinical Endocrinology Metabolism: Clinical and Experimental*, 82(4):1001-1006.

Little, A.C., Pathanjeli, P., Wu, Z., Bao, L., Goo, L.E., Yates, J.A., ... Merajver, S.D. 2019. IL-4/IL-13 stimulated macrophages enhance breast cancer invasion via Rho-GTPase regulation of synergistic VEGF/CCL-18 signaling. *Frontiers in Oncology*, 9:456.

Liu, X., Liu, J., Zhao, S., Zhang, H., Cai, W., Cai, M., ... Chen, J. 2016. Interleukin-4 is essential for microglia/macrophage M2 polarization and long-term recovery after cerebral ischemia. *Stroke*, 47(2):498-504.

Lizneva, D., Rahimova, A., Kim, S.-M., Atabiekov, I., Javaid, S., Alamoush, B., ... Azziz, R. 2019. FSH beyond fertility. *Frontiers in Endocrinology*, 10:136. doi.org/10.3389/fendo.2019.00136

Lu, X., Yang, R., Zhang, L., Xi, Y., Zhao, J., Wang, F., ... Li, Z. 2019. Macrophage Colony-stimulating Factor Mediates the Recruitment of Macrophages in Triple negative Breast Cancer. *International Journal of Biological Sciences*, 15(13):2859.

Lund, J., Ouwens, D.M., Wettergreen, M., Bakke, S.S., Thoresen, G.H. & Aas, V. 2019. Increased glycolysis and higher lactate production in hyperglycemic myotubes. *Cells Tissues Organs*, 8(9):1101.

Mahmoodzadeh, S. & Dworatzek, E. 2019. The role of 17β-estradiol and estrogen receptors in regulation of Ca2+ channels and mitochondrial function in cardiomyocytes. *Frontiers in Endocrinology*, 10:310.

Malinen, M., Jääskeläinen, T., Pelkonen, M., Heikkinen, S., Väisänen, S., Kosma, V.-M., ... Palvimo, J.J. 2013. Proto-oncogene PIM-1 is a novel estrogen receptor target associating with high grade breast tumors. *Molecular and Cellular Endocrinology*, 365(2):270-276.

Marcus, A., Gowen, B.G., Thompson, T.W., Iannello, A., Ardolino, M., Deng, W., ... Raulet, D.H. 2014. Recognition of tumors by the innate immune system and natural killer cells. In. *Advances in Immunology*. 122: Elsevier. pp. 91-128.

Marim, F.M., Silveira, T.N., Lima Jr, D.S. & Zamboni, D.S. 2010. A method for generation of bone marrow-derived macrophages from cryopreserved mouse bone marrow cells. *PloS One*, 5(12), e15263. doi: 10.1371/journal.pone.0015263

Mauvais-Jarvis, F., Clegg, D.J. & Hevener, A.L. 2013. The role of estrogens in control of energy balance and glucose homeostasis. *Endocrine Reviews*, 34(3):309-338.

McCarthy, M.M. 2008. Estradiol and the developing brain. *Physiological Reviews*, 88(1):91-134.

Mercogliano, M.F., Bruni, S., Elizalde, P.V. & Schillaci, R. 2020. Tumor necrosis factor α blockade: an opportunity to tackle breast cancer. *Frontiers in oncology*, 10:584.

Millas, I., Liquidato, B.M., de Sousa Buck, H., Barros, M.D., Paes, R.A.P. & Dolci, J.E.L. 2011. Evaluation of estrogenic receptors in the nasal mucosa of women taking oral contraceptives. *Contraception*, 83(6):571-577.

Millipore, E. 2012. Precise and Accurate Counts and Viability Measurements Across Multiple Cell Lines Using the Muse™ Cell Count & Viability Assay. *Biotechniques*, 52(3):200-203.

Minutti, C.M., Knipper, J.A., Allen, J.E. & Zaiss, D.M. 2017. Tissue-specific contribution of macrophages to wound healing. In. Seminars in Cell & Developmental Biology. Elsevier. pp. 3-11.

Moen, I. & Stuhr, L.E. 2012. Hyperbaric oxygen therapy and cancer—a review. *Targeted Oncology*, 7(4):233-242.

Monteiro, R., Teixeira, D. & Calhau, C. 2014. Estrogen signaling in metabolic inflammation. *Mediators of Inflammation*, 2014,

Mor, G., Yue, W., Santen, R.J., Gutierrez, L., Eliza, M., Berstein, L.M., ... Diano, S. 1998. Macrophages, estrogen and the microenvironment of breast cancer. *The Journal of Steroid Biochemistry Molecular Biology and Evolution*, 67(5-6):403-411.

More, G.K. & Makola, R.T. 2020. In-vitro analysis of free radical scavenging activities and suppression of LPS-induced ROS production in macrophage cells by Solanum sisymbriifolium extracts. *Scientific Reports of the Istituto Superiore di Sanita*, 10(1):1-9.

Mufudza, C., Sorofa, W. & Chiyaka, E.T. 2012. Assessing the effects of estrogen on the dynamics of breast cancer. *Computational Mathematical Methods in Medicine*, 2012, 473572. doi.org/10.1155/2012/473572

Murray, P.J. & Wynn, T.A. 2011. Protective and pathogenic functions of macrophage subsets. *Nature Reviews Immunology*, 11(11):723-737.

Myöhänen, T.T., Schendzielorz, N. & Männistö, P.T. 2010. Distribution of catechol-O-methyltransferase (COMT) proteins and enzymatic activities in wild-type and soluble COMT deficient mice. *Journal of Neurochemistry*, 113(6):1632-1643.

Navarro, F.C., Herrnreiter, C., Nowak, L. & Watkins, S.K. 2018. Estrogen Regulation of T-Cell Function and Its Impact on the Tumor Microenvironment. *Gender and the Genome*, 2(3):81-91.

Németh, B., Doczi, J., Csete, D., Kacso, G., Ravasz, D., Adams, D., ... Tretter, L. 2016. Abolition of mitochondrial substrate-level phosphorylation by itaconic acid produced by LPS-induced Irg1 expression in cells of murine macrophage lineage. *The FASEB Journal*, 30(1):286-300.

Netea-Maier, R.T., Smit, J.W. & Netea, M.G. 2018. Metabolic changes in tumor cells and tumor-associated macrophages: a mutual relationship. *Cancer Letters*, 413:102-109.

Nguyen, H.P. 2010. *Estrogen analysis by liquid chromatography-mass spectrometry.* The University of Texas at Arlington. (Thesis-PhD).

Nichols, H. 2020. *Everything you need to know about estrogen*. https://www.medicalnewstoday.com/articles/277177 Date of access: 19 April

Nielsen, S.R. & Schmid, M.C. 2017. Macrophages as key drivers of cancer progression and metastasis. *Mediators of Inflammation*, 2017, 9624760. doi.org/10.1155/2017/9624760

Obayashi, M., Shimomura, Y., Nakai, N., Jeoung, N.H., Nagasaki, M., Murakami, T., ... Harris, R.A. 2004. Estrogen controls branched-chain amino acid catabolism in female rats. *The Journal of Nutrition, Health & Aging*, 134(10):2628-2633.

Pahl, J.H., Kwappenberg, K.M., Varypataki, E.M., Santos, S.J., Kuijjer, M.L., Mohamed, S., ... Egeler, R.M. 2014. Macrophages inhibit human osteosarcoma cell growth after activation with the bacterial cell wall derivative liposomal muramyl tripeptide in combination with interferon-γ. *Journal of Experimental and Clinical Cancer Research*, 33(1):27.

Palsson-McDermott, E.M., Curtis, A.M., Goel, G., Lauterbach, M.A., Sheedy, F.J., Gleeson, L.E., ... Johnston, D.G. 2015. Pyruvate kinase M2 regulates Hif-1α activity and IL-1β induction and is a critical determinant of the warburg effect in LPS-activated macrophages. *Cell Metabolism*, 21(1):65-80.

Pan, X. 2012. The mechanism of the anticancer function of M1 macrophages and their use in the clinic. *Chinese Journal of Cancer Research. Chung-Kuo Yen Cheng Yen Chiu*, 31(12):557.

Parisi, L., Gini, E., Baci, D., Tremolati, M., Fanuli, M., Bassani, B., ... Mortara, L. 2018. Macrophage polarization in chronic inflammatory diseases: Killers or builders? *Journal of Immunology Research*, 2018, 8917804. doi.org/10.1155/2018/8917804

Park, S. 2018. Catechol Estrogen 4-Hydroxyestradiol is an Ultimate Carcinogen in Breast Cancer. *Biomedical Science Letters*, 24(3):143-149.

Patel, H., Nilendu, P., Jahagirdar, D., Pal, J.K. & Sharma, N.K. 2018. Modulating secreted components of tumor microenvironment: A masterstroke in tumor therapeutics. *Cancer Biology & Therapy*, 19(1):3-12.

Pathria, P., Louis, T.L. & Varner, J.A. 2019. Targeting tumor-associated macrophages in cancer. *Trends in Immunology*, 40(4):310-327.

Pavlou, S., Lindsay, J., Ingram, R., Xu, H. & Chen, M. 2018. Sustained high glucose exposure sensitizes macrophage responses to cytokine stimuli but reduces their phagocytic activity. *BMC Immunology*, 19(1):24.

Pesce, J.T., Ramalingam, T.R., Mentink-Kane, M.M., Wilson, M.S., El Kasmi, K.C., Smith, A.M., ... Wynn, T.A. 2009. Arginase-1–expressing macrophages suppress Th2 cytokine–driven inflammation and fibrosis. *PLoS Pathogens*, 5(4), e1000371. doi.org/10.1371/journal.ppat.1000371

Piarulli, F., Sartore, G., Sechi, A., Basso, D., Fogar, P., Greco, E., ... Lapolla, A. 2017. Low glucose concentrations induce a similar inflammatory response in monocytes from type 2 diabetic patients and healthy subjects. *Oxidative Medicine Cellular Longevity*, 2017, 9185272. doi.org/10.1155/2017/9185272

Pinto, A.T., Pinto, M.L., Cardoso, A.P., Monteiro, C., Pinto, M.T., Maia, A.F., ... Marques, M. 2016. Ionizing radiation modulates human macrophages towards a pro-inflammatory phenotype preserving their pro-invasive and pro-angiogenic capacities. *Scientific Reports of the Istituto Superiore di Sanita*, 6(1):1-15. 615917 doi.org/10.1155/2014/615917

Pizzorno, J.E., Murray, M.T. & Joiner-Bey, H. 2016. *The Clinician's Handbook of Natural Medicine E-Book*. Elsevier Health Sciences.pp.870-890

Podo, F., Buydens, L.M., Degani, H., Hilhorst, R., Klipp, E., Gribbestad, I.S., ... Monleon, D. 2010. Triple-negative breast cancer: present challenges and new perspectives. *Molecular Oncology*, 4(3):209-229.

Poh, A.R. & Ernst, M. 2018. Targeting macrophages in cancer: from bench to bedside. *Frontiers in Oncology*, 8:49.

Pozzi, S., Benedusi, V., Maggi, A. & Vegeto, E. 2006. Estrogen action in neuroprotection and brain inflammation. *Annals of the New York Academy of Sciences*, 1089(1):302-323.

Putti, T.C., Abd El-Rehim, D.M., Rakha, E.A., Paish, C.E., Lee, A.H., Pinder, S.E. & Ellis, I.O. 2005. Estrogen receptor-negative breast carcinomas: a review of morphology and immunophenotypical analysis. *Modern Pathology*, 18(1):26-35.

Qian, B. & Pollard, J.W. 2012. New tricks for metastasis-associated macrophages. *Breast Cancer Research and Treatment*, 14(4):316.

Radde, B.N., Ivanova, M.M., Mai, H.X., Salabei, J.K., Hill, B.G. & Klinge, C.M. 2015. Bioenergetic differences between MCF-7 and T47D breast cancer cells and their regulation by oestradiol and tamoxifen. *Biochemical Journal*, 465(1):49-61.

Raftogianis, R., Creveling, C., Weinshilboum, R. & Weisz, J. 2000. Estrogen metabolism by conjugation. *JNCI Monographs*, 2000(27):113-124.

Raju, G.A.R., Chavan, R., Deenadayal, M., Gunasheela, D., Gutgutia, R., Haripriya, G., ... Patki, A.S. 2013. Luteinizing hormone and follicle stimulating hormone synergy: a review of role in controlled ovarian hyper-stimulation. *Journal of Human Reproductive Sciences*, 6(4):227.

Raschke, W., Baird, S., Ralph, P. & Nakoinz, I. 1978. Functional macrophage cell lines transformed by Abelson leukemia virus. *Cell & Bioscience*, 15(1):261-267.

Ratnakumar, A., Zimmerman, S.E., Jordan, B.A. & Mar, J.C. 2019. Estrogen activates Alzheimer's disease genes. *Alzheimer's Dementia: Translational Research Clinical Interventions in Aging*, 5:906-917.

Redka, D.y.S., Gütschow, M., Grinstein, S. & Canton, J. 2018. Differential ability of proinflammatory and anti-inflammatory macrophages to perform macropinocytosis. *Molecular Biology of the Cell*, 29(1):53-65.

Reichel, D., Tripathi, M. & Perez, J.M. 2019. Biological effects of nanoparticles on macrophage polarization in the tumor microenvironment. *Nanotheranostics*, 3(1):66.

Rettew, J.A., McCall IV, S.H. & Marriott, I. 2010. GPR30/GPER-1 mediates rapid decreases in TLR4 expression on murine macrophages. *Molecular Cellular Endocrinology*, 328(1-2):87-92.

Reynolds, G. & Haniffa, M. 2015. Human and mouse mononuclear phagocyte networks: a tale of two species? *Frontiers in Immunology*, 6:330.

Rezvani, K., Rouce, R., Liu, E. & Shpall, E. 2017. Engineering natural killer cells for cancer immunotherapy. *Molecular Therapy*, 25(8):1769-1781.

Rodríguez-Prados, J., Través, P.G., Cuenca, J., Rico, D., Aragonés, J., Martín-Sanz, P., ... Boscá, L. 2010. Substrate fate in activated macrophages: a comparison between innate, classic, and alternative activation. *The Journal of Immunology*, 185(1):605-614.

Rømer, A.M.A., Thorseth, M.-L. & Madsen, D.H. 2021. Immune modulatory properties of collagen in cancer. *Frontiers in Immunology*:5265.

Rosenberg, S.A. & Restifo, N.P. 2015. Adoptive cell transfer as personalized immunotherapy for human cancer. *Science & Government Report*, 348(6230):62-68.

Rosenfeld, Y. & Shai, Y. 2006. Lipopolysaccharide (Endotoxin)-host defense antibacterial peptides interactions: role in bacterial resistance and prevention of sepsis. *Biochimica et Biophysica Acta (BBA)-Biomembranes*, 1758(9):1513-1522.

Rubinow, K.B. 2018. An intracrine view of sex steroids, immunity, and metabolic regulation. *Molecular Metabolism*, 15:92-103.

Russo, J. & Russo, I.H. 2006. The role of estrogen in the initiation of breast cancer. *The Journal of Steroid Biochemistry and Molecular Biology*, 102(1-5):89-96.

Ryu, A.H., Eckalbar, W.L., Kreimer, A., Yosef, N. & Ahituv, N. 2017. Use antibiotics in cell culture with caution: genome-wide identification of antibiotic-induced changes in gene expression and regulation. *Scientific Reports of the Istituto Superiore di Sanita*, 7(1):7533.

Samavat, H. & Kurzer, M.S. 2015. Estrogen metabolism and breast cancer. *Vaccine & Immunization News*, 356(2):231-243.

Sampson, J.N., Falk, R.T., Schairer, C., Moore, S.C., Fuhrman, B.J., Dallal, C.M., ... Zheng, W.J. 2017. Association of estrogen metabolism with breast cancer risk in different cohorts of postmenopausal women. *Cancer Research and Treatment*, 77(4):918-925.

Santen, R. & Harvey, H. 1999. Use of aromatase inhibitors in breast carcinoma. *Endocrine-Related Cancer*, 6(1):75-92.

Schmidt, M., Kreutz, M., Loffler, G., Scholmerich, J. & Straub, R. 2000. Conversion of dehydroepiandrosterone to downstream steroid hormones in macrophages. *Journal of Endocrinology*, 164(2):161-169.

Seeger, H., Wallwiener, D., Kraemer, E. & Mueck, A.O. 2006. Comparison of possible carcinogenic estradiol metabolites: effects on proliferation, apoptosis and metastasis of human breast cancer cells. *Maturitas*, 54(1):72-77.

Shah, N.R. & Wong, T. 2006. Current breast cancer risks of hormone replacement therapy in postmenopausal women. *Expert Opinion on Pharmacotherapy*, 7(18):2455-2463.

Shrivastava, A. & Gupta, V.B. 2011. Methods for the determination of limit of detection and limit of quantitation of the analytical methods. *Chronicles of Young Scientists*, 2(1):21-25.

Shrivastava, R. & Shukla, N. 2019. Attributes of alternatively activated (M2) macrophages. *Life Sciences*, 224(2019):222-231.

Simpson, E.R. 2003. Sources of estrogen and their importance. *The Journal of steroid Biochemistry Molecular Biology*, 86(3-5):225-230.

Smiley, D.A. & Khalil, R.A. 2009. Estrogenic compounds, estrogen receptors and vascular cell signaling in the aging blood vessels. *Current Medicinal Chemistry*, 16(15):1863-1887.

Starr, T., Bauler, T.J., Malik-Kale, P. & Steele-Mortimer, O. 2018. The phorbol 12-myristate-13-acetate differentiation protocol is critical to the interaction of THP-1 macrophages with Salmonella Typhimurium. *PloS One*, 13(3), e0193601. doi.org/10.1371/journal.pone.0193601

Stout, M.B., Steyn, F.J., Jurczak, M.J., Camporez, J.-P.G., Zhu, Y., Hawse, J.R., ... Pirtskhalava, T. 2017. 17α-Estradiol alleviates age-related metabolic and inflammatory dysfunction in male mice without inducing feminization. *Journals of Gerontology Series A: Biomedical Sciences Medical Sciences*, 72(1):3-15.

Sulistiyani, R.S.C. 1997. Effect of 17 beta-estradiol on metabolism of acetylated low-density lipoprotein by THP-1 macrophages in culture. *Arteriosclerosis, Thrombosis, Vascular Biology*, 17(9):1691-1700.

Sun, X., Li, Y., Deng, Q., Hu, Y., Dong, J., Wang, W., ... Li, C. 2022. Macrophage Polarization, Metabolic Reprogramming, and Inflammatory Effects in Ischemic Heart Disease. *Frontiers in Immunology*, 13,

Sundblad, V., Mathieu, V., Kiss, R. & Rabinovich, G.A. 2013. Galectins: key players in the tumor microenvironment. In. *Cancer Immunotherapy*: Elsevier. pp. 537-563.

Taciak, B., Białasek, M., Braniewska, A., Sas, Z., Sawicka, P., Kiraga, Ł., ... Król, M. 2018. Evaluation of phenotypic and functional stability of RAW 264.7 cell line through serial passages. *PloS One*, 13(6), e0198943. doi:10.1371/journal.pone.0198943

Tamir, S., Izrael, S. & Vaya, J. 2002. The effect of oxidative stress on ERα and ERβ expression. *The Journal of Steroid Biochemistry Molecular Biology and Evolution*, 81(4-5):327-332.

Tedesco, S., De Majo, F., Kim, J., Trenti, A., Trevisi, L., Fadini, G.P., ... Vitiello, L. 2018. Convenience versus biological significance: are PMA-differentiated THP-1 cells a reliable substitute for blood-derived macrophages when studying in vitro polarization? *Frontiers in Pharmacology*, 9:71.

Terrazas, S., Escoto, A.-K., Wolkowicz, P. & Giordano, S. 2018. Investigating the anti-oxidant effects of estrogen in RAW cell macrophages. *Free Radical Biology Medicine & Health*, 128:S111.

Thapa, B. & Lee, K. 2019. Metabolic influence on macrophage polarization and pathogenesis. *BMB Reports*, 52(6):360.

Theret, M., Mounier, R. & Rossi, F. 2019. The origins and non-canonical functions of macrophages in development and regeneration. *Development and Psychopathology*, 146(9):dev156000.

Toran-Allerand, C.D., Tinnikov, A.A., Singh, R.J. & Nethrapalli, I.S. 2005. 17α-Estradiol: a brain-active estrogen? *Endocrinology and Metabolism Clinics of North America*, 146(9):3843-3850.

Torgovnick, A. & Schumacher, B. 2015. DNA repair mechanisms in cancer development and therapy. *Frontiers in Genetics*, 6:157.

Trenti, A., Tedesco, S., Boscaro, C., Trevisi, L., Bolego, C. & Cignarella, A. 2018. Estrogen, angiogenesis, immunity and cell metabolism: solving the puzzle. *International Journal of Molecular Sciences*, 19(3):859.

Unger, R.E., Krump-Konvalinkova, V., Peters, K. & Kirkpatrick, C.J. 2002. In vitro expression of the endothelial phenotype: comparative study of primary isolated cells and cell lines, including the novel cell line HPMEC-ST1. 6R. *Microvascular Research*, 64(3):384-397.

Van den Bossche, J., Baardman, J. & de Winther, M.P. 2015. Metabolic characterization of polarized M1 and M2 bone marrow-derived macrophages using real-time extracellular flux analysis. *JoVE*, (105):e53424.

Van der Windt, G.J., Chang, C.H. & Pearce, E.L. 2016. Measuring bioenergetics in T cells using a seahorse extracellular flux analyzer. *Current Protocols in Immunology*, 113(1):1-3.16.

Venter, G., Oerlemans, F.T., Wijers, M., Willemse, M., Fransen, J.A. & Wieringa, B. 2014. Glucose controls morphodynamics of LPS-stimulated macrophages. *PloS One*, 9(5), e96786. doi.org/10.1371/journal.pone.0096786

Villa, A., Rizzi, N., Vegeto, E., Ciana, P. & Maggi, A. 2015. Estrogen accelerates the resolution of inflammation in macrophagic cells. *Scientific Reports of the Istituto Superiore di Sanita*, 5:15224.

Viola, A., Munari, F., Sánchez-Rodríguez, R., Scolaro, T. & Castegna, A. 2019. The metabolic signature of macrophage responses. *Frontiers in Immunology*, 10(2019):1462.

Wagner, B.A., Venkataraman, S. & Buettner, G.R. 2011. The rate of oxygen utilization by cells. *Free Radical Biology Medicine & Health*, 51(3):700-712.

Wang, C., Mayer, J.A., Mazumdar, A., Fertuck, K., Kim, H., Brown, M. & Brown, P.H. 2011. Estrogen induces c-myc gene expression via an upstream enhancer activated by the estrogen receptor and the AP-1 transcription factor. *Molecular Endocrinology*, 25(9):1527-1538.

Wang, F., Zhang, S., Jeon, R., Vuckovic, I., Jiang, X., Lerman, A., ... Herrmann, J. 2018. Interferon gamma induces reversible metabolic reprogramming of M1 macrophages to sustain cell viability and pro-inflammatory activity. *EBioMedicine*, 30:303-316.

Wang, M., Zhao, J., Zhang, L., Wei, F., Lian, Y., Wu, Y., ... Cao, K. 2017. Role of tumor microenvironment in tumorigenesis. *Journal of Cancer*, 8(5):761.

Wang, N., Liang, H. & Zen, K. 2014. Molecular mechanisms that influence the macrophage M1–M2 polarization balance. *Frontiers in Immunology*, 5:614.

Wang, S., Cyronak, M. & Yang, E. 2007. Does a stable isotopically labeled internal standard always correct analyte response?: A matrix effect study on a LC/MS/MS method for the determination of carvedilol enantiomers in human plasma. *Journal of Pharmaceutical Biomedical Analysis*, 43(2):701-707.

Wang, Z., Guan, D., Wang, S., Chai, L.Y.A., Xu, S. & Lam, K.-P. 2020. Glycolysis and oxidative phosphorylation play critical roles in natural killer cell receptor-mediated natural killer cell functions. *Frontiers in Immunology*, 11:202.

Wei, C., Yang, C., Wang, S., Shi, D., Zhang, C., Lin, X., ... Xiong, B. 2019. Crosstalk between cancer cells and tumor associated macrophages is required for mesenchymal circulating tumor cell-mediated colorectal cancer metastasis. *Molecular Cancer*, 18(1):64.

Werfel, T.A. & Cook, R.S. 2018. Efferocytosis in the tumor microenvironment. In. Seminars in Immunopathology. Springer. pp. 545-554.

Williams, C. & Lin, C. 2013. Oestrogen receptors in breast cancer: basic mechanisms and clinical implications. *Ecancermedicalscience*, 7(370), 24222786. doi: 10.3332/ecancer.2013.370

Wits, I. 2009. The Tumor Microenvironment: The Making of a Paradigm. *Cancer Microenvironment: Official Journal of the International Cancer Society*, 2:9-17. 10.1007/s12307-009-0025-8

Xuan, Q., Wang, J., Nanding, A., Wang, Z., Liu, H., Lian, X. & Zhang, Q. 2014. Tumor-associated macrophages are correlated with tamoxifen resistance in the postmenopausal breast cancer patients. *Pathology Oncology Research*, 20(3):619-624.

Yang, H., Yin, J., Ficarrotta, K., Hsu, S., Zhang, W. & Cheng, C. 2016. Aberrant expression and hormonal regulation of Galectin-3 in endometriosis women with infertility. *Journal of Endocrinological Investigation*, 39(7):785-791.

Yao, J., Chen, S., Cadenas, E. & Brinton, R.D. 2011. Estrogen protection against mitochondrial toxin-induced cell death in hippocampal neurons: antagonism by progesterone. *Brain Research Bulletin*, 1379:2-10.

Yersal, O. & Barutca, S. 2014. Biological subtypes of breast cancer: Prognostic and therapeutic implications. *World Journal of Clinical Oncology*, 5(3):412.

Yu, F. & Bender, W. 2001. The mechanism of tamoxifen in breast cancer prevention. In. Breast Cancer Research. Springer. pp. 1-1.

Zhang, M., He, Y., Sun, X., Li, Q., Wang, W., Zhao, A. & Di, W. 2014. A high M1/M2 ratio of tumor-associated macrophages is associated with extended survival in ovarian cancer patients. *Journal of Ovarian Research*, 7(1):19.

Zheng, X., Hong, Y., Feng, G., Zhang, G., Rogers, H., Lewis, M.A., ... Wei, X. 2013. Lipopolysaccharide-induced M2 to M1 macrophage transformation for IL-12p70 production is blocked by Candida albicans mediated up-regulation of EBI3 expression. *PloS One*, 8(5), e63967. doi.org/10.1371/journal.pone.0063967.

Zhong, X., Lee, H., Kim, S.H., Park, S., Kim, W., Cha, Y. & Surh, Y. 2018. Myc-nick promotes efferocytosis through M2 macrophage polarization during resolution of inflammation. *The FASEB Journal*, 32(10):5312-5325.

Zhou, W., Yang, S. & Wang, P.G. 2017. Matrix effects and application of matrix effect factor. *Bioanalysis*, 9(23):1839-1844.

Zhu, B.T. & Conney, A.H. 1998. Functional role of estrogen metabolism in target cells: review and perspectives. *Carcinogenesis*, 19(1):1-27.

Zimmerman, M.A., Budish, R.A., Kashyap, S. & Lindsey, S.H. 2016. GPER-novel membrane estrogen receptor. *Clinical Science (London, England: 1979)*, 130(12):1005.

Zlotos, D.P., Kronenberger, T. & Laufer, S. 2023. Anticancer Drug Conjugates Incorporating Estrogen Receptor Ligands. *Pharmaceutics*, 15(1):67.